# CORRELATION STUDIES RELATIVE TO THE $\gamma$-RAYS EMITTED IN THE DEUTERON BOMBARDMENT OF BERYLLIUM.

THESIS

submitted by

Robert B. Galloway, B.Sc.

for the degree of

DOCTOR OF PHILOSOPHY

University of Edinburgh,

November, 1959.

# CONTENTS

# CHAPTER I.

## INTRODUCTION

Much work has been done to elucidate the level structure of the light nuclei, with the result that a well established general picture of each is now available, in which only points of detail require further study.

The level structure, below 4 Mev excitation, and decay scheme of one such nucleus, that of Boron 10, has been studied extensively. The reactions that have been used for this purpose are,

$$Be^9(d, n)B^{10}$$

$$B^{10}(p, p')B^{10*} \text{ and } B^{10}(d, d')B^{10*}$$

$$Li^7(\alpha, n)B^{10}$$

The reaction $Be^9(p, \gamma)B^{10}$ can excite levels up to ~ 6.5 Mev in $B^{10}$. This reaction is therefore unsuitable for the study of the levels below 4 Mev, since $\gamma$-ray cascades from the higher levels complicate the interpretation of the observations.

### 1.1. The Spectrum of the Neutrons from $Be^9(d, n)B^{10}$

Many workers have studied the energy spectrum of the neutrons produced in the $Be^9(d, n)B^{10}$ reaction, and so have deduced the energies of the excited levels of the product nucleus. In the early work, by Bonner and Brubaker[1] in 1936, and Staub and Stephens[2] in 1939, the neutron spectrum was obtained by observing recoil protons in a cloud chamber. They found neutron groups corresponding to levels in $B^{10}$ at 0.72, 2.2 and 3.6 Mev.

Later nuclear emulsions were used, first in 1943 by Powell[3], who confirmed these levels. Similar results were obtained by Whitehead and Mandeville[4] in 1950. In 1951 Ajzenberg[5], using 3.4 Mev deuterons and a thin target, found levels at 0.77, 1.79 2.22, and 3.59 Mev. Pruitt, Swartz and Hanna[6] confirmed these levels in 1953 using 0.95 Mev deuterons. In 1953, Dyer and Bird[7] bombarded a thick target with 600 Kev deuterons and found the above four levels and evidence for a previously unobserved level at 2.85 Mev. They also drew attention to a very weak peak, of doubtful statistical significance, in the neutron spectra of Staub and Stephens[2] and Powell[3] which could correspond to a level in $B^{10}$ at about 2.8 Mev.

Reid[8], using a neutron counter telescope, obtained a spectrum similar to that of Dyer and Bird[7], with a barely significant peak that could be attributed to a level at 2.86 Mev in $B^{10}$.

More recently however, Green, Scanlon and Willmott[9], using photographic plates, found no trace of a weak neutron group corresponding to a level near 2.8 Mev.

## 1.2. Inelastic Scattering - $B^{10}(p, p')B^{10*}$ and $B^{10}(d, d')B^{10*}$

Craig, Donahue and Jones[10] used electrostatic analysis of the scattered protons from $B^{10}(p, p')B^{10*}$ to find the energy of the first excited state, and obtained a value of 719 ± 1.6 Kev. Both $B^{10}(p, p')B^{10*}$ and $B^{10}(d, d')B^{10*}$ have been studied by Bockelman, Browne, Sperduto and Buechner[11], who employed magnetic analysis of the scattered particles, and gave the low lying levels of $B^{10}$ as 0.717, 1.739, 2.152 and 3.583 Mev.

## 1.3. $Li^7(\alpha, n)B^{10}$

Boron loaded Geiger counters were used by Haxel and Stuhlinger[12] (1939) to obtain the threshold $\alpha$-particle energies for the production of the ground state and first three excited states of $B^{10}$. They deduced excitation energies of 0.8, 1.3 and 2.1 Mev (all $\pm$ 0.1 Mev.).

More recently this reaction has been studied by Robbins[13] who employed a counter telescope to obtain the energy spectrum of the neutrons, and also obtained the reaction threshold for each level with the aid of a $BF_3$ counter. The targets used were 99% pure isotope and a run was made with a $Li^6$ target to check on the possible effect of $Li^6$ impurity in the $Li^7$ targets. The results indicated levels in $B^{10}$ at 0.74, 1.31 and 1.72 Mev (all $\pm$ 0.06 Mev).

No other reaction has yielded evidence for a level at 1.31 Mev in $B^{10}$.

## 1.4. $B^{10}$ $\gamma$-ray Spectra

Rasmussen, Hornyak and Lauritsen[14] used a magnetic lens spectrograph to measure the energy of photoelectrons from radiators irradiated by the $\gamma$-rays emitted by the excited $B^{10}$ nucleus produced by the reaction $Be^9(d, n)B^{10}$. They found $\gamma$-rays of the following energies; 413.5 $\pm$ 1, 716.6 $\pm$ 1, 1021.6 $\pm$ 2, 1432.9 $\pm$ 5, 2152.0 $\pm$ 15, 2871.0 $\pm$ 15 and 3604.0 $\pm$ 30 Kev.

Day and Huus[15], with a NaI scintillation counter, observed a 718 $\pm$ 5 Kev $\gamma$-ray resulting from the proton bombardment of $B^{10}$, and attributed it to the inelastic scattering reaction, $B^{10}(p, p')B^{10*}$.

Shafroth and Hanna[16] operated two NaI scintillation spectrometers in coincidence to study the decay scheme of $B^{10}$ produced by

the reaction $Be^9(d, n)B^{10}$. Their results are summarised in Fig. 1. They found no definite evidence for a level at 2.86 Mev, which is shown dotted, though their results were not inconsistent with its existence.

1.5. The Proposed Investigation

Fig. 1 gives the currently accepted level structure and decay scheme of $B^{10}$, e.g. as summarised by Ajzenberg and Lauritsen[17] in 1955.

Following the work of Dyer and Bird[7] and Reid[8] a photographic emulsion study of the neutrons from the reaction $Be^9(d, n)B^{10}$ was undertaken in this laboratory by Karadeniz. The spectra, in which the resolution was probably as good as can be obtained by this method (see Bird and Spear[18]) show neutron groups corresponding to the "established" levels of fig. 1 and in addition two groups indicating levels in the 2.8 Mev region, at 2.70 and 3.20 Mev. The poorer energy resolution in the spectra of Dyer and Bird[7] and Reid[8] could have masked any structure corresponding to a 3.2 Mev level.

As the only reported investigation of the $B^{10}$ $\gamma$-ray cascades, by Shafroth and Hanna[16] was not conclusive about the possible existence of such levels, it was felt that a careful study should be undertaken of those cascades likely to yield evidence for or against the levels near 3 Mev suggested by some of the neutron spectra. The department's H.T. set was used to bombard a thick beryllium target with 600 Kv deuterons and so produce the reaction $Be^9(d, n)B^{10}$ under conditions similar to those of the experiment of Karadeniz.

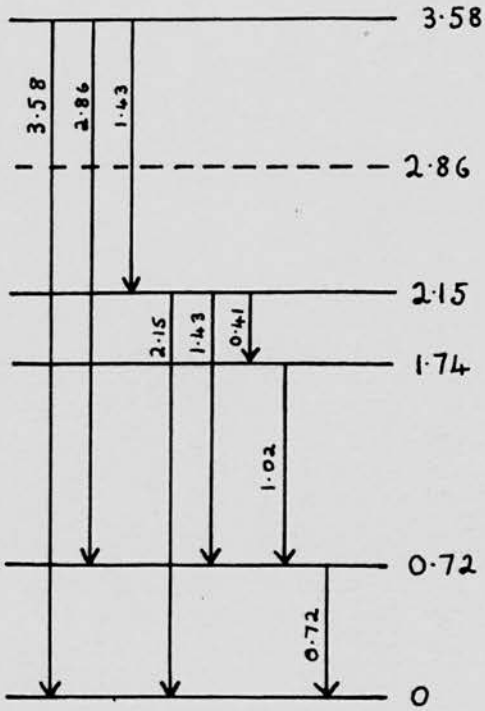


FIG 1 ENERGY LEVELS AND γ-RAY TRANSITIONS OF $B^{10}$ (SHAFROTH AND HANNA [16]).

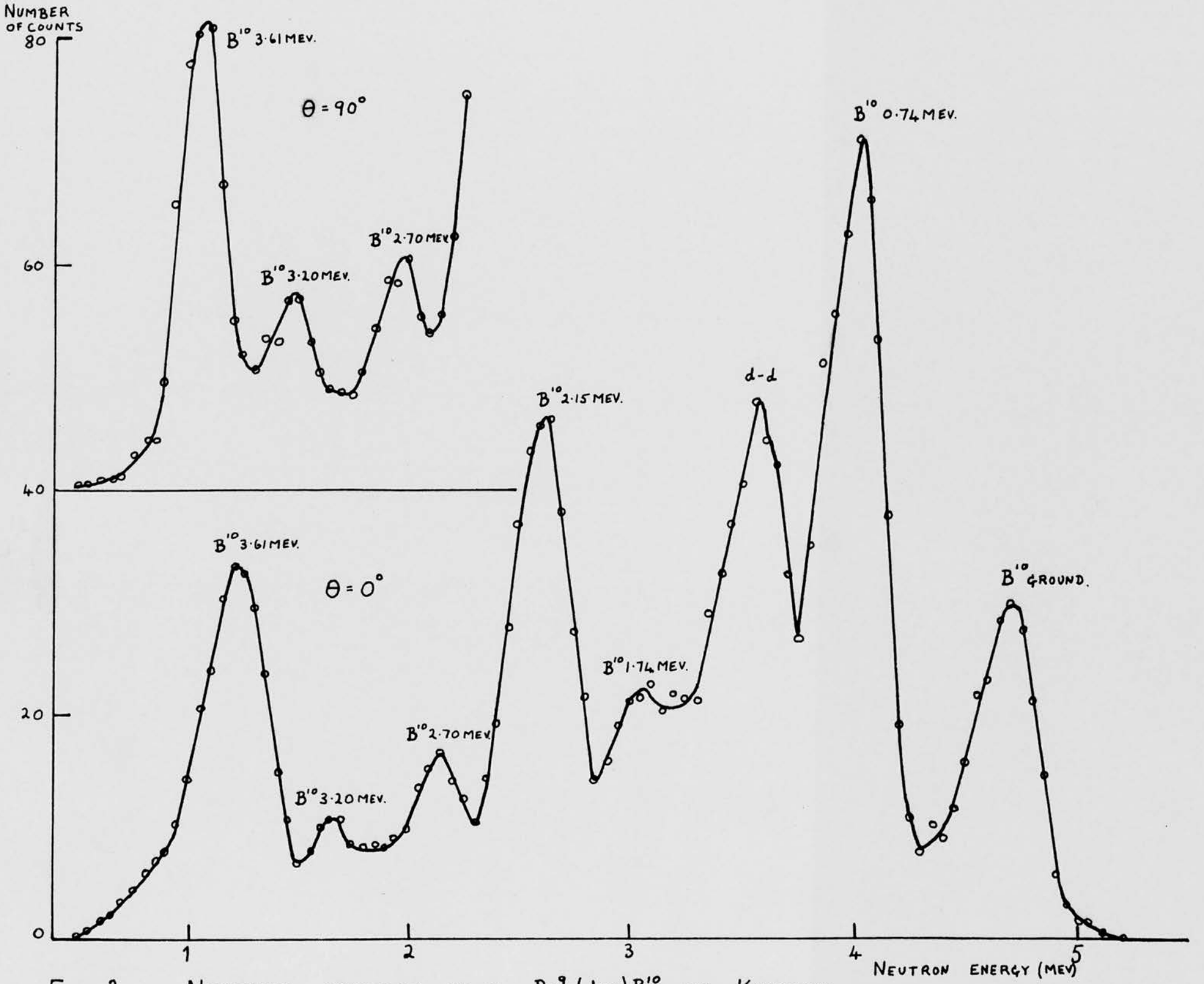


FIG. 2 NEUTRON SPECTRUM FROM $Be^{9}(d,n)B^{10}$ BY KARADENIZ.

Energy levels and spins of states of nuclei in the 1-p shell, $He^4$ to $O^{16}$, have been calculated by Kurath[19], assuming a central two-body interaction and an intermediate strength of spin-orbit coupling. The results for the first four excited states of $B^{10}$ agree well with the states clearly established by experiment, and this provides additional interest in the investigation of any other possible low lying levels.

# CHAPTER 2.

## PRELIMINARY WORK - UNGATED SPECTRA

### 2.1. Scintillation Spectrometers

It was decided to use sodium iodide scintillation counters, and two conventional counter heads were built. The crystals were $1\frac{1}{4}$" diameter x 1" long, and 11-stage E.M.I. photomultipliers were used, type 6260B in one case, and the electrically equivalent type 6097B in the other. The photomultiplier base and the resistor chain for the dynode voltages (fig. 3a), which was based on the recommendations issued by the makers, were in a brass holder; a thin aluminium can which was a tight push fit in this holder surrounded the photomultiplier and crystal, and a perspex ring held the crystal centrally on the end of the photomultiplier. Two light springs were included, one to hold the perspex ring in place, the other to ensure good optical contact between the crystal and photomultiplier, this being aided by placing a drop of oil between them.

The performance of each counter was checked using the 0.66 Mev $\gamma$-rays from a $Cs^{137}$ source, and the 1.17 and 1.33 Mev $\gamma$-rays from a $Co^{60}$ source. The dynode resistor chain was connected to a type 1033A E.H.T. power unit. The signal from the photomultiplier was fed through a cathode follower into an Ekco type N567 amplifier and thence into a type 1074A five channel kicksorter, whose channel width was set at $\frac{1}{2}$ volt. This kicksorter has four channels which can be used to scan a spectrum, and a fifth channel which counts all pulses above the range of the four. Because of the difficulty of setting the widths of each of the four channels to exactly the same value, spectra were scanned by moving the four channels in steps of one channel width, the counting rate at a

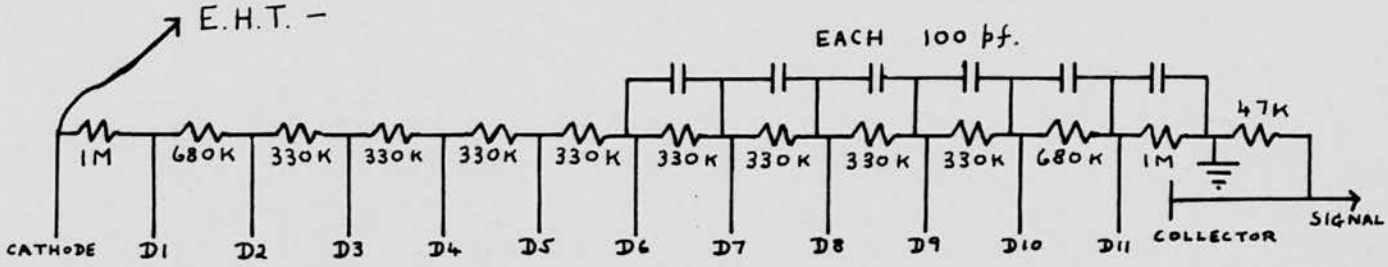


FIG. 3A ORIGINAL DYNODE RESISTOR CHAIN.

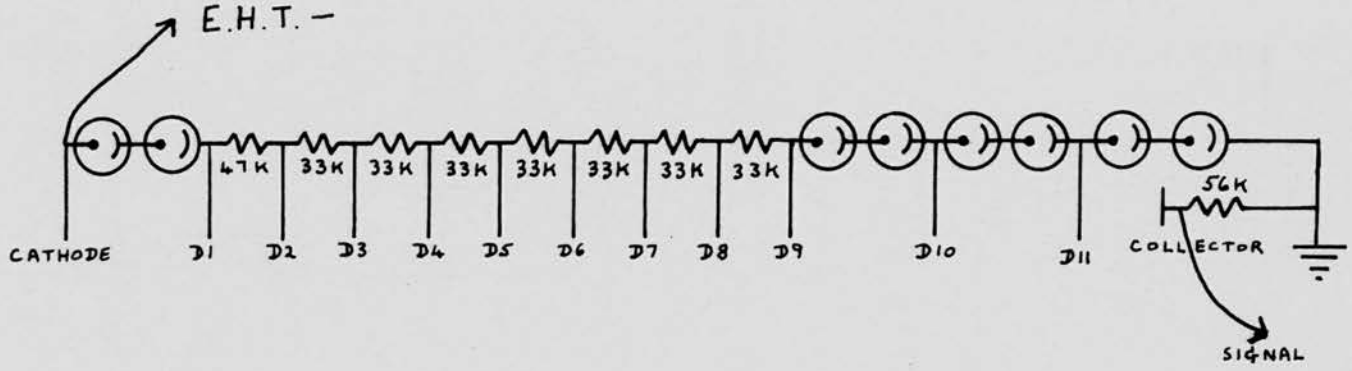


FIG. 3B IMPROVED DYNODE VOLTAGE SUPPLY SYSTEM.

ALL NEON STABILIZERS TYPE 90C1.
CURRENT DRAWN 1·2 M.A. AT 1 KV.
VOLTAGE ACROSS EACH NEON ~85 V.

given position in the spectrum being obtained by adding together the number of counts registered in each channel when it occupied that position.

Spectra were obtained using the Cs source, with several values of E.H.T., and the resolution, i.e. ratio of width of photopeak at half the maximum counting rate to photopeak pulse amplitude, was calculated in each case. With both counters the resolution was never better than 20% and with this resolution it was not possible to separate the two $Co^{60}$ photopeaks. However the use of a borrowed crystal, known to exhibit good resolution, showed that the crystals were at fault; after they had been re-canned by the makers, resolutions of 9% and 10% were obtained for the two counters.

A comparison of the positions of the Co and Cs photopeaks showed that the response of the counters was non-linear for values of E.H.T. greater than 1.25 kv. Further a linear response up to 2.62 Mev ( $\gamma$ -ray from $ThC^{11}$) could not be obtained even by reducing the E.H.T. to 600 V, at which value the resolution was seriously impaired. Several voltage distributions on the dynodes of the photomultiplier were tried, by altering the resistor chain, and the decoupling capacitors at the anode end of the chain were increased in an attempt to extend the region of linearity, but without success.

Messrs. E.M.I. suggested that the connections of the photomultiplier tube should be rearranged to give a constant 150 - 200V between the cathode and dynode 1, and to keep a moderately high fixed voltage between dynode 9 and the anode, the

gain of the remainder of the tube being varied as required. It was suggested that neon stabiliser tubes should be used to maintain the fixed voltages. Accordingly the arrangement shown in fig. 3b was fitted up. Type 90C1 neons, which stabilise at 90V, were selected for their ability to function with a burning current as low as 1 m.a. Linearity up to the $ThC^{11}$ photopeak was obtained with good resolution using this system with an overall voltage of 1 kv. A typical spectrum, showing the Cs, Co and $ThC^{11}$ $\gamma$-rays, is given in fig. 4, curve (i). The positions of the photopeak, Compton edge and escape peaks due to the $ThC^{11}$ $\gamma$-ray are marked; only the photopeaks of the Co and Cs $\gamma$-rays are shown. The straight line (ii) shows the relation between pulse height and $\gamma$-ray energy for these peaks.

## 2.2. The Target Holder

A target holder was designed which would be suitable for angular correlation studies, and provision was made for changing targets easily and with a minimum effect on the accelerating column vacuum system. Fig. 5 shows a sectional view of the target holder, with a plan view to a smaller scale on the right hand side. It consists essentially of a cylindrical box A, with the target B, located at the centre, and a tube C, through which the deuteron beam can enter. The moveable tube D is used, when changing targets, to isolate the target from the main vacuum system. In the position shown it seals off the target B from the vacuum system, by pressing against the neoprene gasket E, so that the target can be removed without affecting the vacuum. The target is fixed to the top plate F, and is removed by lifting the top plate off, after undoing the four screws G. The lower

FIG. 4 TYPICAL SPECTRA, SHOWING LINEARITY

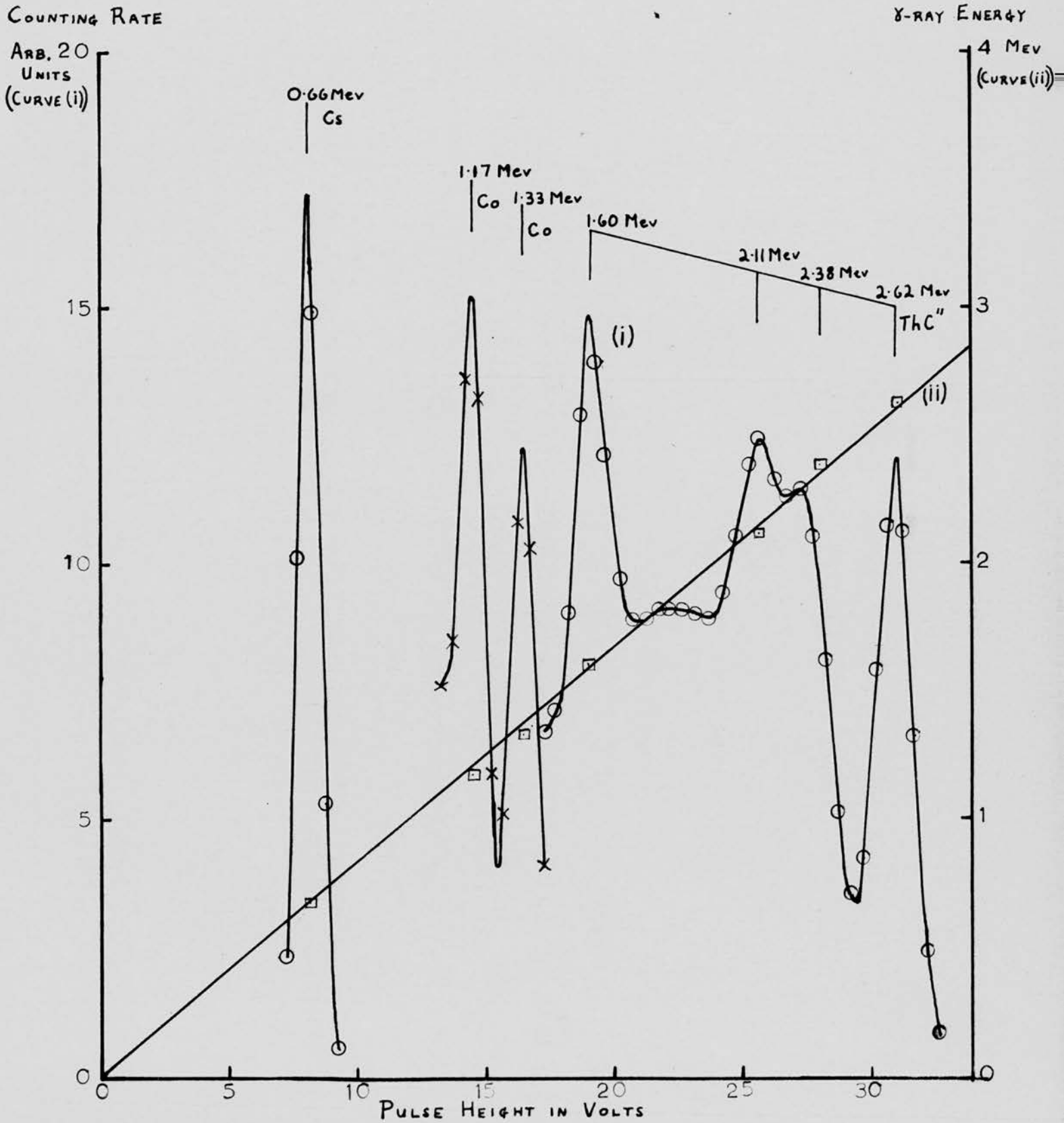

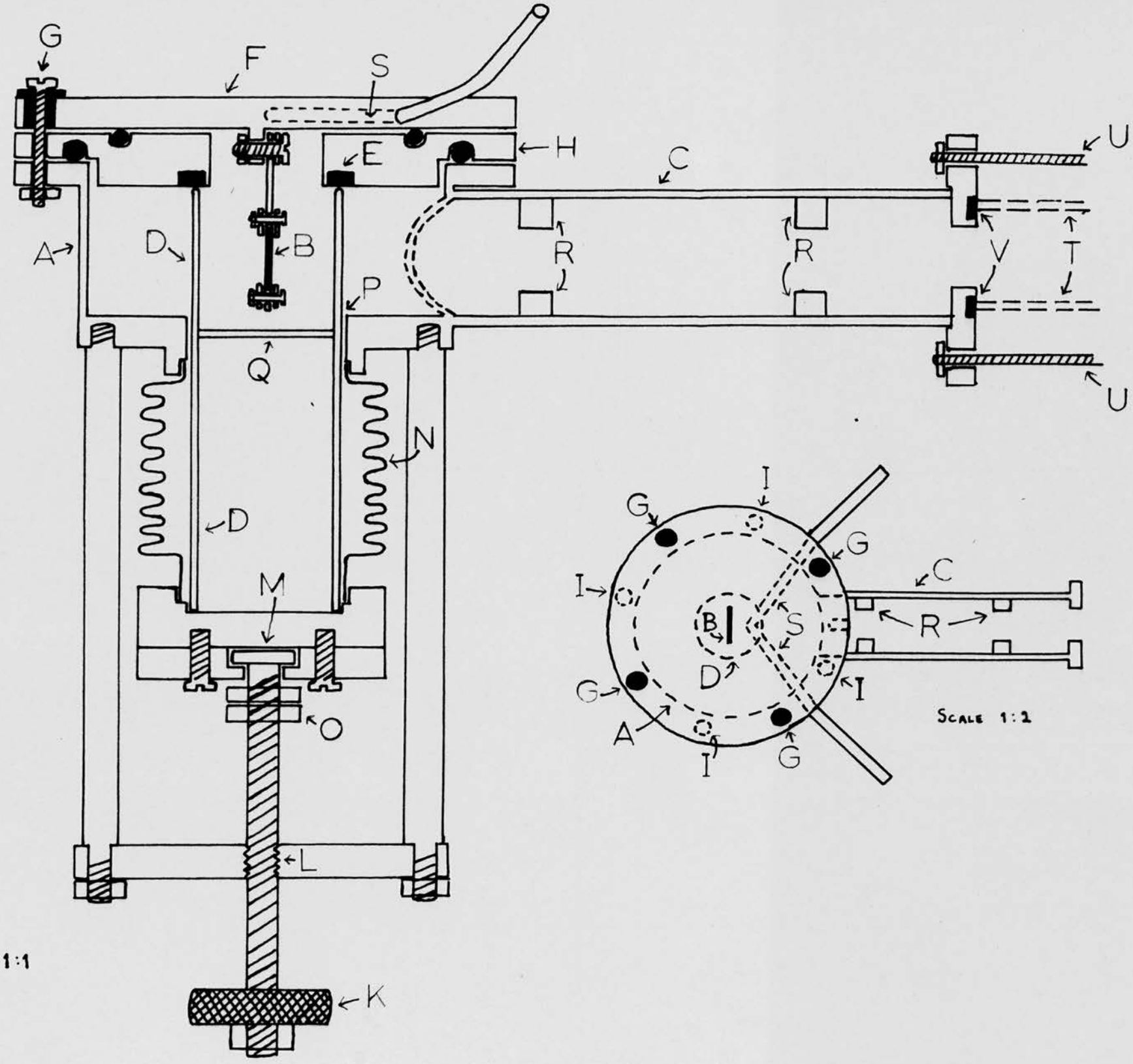
G
F
S
H
E
C
U
A
D
B
R
R
V
T
P
Q
N
D
M
O
L
K
U
I
G
G
I
C
R
B
S
D
I
G
A
I
G
Scale 1:2
Scale 1:1

plate H is not affected by this operation as it is fixed by an independent set of four screws I (shown only on the plan view), which pass through this plate (H) and the flange on the target box A.

When the target has been changed and the top plate replaced, the tube D can be withdrawn from around the target by turning the knob K, which operates the screw drive L. The screw is attached to the tube D at M by a simplified version of a 'ball and socket' joint, which could be called a 'disc and socket' joint, so that the screw can turn without the tube turning. A metal bellows N is used to provide a vacuum tight connection between the tube D and the target box A, and permits the required movement. Lock nuts O prevent excessive straining of the metal bellows, by stopping the extraction of tube D when its top becomes level with the bottom of the target box, i.e. when it reaches P. A disc Q blocks tube D so that the minimum possible amount of air is introduced into the vacuum system after changing a target. Stops R limit the diameter of the deuteron beam, to prevent the gasket E and the top of tube D (in position P) being bombarded by the deuteron beam when the target holder is in use.

O-rings are included between the top plate F and the plate H, and between plate H and the flange on A. The top plate F is insulated from the rest of the target holder by a thin washer of oil-cloth between it and plate H, and by ebonite insulators round the four screws G, so that the beam current striking the target can be measured. A hole drilled in the edge of the top plate to take a wander-plug provides a suitable connection for measuring the current. Water cooling of the top plate, and hence of the

target, is provided through two holes, S, drilled into the edge of the plate, so as to meet near the centre.

The target holder is fitted on the end of a quartz tube T, the other end of which joins the H.T. set's vacuum system where the deuteron beam emerges after resolution and deflection through 30° by a magnetic field. The screwed rods U are fixed at their other end and pull the gasket V against the quartz tube, making a vacuum-tight joint. The weight of the target holder is supported independently by a clamp round tube C. The target holder can be seen in the centre of fig. 24.

After changing a target the pressure in the main vacuum system returns to its normal working value in the time taken to screw the tube D clear of the target. The whole operation of changing a target can be done in about ten minutes.

The target used in the present experiment was a small disc of beryllium, $\frac{3}{4}$" in diameter and about 1/32" thick. It was clamped in a $\frac{3}{4}$" hole in a strip of copper, which was attached to the top plate of the target holder.

## 2.3. Counting Rate

As the pulses forming a spectrum are randomly distributed in time, there will be some cases in which two adjacent pulses occur closer together than the pulse length. Such pairs of pulses will appear at the kicksorter as a single larger pulse, and if sufficiently common will distort the spectrum. An estimate was made of the magnitude of this effect.

In a random sequence of pulses, the probability of observing a pulse in a small interval of time, dt, is proportional to dt. If n is the average counting rate, the probability of observing

a pulse in dt is ndt.

Let p(t) be the probability that no pulse occurs during time t.

Then the probability that a pulse-free interval t is followed by an interval dt in which a pulse occurs is p(t) x n dt, and this must equal the decrease in the probability that no pulse will occur, -dp.

$$\text{i.e. } -dp = p(t) \cdot n\,dt$$

$$\therefore\ p(t) = A\,e^{-nt}$$ and the constant A = 1,

as p(0) = 1,

$\therefore$ the probability of some pulses in time t is

$$1 - p(t) = 1 - e^{-nt}$$

When obtaining spectra the counting rate, of pulses larger than 5V, was normally about $10^3$/sec., and the pulses were 3/us long. With this counting rate, the probability of a pulse following another within 3/us is,

$$1 - p(3 \times 10^{-6}) = 1 - \exp(-10^3 \times 3 \times 10^{-6})$$

$$\approx 1 - 1 + 3 \times 10^{-3} = 3 \times 10^{-3}$$

Thus only about 0.3% of the pulses overlap, and it should be quite safe to obtain spectra at this rate. This was checked roughly using a Cs source by observing the very small number of pulses with amplitude considerably larger than those in the photopeak. When observing the $\gamma$-rays from the $Be^9(d, n)B^{10}$ reaction it was found that considerably larger counting rates distorted the spectrum, whereas lower counting rates did not alter its shape. Fig. 6 illustrates the effect of counting rate

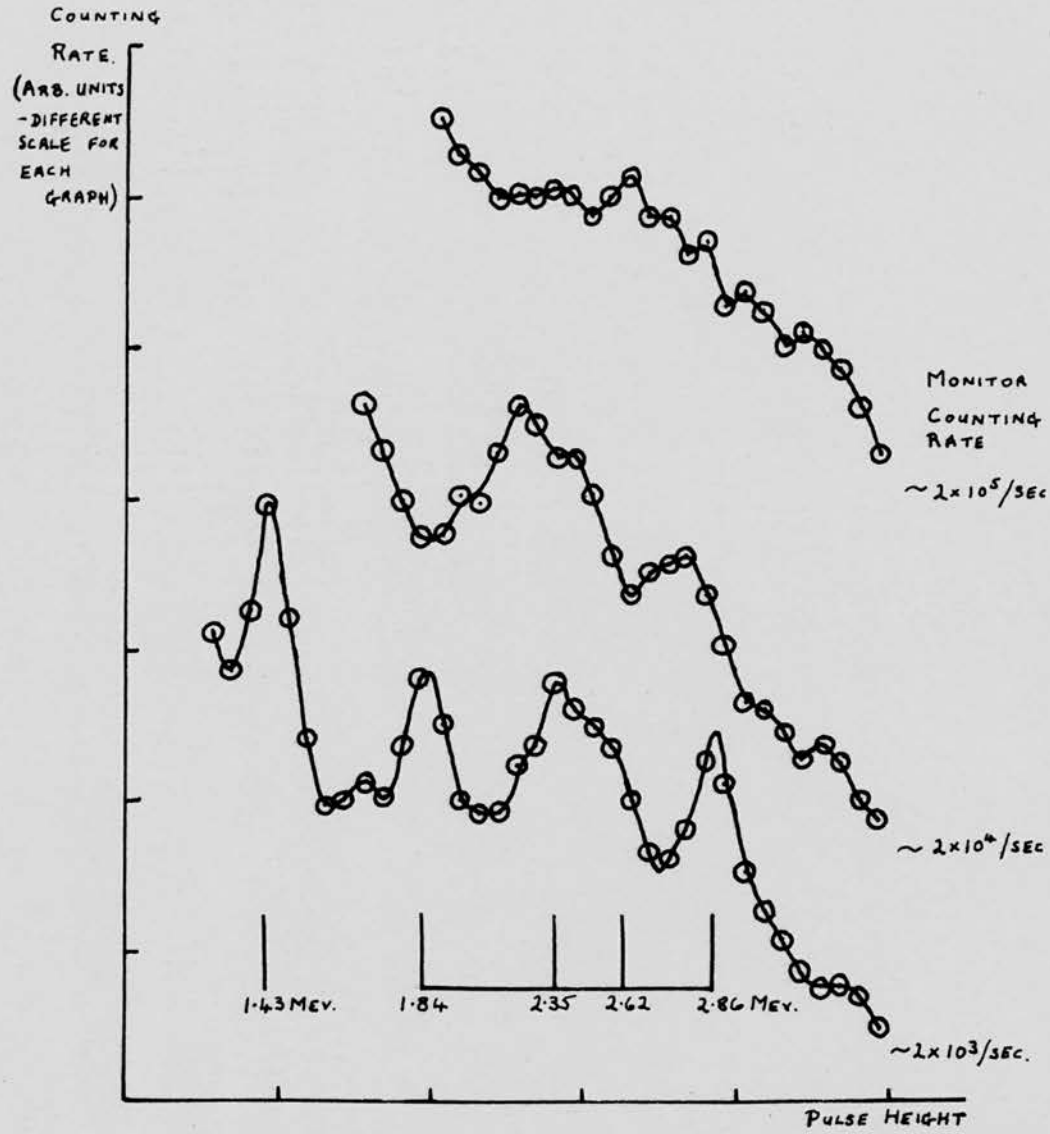


FIG. 6 SPECTRA OF THE HIGH ENERGY $B^{10}$ $\gamma$-RAYS, OBTAINED WITH DIFFERENT BEAM CURRENTS, SHOWING DISTORTION AT HIGH COUNTING RATES.

on the shape of part of the spectrum from the $Be^9(d, n)B^{10}$ reaction.

2.4. γ-rays from the Deuteron Bombardment of Beryllium

The beryllium target was bombarded with 600 kv deuterons from the department's Cockcroft-Walton generator. Fluctuations in the intensity of the deuteron beam while scanning the spectrum were allowed for by including a monitor scaler, fig. 7, at the amplifier output and obtaining the number of counts in the kicksorter for a given count on the scaler, rather than the number of counts in a given time. Calibration spectra similar to fig. 4 were used to analyse the $B^{10}$ spectra; typical examples are shown in figs. 8, 9 and 10, along with the interpretation of the various peaks. Vertical marks indicating the position of the photopeak, Compton edge, and escape peaks for the same γ-ray are joined by a horizontal line. Fig. 8 covers the range of all the expected γ-rays except that at 0.41 Mev, which is shown in fig. 9; fig. 10 is an expanded spectrum of the higher energy peaks, above 1.5 Mev.

The $B^{10}$ γ-rays at 0.41, 0.72, 1.02, 1.43, 2.15 and 2.86 Mev are all observed. The two remaining peaks do not fit the $B^{10}$ decay scheme. One, in fig. 10, is attributed to the 3.37 Mev γ-ray from $Be^{10}$ produced by the competing reaction $Be^9(d, p)Be^{10}$, while the other, fig. 9, at 0.48 Mev is attributed to $Li^7$ from the $Be^9(d, \alpha)Li^7$ reaction[17]. The 3.58 Mev $B^{10}$ γ-ray was not resolved, because of its very low intensity. As it is not necessary to resolve this line for the investigation of a level near 2.8 Mev, no special attempt was made to do so, and this region of the spectrum is not shown.

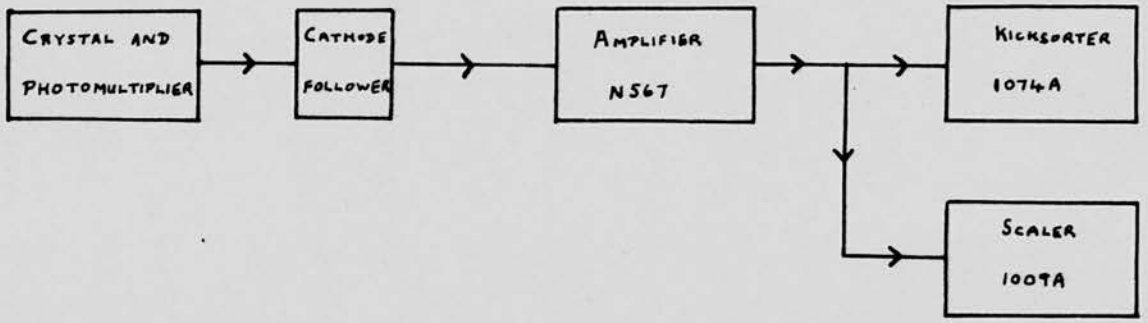


FIG. 7 ELECTRONIC SYSTEM USED FOR UNGATED SPECTRA.

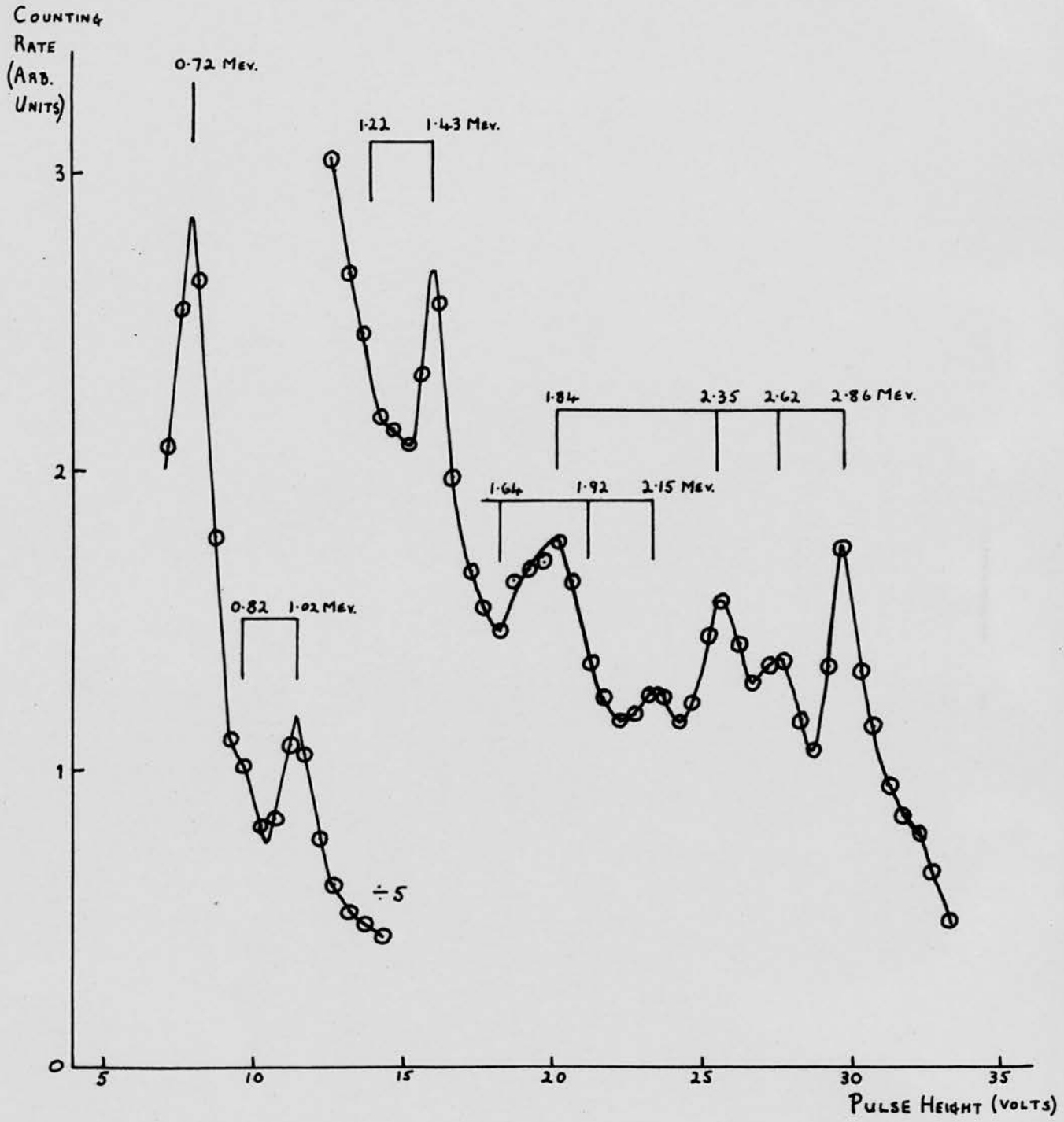


FIG. 8 SPECTRUM OF THE $\gamma$-RAYS FROM THE $Be^{9}(d,n)B^{10}$ REACTION.

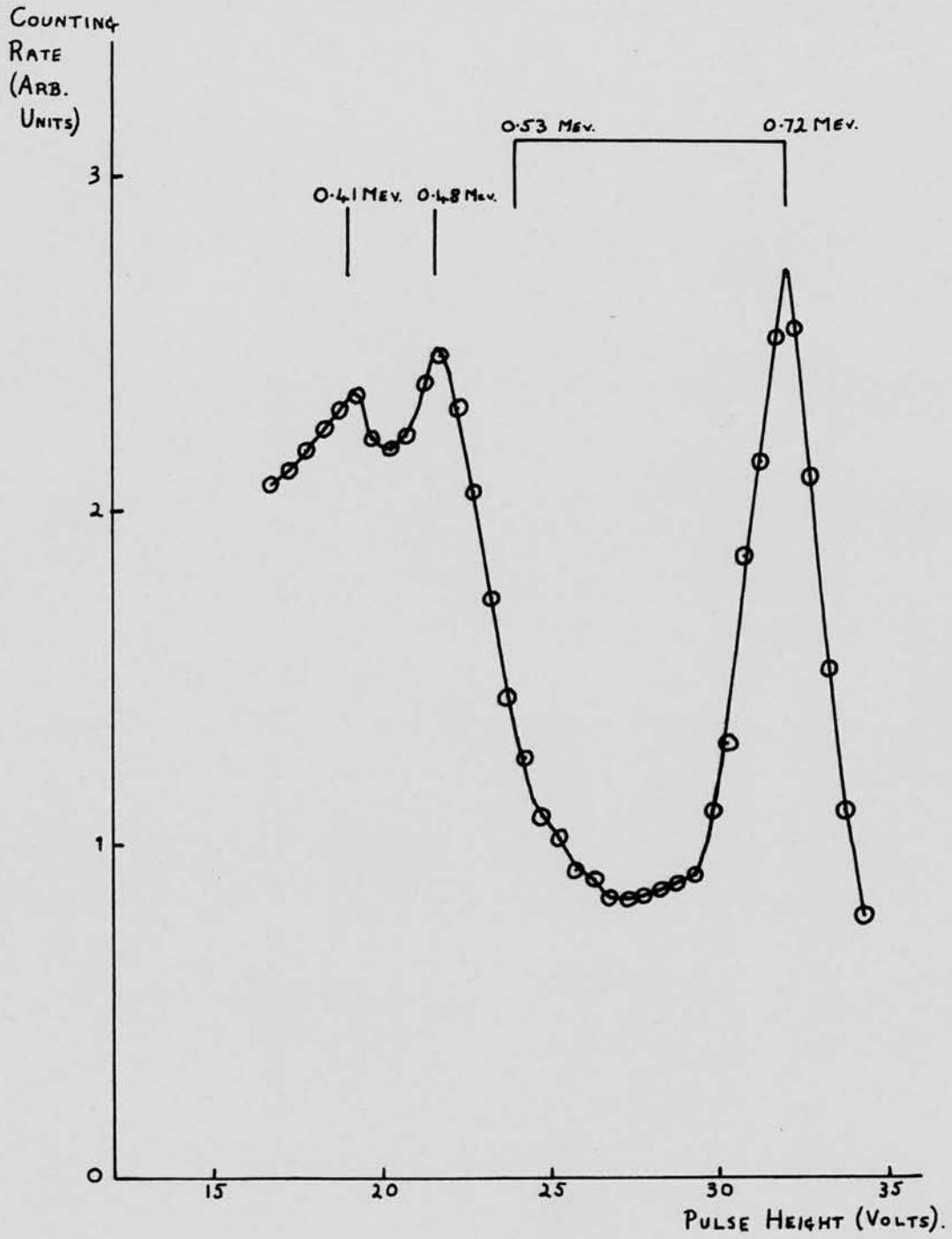


FIG. 9 SPECTRUM OF γ-RAYS FROM $Be^9 + d$

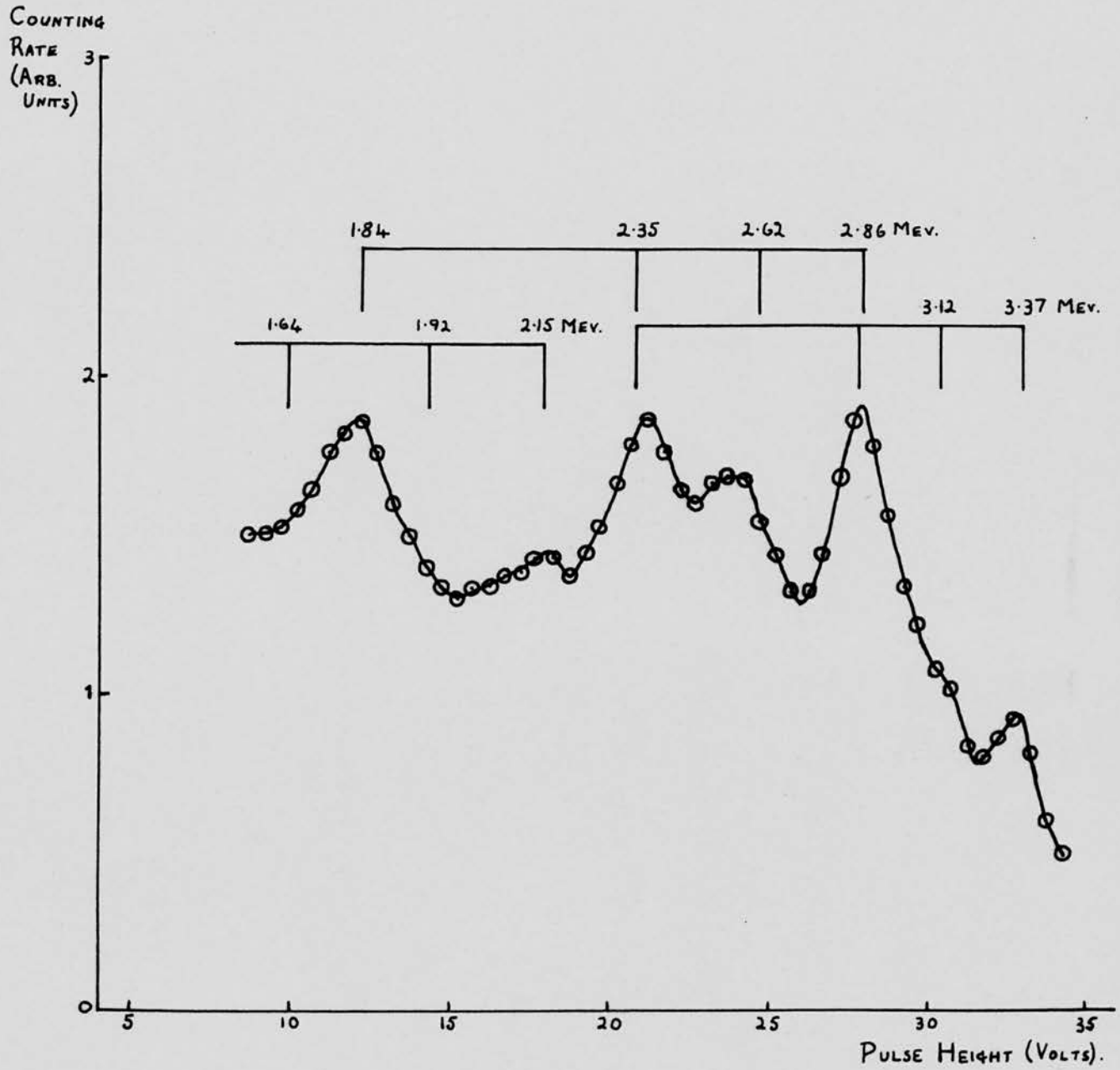


Fig. 10. Spectrum of the γ-rays of energy greater than 1·5 Mev. from $Be^{9} + d$.

# CHAPTER 3.

## COINCIDENCE EQUIPMENT

The electronic units that were required for the experiment are discussed below. Section 3.1. deals with the construction of a coincidence gate unit and the slow coincidence system in which its operation was tested. There follows in section 3.2. a discussion of the problem of pulse height analysis in a coincidence experiment, and the proposal of a design for a 30- channel kicksorter. As the construction of a kicksorter of this type was too large an undertaking to form part of the present investigation, the department's Sunvic kicksorter was used. Section 3.3. contains a description of the method employed to feed pulses from the H.T. laboratory to the laboratory where the Sunvic kicksorter was situated. The present experiment required a more complicated coincidence system than that described in section 3.1; section 3.4. deals with this fast-slow coincidence system and the equipment required to complete it.

### 3.1. Slow Coincidence System

The spectrum of $\gamma$-rays in coincidence with a $\gamma$-ray of a particular energy might be obtained in a straightforward way using the electronic equipment indicated in the block diagram, fig. 11. A pulse from the right hand counter head is allowed to pass through the gate to the kicksorter only if the gate has been opened by a pulse from the single channel pulse height analyser, which is set to provide an output when a $\gamma$-ray of the desired energy has been detected by the left hand counter. In such a system the gate must open for a length of time about equal to the length of the

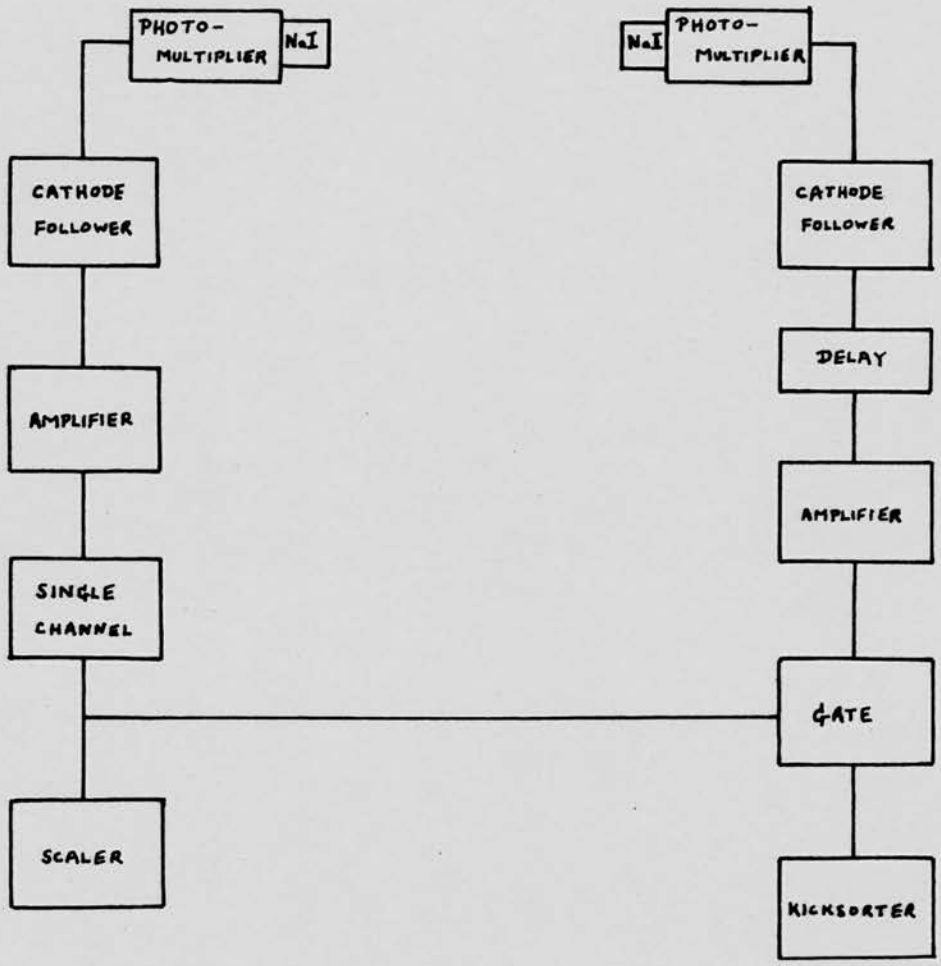


FIG. 11 BLOCK DIAGRAM OF "SLOW" COINCIDENCE SYSTEM.

pulses to be fed through it, and this limits the resolving time that can be obtained to a few $\mu$s, hence the description "slow". A small delay is included in the right hand side to ensure that, when coincident $\gamma$-rays are detected, the gate is fully open before the right hand pulse passes through to be recorded.

Coincidence Gate

The gate unit to be described was based on the circuit of an input amplifier for a pulse height analyser described by Folkierski[20] which included an amplifier, a coincidence gate, and provision for expanding a portion of the spectrum. A block diagram of the unit that was built is shown in fig. 12. The positive going input is applied via a single stage amplifier with a gain of two to the gate which, depending on the position of the switch S1, is either held permanently open or is opened for 5 $\mu$s when a positive pulse fires the trigger circuit. A single stage of amplification at the input of the trigger circuit ensures adequate sensitivity. The subtractor enables up to 100V to be subtracted from the pulses that come through the gate, i.e. the equivalent of up to 50V from pulses at the input to the unit. The tops of the pulses can then be amplified as desired to give an expanded picture of the high energy end of the spectrum. The switch S2 allows the subtractor to be bypassed, while S3 selects the gain of the stage following the subtractor. The unit has a cathode follower output. As an example of the use of the subtractor, the type 1074A kicksorter can scan only the range 5 - 32.5 V, whereas the N567 amplifier that precedes it can provide a spectrum that extends up to 60V before becoming non-linear. If 30V is subtracted from the N567 amplifier

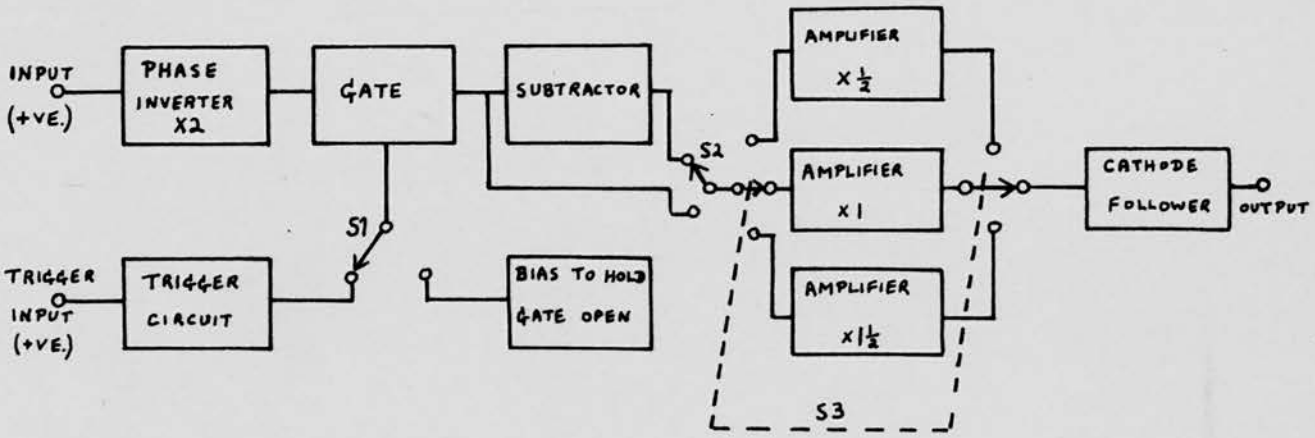


FIG. 12. GATE AND SUBTRACTOR UNIT.

output, the number of channels per peak in the upper part of a spectrum can be doubled. Fig. 10 was obtained in this way and can be compared with the higher energy end of fig. 8.

The circuit of the unit is given in fig. 13. V1 acts as a phase changer with a gain of two. The gate comprises V2, V3 and V4. (There appears to be an error in the circuit shown in Folkierski's paper[20]; the valve corresponding to V4b in fig. 13 is shown connected the wrong way round, cf. Wilkinson[21]). The potential applied to the right hand grid of V2 determines whether the gate is open or closed. If the right hand side of V2 is cut off, the left hand side can act as a cathode follower with V3 as the load, and the gate is open. However if the right hand side of V2 is conducting, the common cathode will be held at the potential of the right hand grid and negative pulses applied to the left hand grid will not appear at the cathode. Under these conditions the gate is closed. The trigger circuit, V7 and V8, that controls the gate is of standard type and provides a pulse 5 $\mu$s long. It is preceded by an amplifier, V5. When the gate is operated by the trigger circuit a small negative pulse about 1V high is produced at the cathode of V2, as the current passing through this valve when the gate is open is not exactly the same as when it is closed. This means that when a pulse is passed by the gate it is superimposed on a small pedestal. The biased diode V8 acts as the subtractor. The amount it subtracts is shown on the meter M and is controlled by the 5 k$\Omega$ potentiometer. V9, V10 and V11 provide gains of 0.5, 1.0 and 1.5 respectively; the only difference between these three stages is the value of

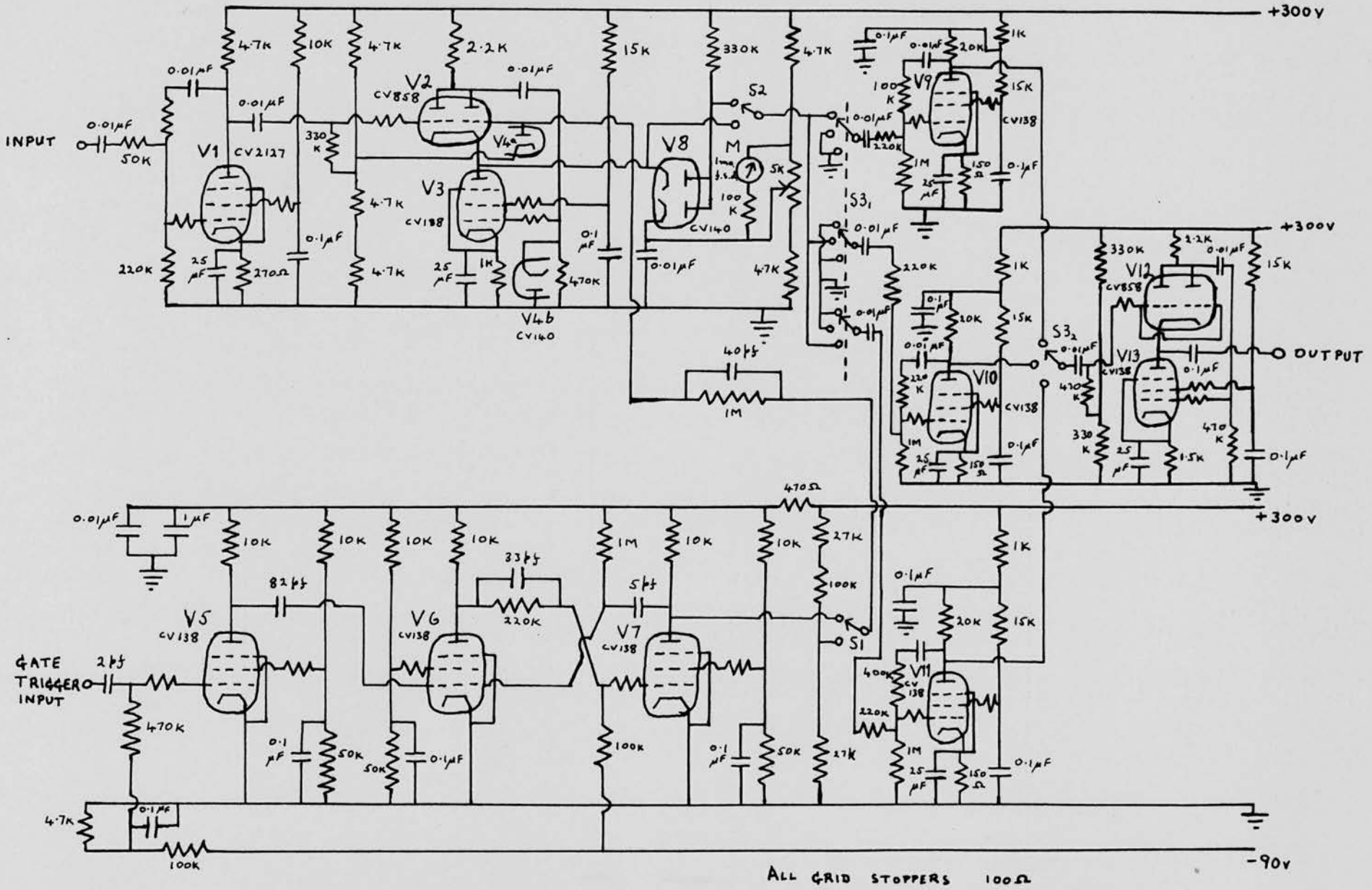


Fig. 13 Circuit of gate unit.

the feedback resistor. The cathode follower output stage consists of V12 and V13. The power requirements of the unit are, 180 m.a. at +300V, 2 m.a. at -90V, and 4.7 A at 6.3 V a.c. for valve heaters. The positive line is electronically stabilized and is provided by a Roband, type M35A subchassis power unit. The negative line is provided by a simple full wave rectifier circuit and is neon stabilized.

Testing the Gate Unit

Thorough testing was carried out using a type 1013C double pulse generator, which provided two independent outputs whose separation could be varied at will. Pulses of at least 5V were required to operate the gate, and the coincidence resolving time was measured as 5/us. A graph of the amplitude of the output from the unit against that of the input is shown in fig. 14a, from which the three values of overall gain, nominally 1, 2 and 3, were found to be 0.75, 1.4 and 2.5. The amplifiers are also shown to be linear for outputs of up to 40V, which is quite adequate. The working of the subtractor was checked and is illustrated in fig. 14b, in which output is plotted against input for four different subtractor settings, with the gain set to the nominal X1 position.

The Delay

A delay, variable in 1/us steps over the range 0 - 20/us, with a characteristic impedance of 100 $\Omega$ to match the input impedance of the N567 amplifier, was constructed to complete the slow coincidence system of fig. 9. It is a $\pi$ -type network, fig. 15, designed to have a cut-off frequency of 1 Mc/s.

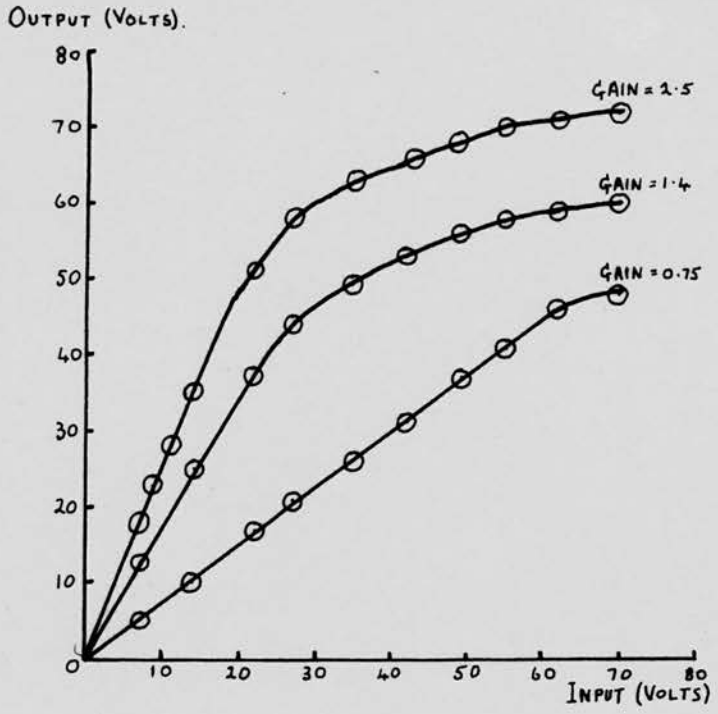


Fig. 14a. OUTPUT OF GATE UNIT PLOTTED AGAINST INPUT (SUBTRACTOR NOT IN USE).

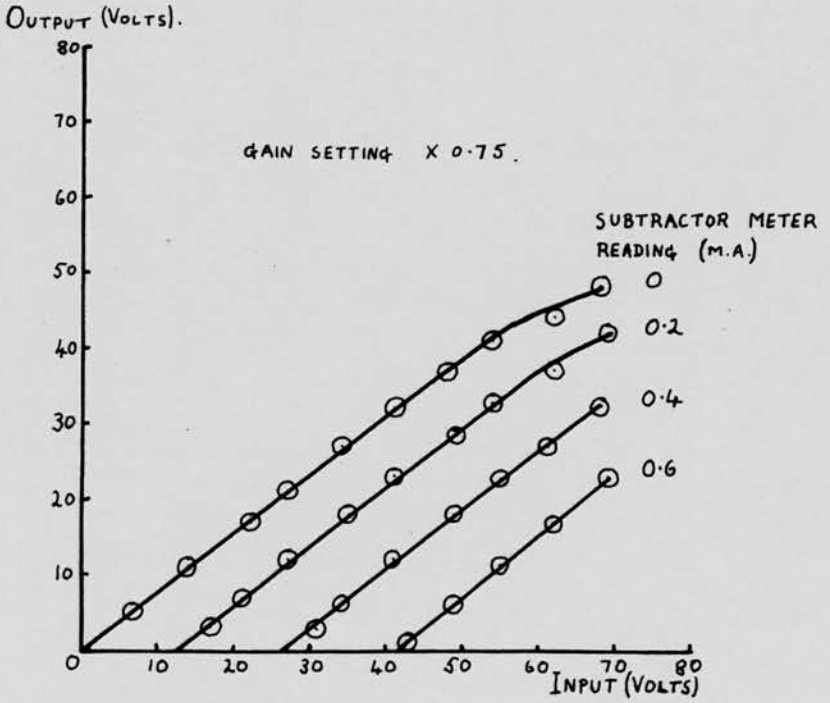


Fig. 14b. OUTPUT OF GATE UNIT PLOTTED AGAINST INPUT, WITH SUBTRACTOR IN USE.

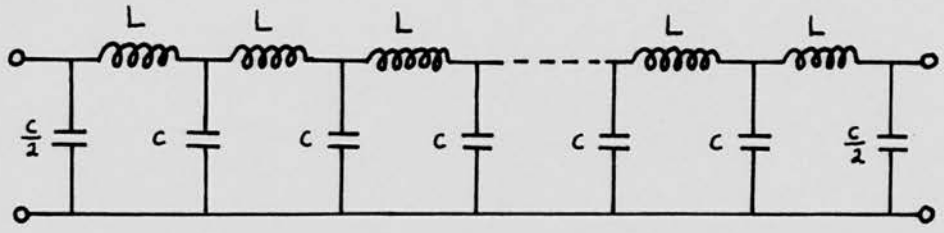


FIG. 15 DELAY NETWORK.

The characteristic impedance, $Z_o = \sqrt{\frac{L}{C}} = 100\ \Omega$ , (1),

the delay per section, $T_D = \sqrt{LC}$ ,

and the cut-off frequency, $f_c = \frac{1}{\pi\sqrt{LC}} = 1$ Mc/s.

$$\therefore\ T_D = \sqrt{LC} = \frac{1}{\pi} \times 10^{-6} \text{ secs.} \qquad (2)$$

(1) x (2) $\quad L = \frac{1}{\pi} \times 10^{-4} \approx 32\ \mu H.$

(2) ÷ (1) $\quad C = \frac{1}{\pi} \times 10^{-8} \approx 3{,}300$ pf. (nearest standard value)

Sixty sections were made, with tappings every three sections, which should give a total delay of 19 μs. The inductances consisted of 50 turns of 38 s.w.g. silk covered copper wire wound to form coils $\frac{1}{8}$" wide on $\frac{1}{2}$" diameter paxolin tube.

The total delay measured on an oscilloscope was 18 μs, 0.9 μs between adjacent tappings. The total attenuation was 11 db, 0.55 db between neighbouring tapping points.

Testing of Gate Unit with a $Co^{60}$ Source

The pulses from a single counter were fed into the gate unit, and used to trigger open the gate, so that they should all be passed to the kicksorter. The resulting spectrum, from a $Co^{60}$ source, is shown in fig. 16a, with a spectrum obtained in the same time with the gate held open, for comparison. From this it is clear that the gate opens quite reliably and that none of the coincident pulses were missed. The shift of about a volt due to the operation of the gate can be seen.

The slow coincidence system of fig. 11 was assembled and the single channel set to accept pulses from the 1.33 Mev $Co^{60}$ photopeak. The coincidence spectrum obtained is shown in

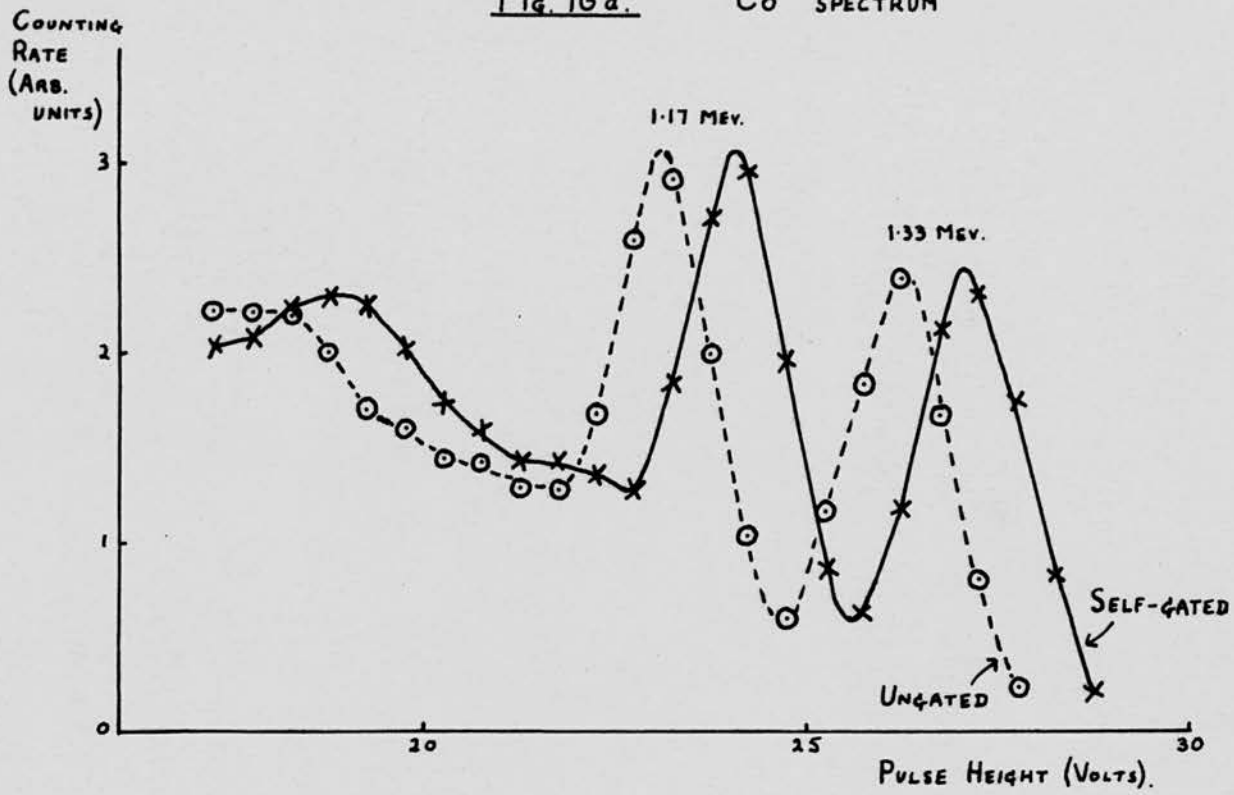
Fig. 16a. Co 60 spectrum
Counting Rate (Arb. units)
1·17 Mev.
1·33 Mev.
Self-gated
Ungated
0
1
2
3
20
25
30
Pulse Height (Volts).

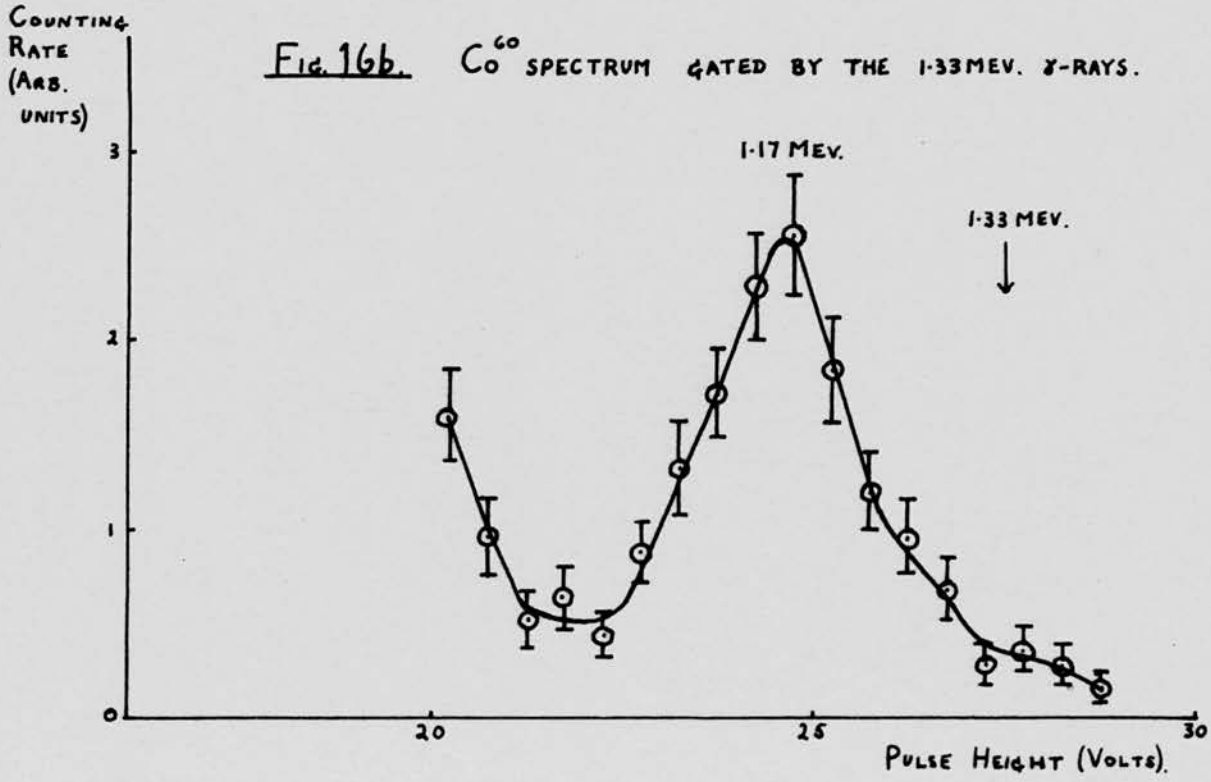
Fig. 16b. Co 60 spectrum gated by the 1·33 Mev. γ-rays.
Counting Rate (Arb. units)
1·17 Mev.
1·33 Mev.
0
1
2
3
20
25
30
Pulse Height (Volts).

fig. 16(b). It shows, as it should, only the 1.17 Mev $Co^{60}$ $\gamma$-ray.

3.2. Pulse Height Analysis

The counting rate in a coincidence spectrum is necessarily very much lower than in an ungated one, e.g. the curves in fig. 16a were each obtained in about half an hour, whereas fig. 16b took three and a half hours and the peak represents only 64 counts compared with several thousand in fig. 16a. Fig. 16b could have been obtained in only 12 mins. with a 60-channel kicksorter. The time required to scan the energy range of interest in a coincidence experiment on the $Be^9(d, n)B^{10}$ reaction using the 1074A five-channel kicksorter would be prohibitive; a multichannel kicksorter is necessary for a study of the kind proposed.

Proposals for a 30 Channel Kicksorter

An attempt was made to devise a system of pulse height analysis that could conveniently be built using transistors throughout, in order to benefit from the trouble-free operation claimed for semi-conductor devices. The kicksorter should have a minimum of preset controls to adjust in setting up, and for simplicity a fixed channel width of $\frac{1}{2}$V. The 30 channels should be capable of covering any desired 15V range between 0 and 60V, the limit of linearity of the type 1008 amplifiers available in the laboratory.

The obvious system of 30 independent discriminators with thresholds $\frac{1}{2}$V apart, was rejected as one would expect it to require a lengthy setting up procedure. This type of kicksorter, e.g. A.E.R.E. type 1091A, is no longer favoured by those with experience of them. Essentially the system proposed uses the same discriminator 30 times. A block diagram of the proposal is shown

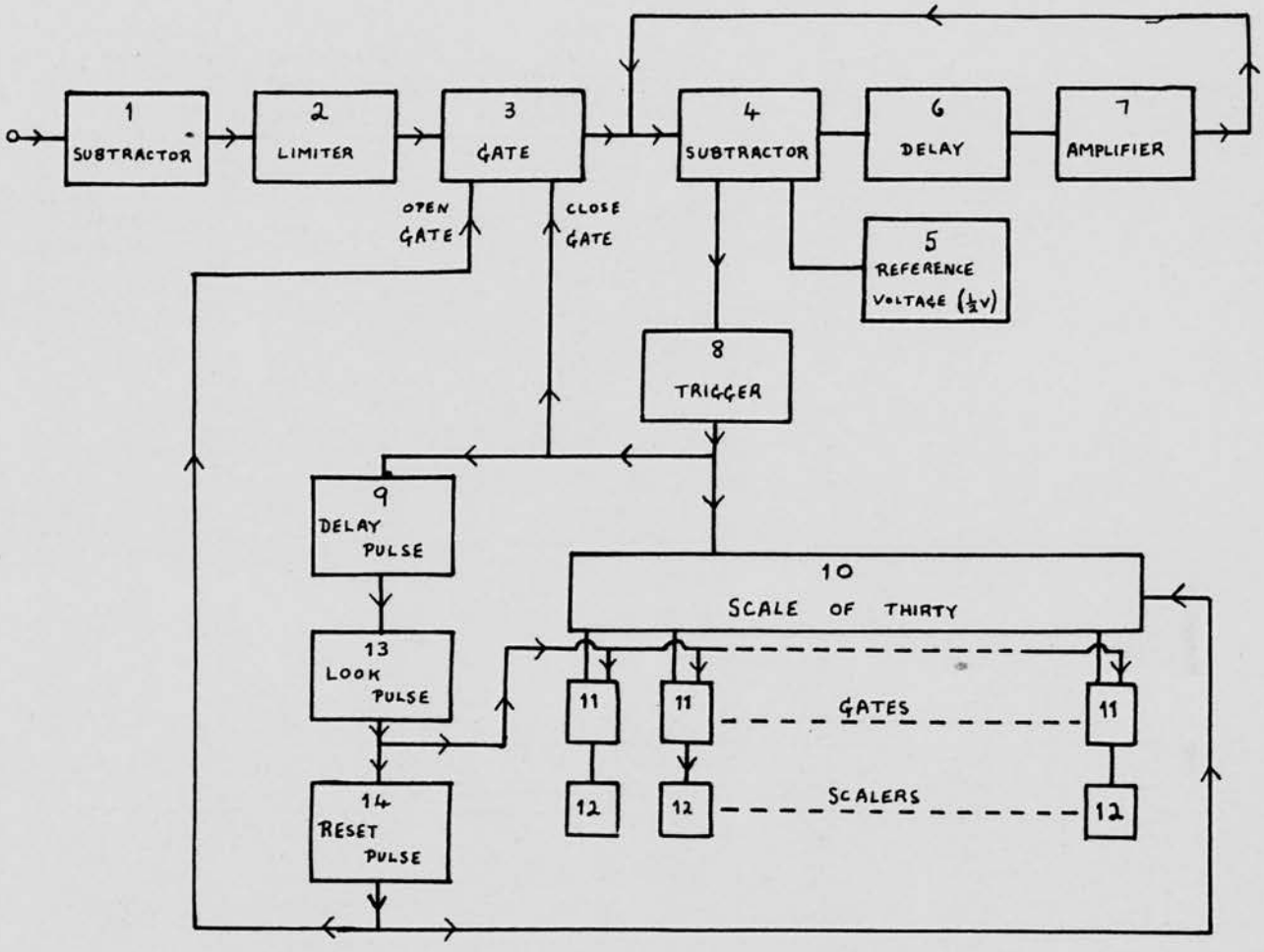


FIG. 17. PROPOSED SCHEME FOR A 30-CHANNEL KICKSORTER.

in fig. 17. The heart of the system is the loop of blocks 4, 6 and 7. The subtractor (4) removes $\frac{1}{2}$V, determined by reference voltage (5), from the bottom of a pulse applied to it, the top of the pulse being passed into the delay (6), which is made long enough for the subtractor to return to its quiescent state before this pulse reaches the amplifier (7), which serves only to compensate for the attenuation inevitably present in the delay. From the amplifier (7) the top of the original pulse is passed back into the subtractor and the process repeated until the pulse is reduced to zero. The height of the original pulse is determined by the number of subtractions performed. Each time a pulse enters the subtractor the sensitive trigger circuit (8) is fired and this passes a standard pulse into the scale of 30 (block 10) which counts the number of subtractions performed and indicates the pulse height by the stage which is left 'on' after the input pulse has been reduced to zero, fig. 18. This stage is used to gate a pulse, via block (11), into the appropriate scaling unit (12).

The subtractor (block 1) is to enable the 30 channel analysis to be performed in any 15V section of a 60V spectrum, i.e. it is to subtract any desired voltage between 0 and 45V from the input pulses. Block 2 limits all pulses at 15V. This ensures that no pulse makes more than 30 circuits of the loop of units 4, 6 and 7, and that the dead time of the instrument need only be 30 times the length of delay (6). The limiter (2) also causes all pulses above the range of the analyser to be recorded in the 30th channel, a facility of some help in determining the desired portion of a

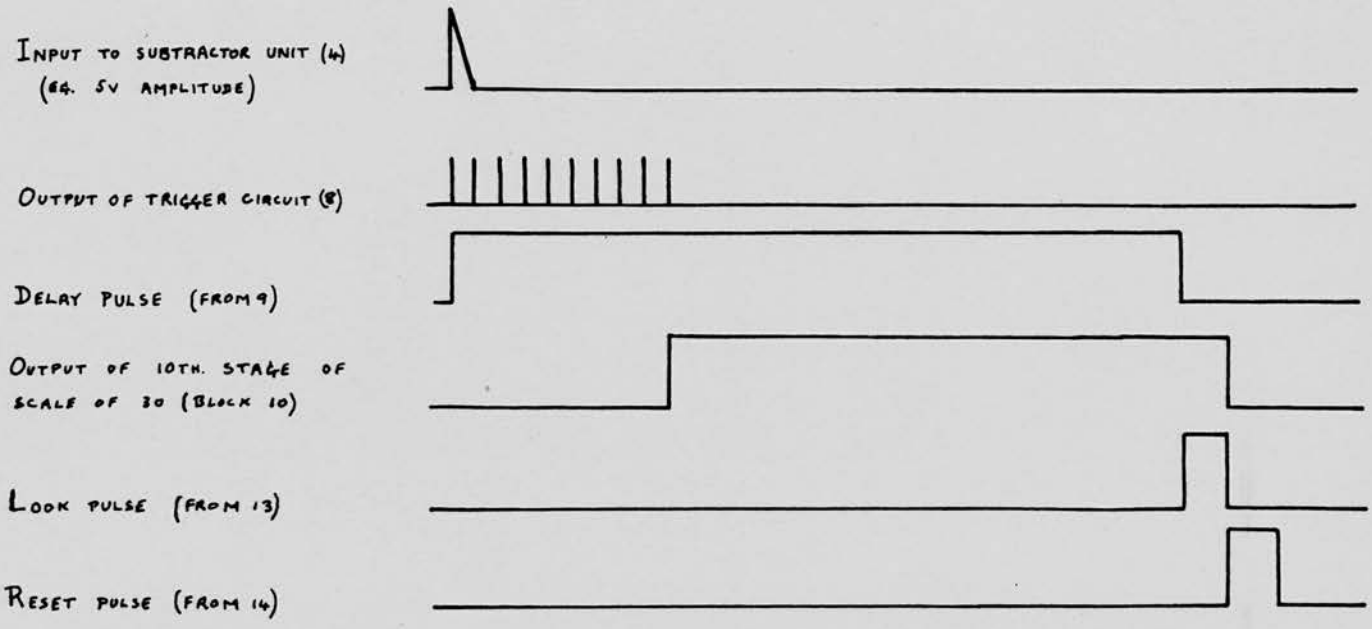


FIG. 18. RELATIONSHIP IN TIME OF SOME OF THE PULSES OCCURING IN THE PROPOSED 30-CHANNEL KICKSORTER.

spectrum for analysis. The gate (3) is closed when a pulse has entered the instrument and remains closed until the pulse has been disposed of. The trigger circuit (8), as well as feeding standard pulses into the scale of thirty (10), closes the gate (3) and triggers the delay pulse generator (9) on the entry of each new pulse into the analyser (fig. 18). Block (9) produces a pulse of length 30 x (length of delay 6). By the time the trailing edge of this pulse is produced, the scale of thirty (10) is in a steady state indicating the channel in which a count should be registered. This trailing edge produces a 'look' pulse in unit (13) which is passed through one of the gates (11) into the appropriate scaler (12). A reset pulse is then produced in (14) which sets the scale of thirty (10) to zero and opens the gate (3), after which another pulse can be measured.

It seems possible that the delay (6) could be about 10/us, giving a dead time of 300/us. Thus the instrument should be capable of sorting 3,000 regularly spaced pulses per sec. and scalers consisting of a dekatron followed by a mechanical register should be adequate. The proposals are limited to thirty channels because a larger number would require the transistorized units (3) and (7) to handle linearly pulses in excess of 15V, which would probably be difficult to achieve. Also the delay (6) will have to be of very good quality to enable a pulse to be passed through it 30 times without introducing excessive distortion.

To build such an instrument would require the investigation of the properties of the basic transistorized circuits involved, and in the final stages of the project the construction of a considerable amount of circuitry. Thorough testing would have

to follow before the kicksorter could be used with confidence in an experiment. The project was therefore too large to fit into this investigation; but work on it is proceeding in this laboratory, with the aid of a grant from the Paul Instrument Fund.

### 3.3. Use of Sunvic, Hutchinson-Scarrott type, Kicksorter

For the present work it was decided to use the department's Sunvic (Mk. I) pulse height analyser. This was situated in a laboratory about 150 yds. from the H.T. set and it was necessary to feed pulses along a coaxial cable to it. The low impedance of the cable, 69Ω, loaded even a cathode follower output stage to such an extent that pulses larger than a volt or two were severely distorted. This was overcome by the simple expedient of including a 2.2 KΩ resistor in series with the cable, fig. 19, at the output of the gate unit. This attenuated the pulses considerably and an amplifier was required at the end of the cable, before the kicksorter. Pulses of up to 30V at the output of the gate unit were reduced by the 2.2 KΩ resistor to under $\frac{1}{2}$V on the cable and were thus small enough to be fed into a standard type 1008 amplifier, which had its time constants set so as to have a minimum effect on the pulse shape, i.e. the time constant of integration at a minimum, 0.15 μs, and of differentiation at a maximum, 1.5 m.s.. The system was tested using sources and the spectra obtained in this way were in all respects as good as those already obtained with the five channel kicksorter.

### 3.4. Fast-Slow Coincidence System

To obtain an appreciably shorter resolving time than is possible with the simple slow coincidence arrangement of fig. 11, the so-called "fast-slow" system of fig. 20 is required.

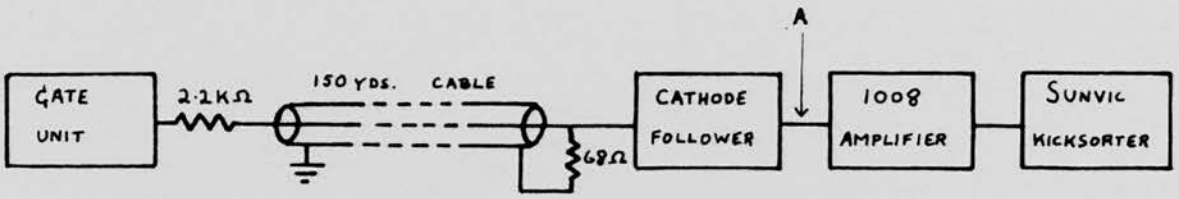


FIG. 19. METHOD USED TO FEED PULSES TO THE SUNVIC KICKSORTER. AN ATTENUATOR, VARIABLE IN ½ DB. STEPS, WAS INCLUDED AT A TO PROVIDE A FINE GAIN CONTROL.

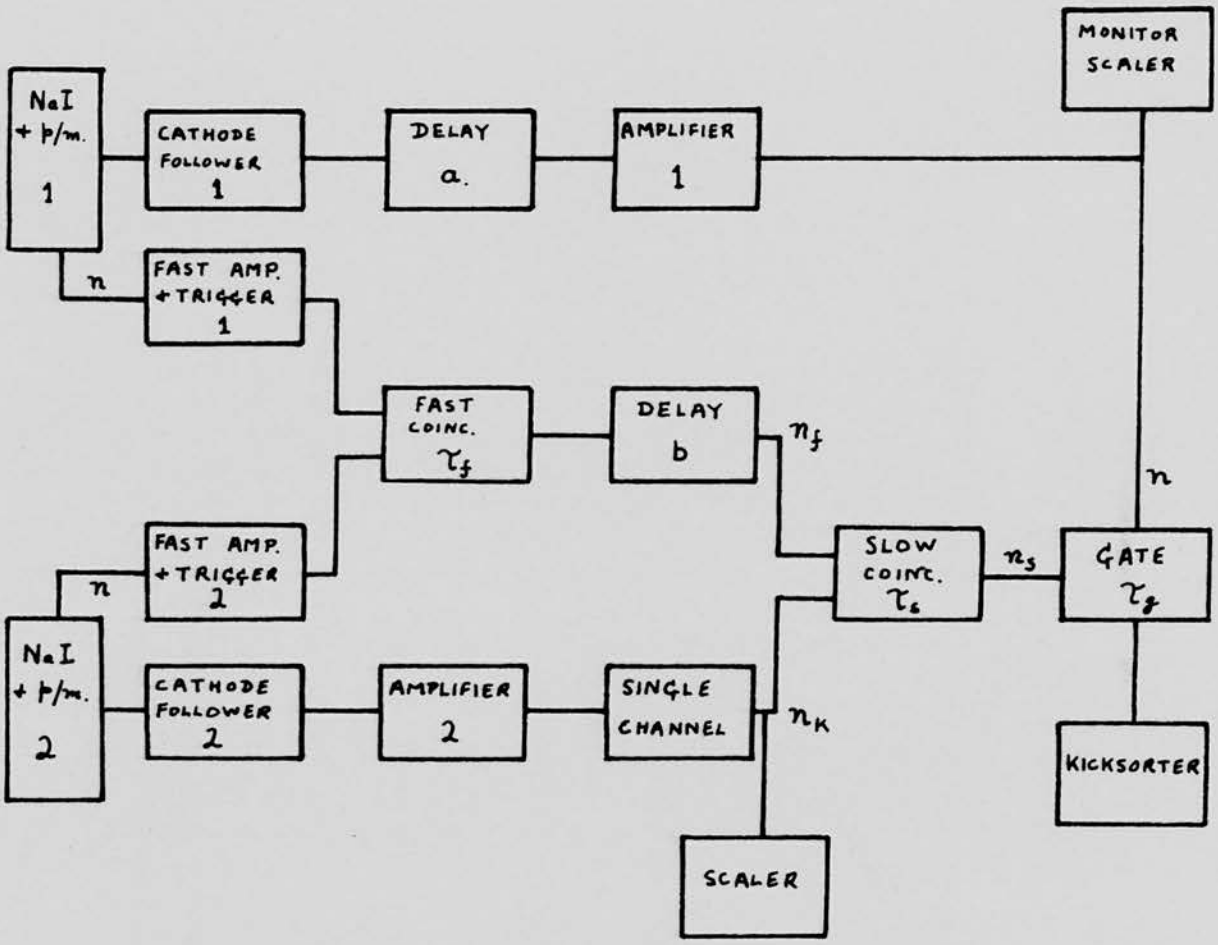


FIG. 20. FAST - SLOW COINCIDENCE SYSTEM.

Coincident events in counters 1 and 2 are selected by the fast coincidence unit, with a resolving time of about $10^{-8}$ sec. As the aim is to obtain a spectrum of the pulses from counter 1 that are in coincidence with $\gamma$-rays of a particular energy in counter 2, not all the coincident events are of interest. The single channel selects the pulses from counter 2 that correspond to $\gamma$-rays of the desired energy. Thus a coincidence between the single channel output and the fast coincidence output indicates an event of the kind sought, and causes the gate to open, allowing the delayed pulse from counter 1 into the kicksorter.

To use a fast coincidence unit a sharply rising pulse is required from the photomultiplier, which means that it must have a sufficiently high gain to cause the fast trigger circuit to fire when the first few photoelectrons are emitted from the photocathode. When the multiplier is operated at a high gain its last few stages will saturate and the size of the output pulse will no longer be proportional to the energy of the $\gamma$-ray that causes it. This prevents energy selection from being included in the fast circuitry. The photomultiplier output for use in spectroscopy must be taken from an early dynode, which does not suffer from any saturation effects. The unit that selects coincidences between the single channel and fast coincidence outputs need not have a particularly short resolving time, as the counting rates in this part of the system are much lower than at the photomultiplier outputs. The variable delays a and b are adjusted as required to compensate for any delays introduced in the circuitry.

Fast Coincidence Unit

A fast coincidence unit, with a resolving time of 20 m/us, and associated fast amplifiers and trigger circuits were built to the design of Collinge, Marrison and Eccleshall[22], with slight modification based on the information in Fisher and Schute[23]. The latter authors described a system using NaI crystals and 14-stage E.M.I. photomultipliers, in which the pulses for spectroscopy are taken from the 9th dynode and the "fast" pulses are taken from the anode. As it was decided to adopt a similar arrangement of 14-stage photomultipliers the gain of the amplifier section of the circuit described in ref. 22 would be unnecessarily high and the first stage of amplification was omitted. A type CVX2276 valve, which could not be obtained readily, was replaced by an EFP60 with appropriate alteration of operating voltages. The variable delay, b in fig. 20, was included after the fast coincidence circuit, with a cathode follower at the output. An amplitude discriminator is included in the design of ref. 22 which can be set to prevent the trigger circuit from being operated by photomultiplier noise and pulses too small to be of interest in an experiment.

Fast Amplifier, Discriminator, and Trigger Circuit

The circuit of this part of the unit, two of which were required, is shown in fig. 21. V1, a secondary emission pentode, amplifies the negative-going pulse from the photomultiplier. The positive amplified pulse is fed by the cathode follower V2a, to the diode discriminator, D1 and D2. The backbias across D1 is the difference between the potential of the slider of VR1 and that of VR2, applied via the cathode followers V2a and V2b respectively.

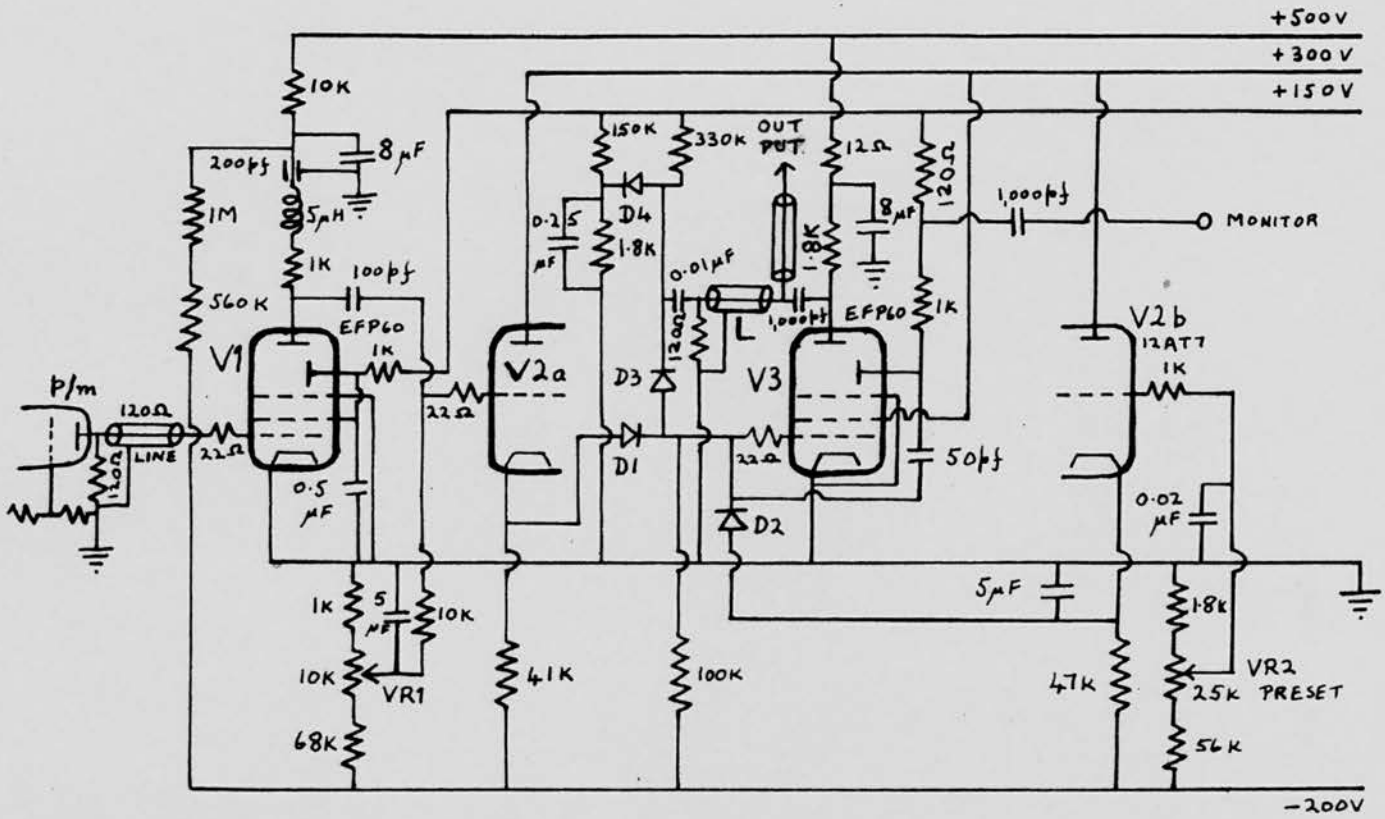


L – 2 METRES OF 120Ω CABLE (10 m μs).

Fig. 21. Circuit of fast amplifier and trigger circuit.

After passing the discriminator the pulse reaches the control grid of V3, a secondary emission pentode connected as a trigger circuit. The valve is normally cut off. A positive-going change of control grid potential causes it to start conducting, the changeover being assisted by feeding the amplified positive step produced at the dynode back to the control grid. The negative voltage step produced at the anode proceeds along the cable L and on reaching the end is fed through the diode D3 to the control grid, cutting the valve off regeneratively because of the dynode-to-grid coupling. The length of the pulse produced is determined by the length of the cable L. To prevent continuous oscillation the diodes D3 and D4 are biased in such a way that the positive-going change produced at the anode when the valve is switched off does not reach the control grid after passing along the delay L, but is short-circuited to earth through D4 and the 0.25/uF condenser in series with it.

The pulse from V3 anode is fed to the coincidence mixer.

Coincidence Mixer

The circuit of the mixer is shown in fig. 22. The output of one trigger circuit is connected to the anode of D1, and that of the other to the anode of D2. These two diodes form the actual mixer circuit. A pulse from a trigger circuit cuts off its associated diode, producing a signal across the common cathode resistor which is small when one diode is cut off, but is much larger when both diodes are cut off at the same time. The bias applied to the discriminator, D3 and D4, by the cathode follower V1, is set to pass only the pulses that correspond to coincidences. The pulses that overcome the discriminator bias are fed through a

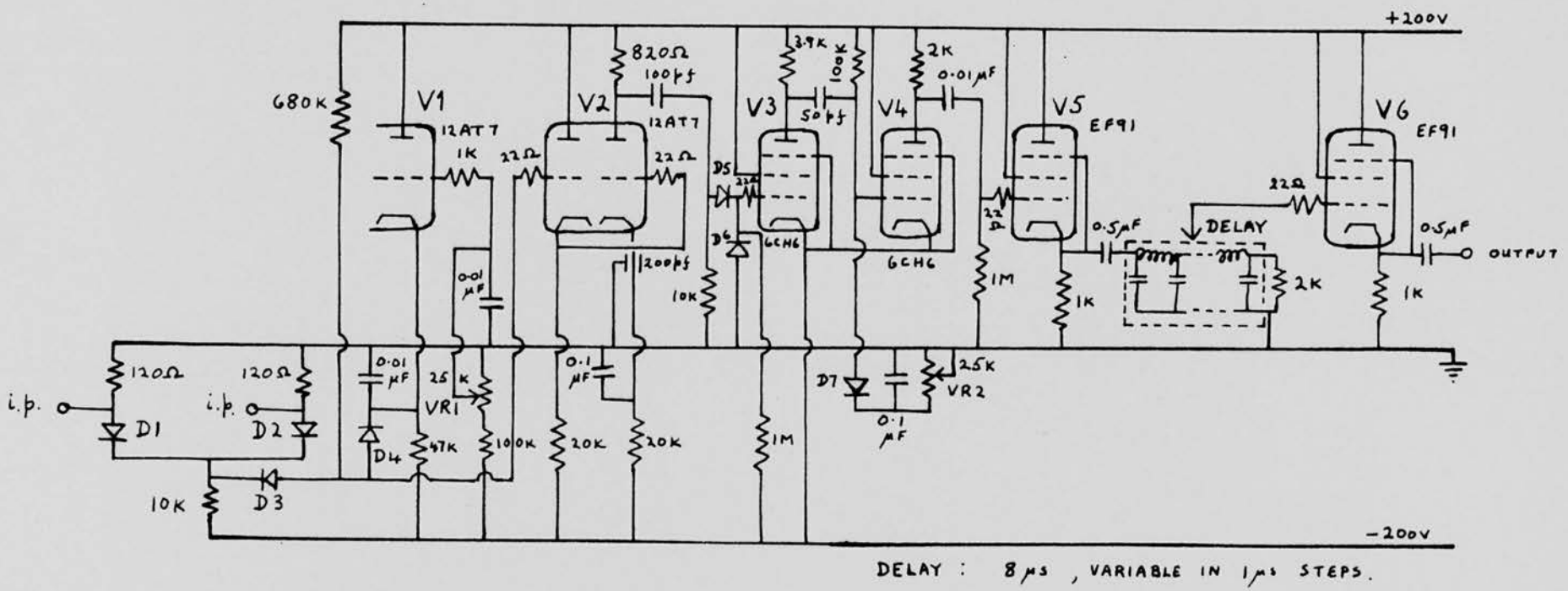


Fig. 22 Circuit of fast coincidence mixer.

cathode follower and an amplifier (the two sections of V2) to a trigger circuit, V3 and V4, that provides a standard pulse 1 μs long. A cathode follower, V5, couples the trigger circuit to a delay network whose delay is variable in 1 μs steps from 0 to 8 μs. V6 and the associated components form a cathode follower output stage.

Power Supplies

All the positive H.T. lines are obtained from the +500V line via dropping resistors and neon stabilizers. The +500V, 170 m.a. supply is obtained from a Solartron power unit type SRS151, and the -200V, 100 m.a. supply from a simple neon stabilized full wave rectifier system.

Testing the Fast Coincidence Unit

The complete fast coincidence unit was tested with a pulse generator, type 1147A, which provided two outputs whose separation could be varied accurately; it was found to have a sharply defined resolving time of 20 m μs.

3.5. Counter Heads with 14-stage Photomultipliers

Two identical counter heads were constructed. The crystal and photomultiplier assembly was contained in a light tight brass tube, with a thin aluminium plate covering the crystal end and a brass plate the other end. Threaded rods fixed to the brass end plate carried a brass ring on which the photomultiplier base was mounted, and two paxolin rings which held the photomultiplier and crystal securely in place, as shown in fig. 23. In this way the crystal, photomultiplier and associated components can be easily removed from the brass tube when required, e.g. for alteration of the dynode resistor chain. The resistors were mounted between the

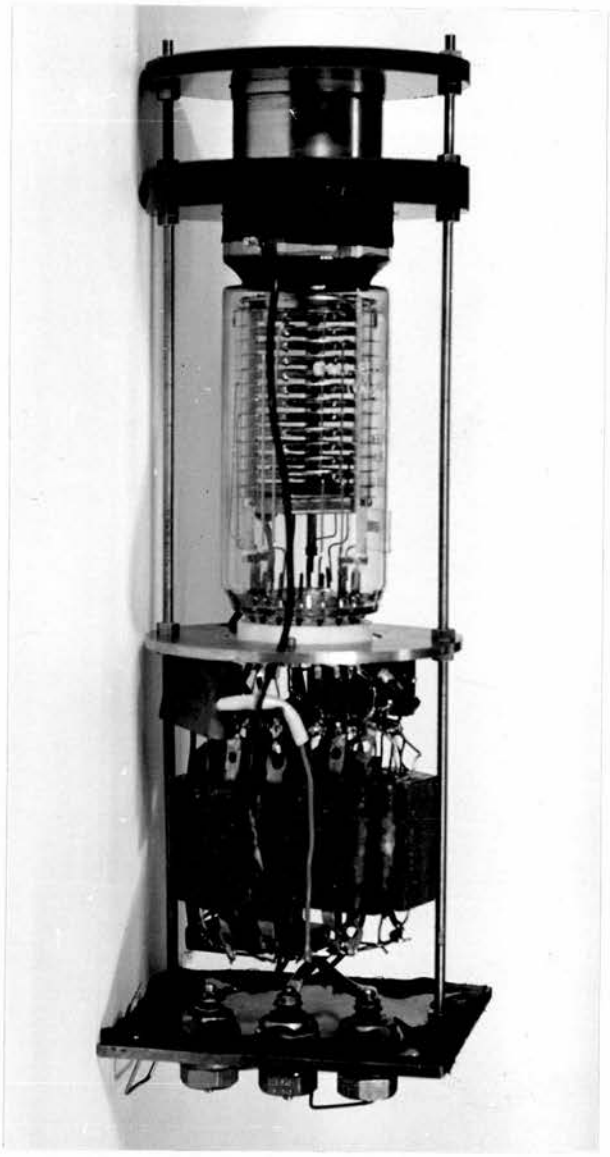

Fig. 23. THE PHOTOMULTIPLIER AND CRYSTAL MOUNTING.

tags on two switch wafers, not directly to the photomultiplier holder. This enabled alterations to the dynode chain to be made very quickly, as it was not necessary to apply a soldering iron to the connections on the photomultiplier holder itself and the tube could safely be left in place. By means of two screws on the brass tube the counter head could be clamped to an aluminium plate in any of a large number of preselected positions around the target, fig. 24. It was found necessary to fix a block of lead between the two crystals to eliminate coincidences due to scattering of $\gamma$-rays from one crystal to the other.

E.M.I. type 6262B 14-stage photomultipliers were used. The pulses for energy determinations were taken from the 9th dynode and those for operating the fast coincidence unit from the anode. A dynode resistor chain that seemed likely to give the required outputs with an overall voltage of about 1.5 KV was assembled and tested with Cs, Co and Th sources to ensure that the pulses from the anode could operate the fast coincidence unit, and that the output from the 9th dynode was proportional to the $\gamma$-ray energy and exhibited good resolution. The chain was adapted until both conditions were satisfied, resulting in the arrangement of fig. 25. Adequate decoupling of the resistor chain was found to be a very important factor in obtaining a linear response from the 9th dynode. The resolution depended on the value of E.H.T. applied to the photomultiplier. The ratio of counting rate on the higher energy Co peak to the counting rate in the valley between the two peaks was used as a sensitive test of the resolution to find the best value of E.H.T. for each photomultiplier. The result, for both counters, is shown in fig. 26, the best resolution being obtained at 1.4 KV

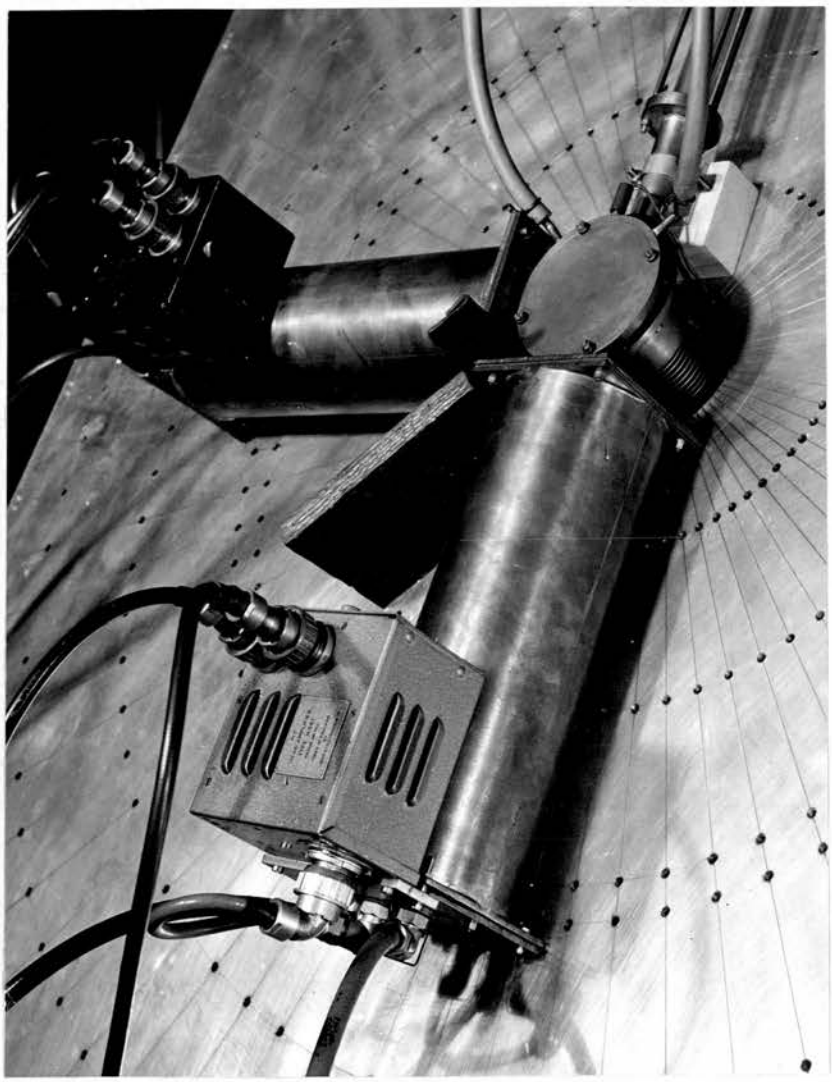

Fig. 24. THE COUNTER HEADS MOUNTED BESIDE THE TARGET HOLDER.

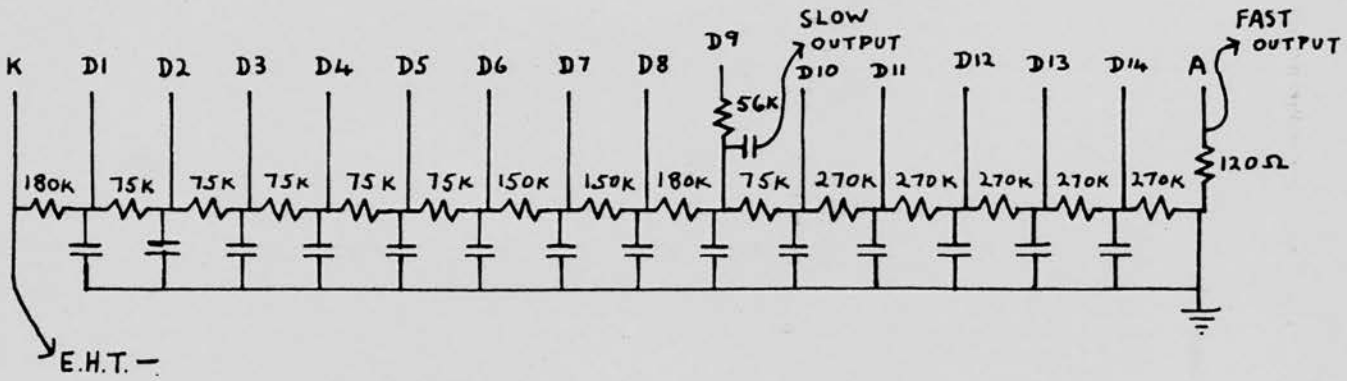


ALL CAPACITORS 0·01 μF

Fig. 25. DYNODE RESISTOR CHAIN USED WITH 14-STAGE PHOTOMULTIPLIERS.

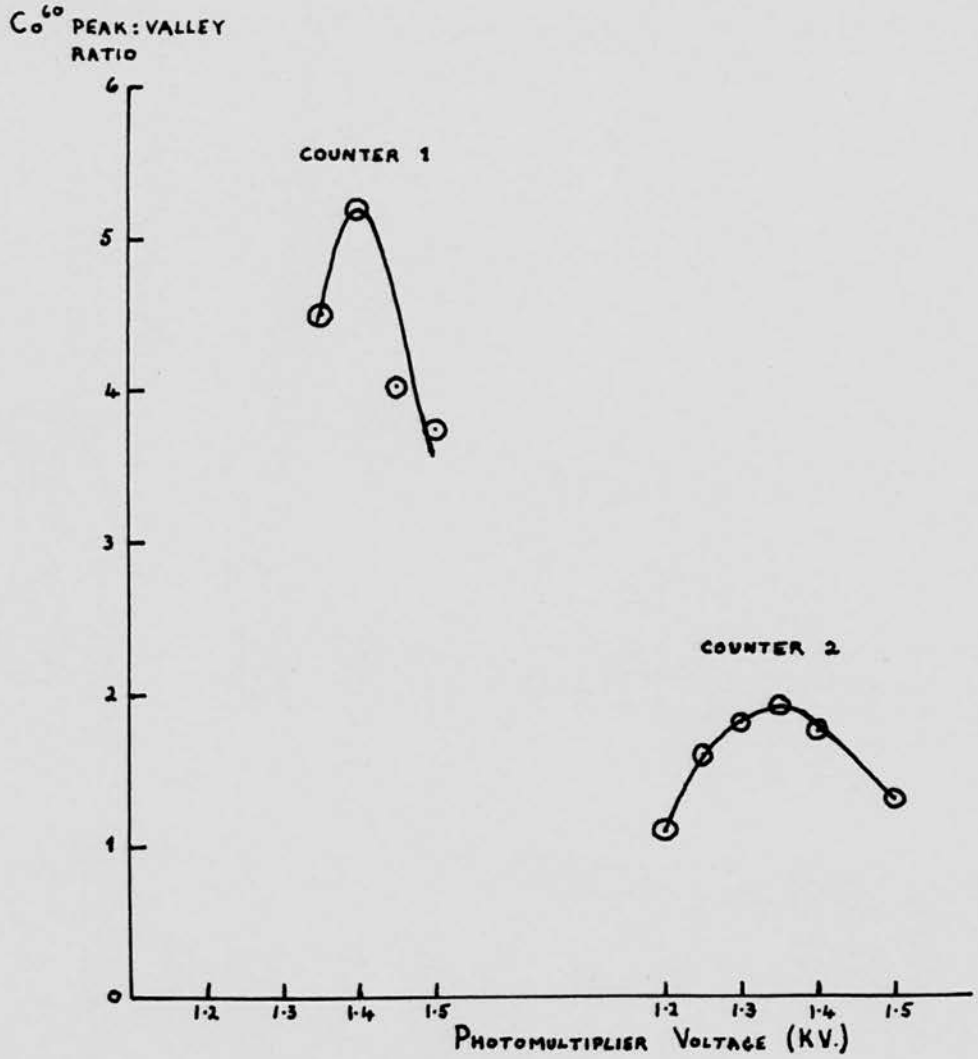


Fig.26. $Co^{60}$ PEAK : VALLEY RATIO AS A FUNCTION OF E.H.T., FOR BOTH COUNTERS.

for counter 1 and at 1.35 KV for counter 2. Spectra from both counters of Cs, Co and Th $\gamma$-rays are shown in fig. 27. The performance of the counters is summarised in the table below. The figures quoted for the crystals by the manufacturer are given for comparison.

Performance of the Counters

| | Counter 1 | | Counter 2 | |
|---|---|---|---|---|
| | Observed | Quoted by manufacturer | Observed | Quoted by manufacturer |
| Best E.H.T. | 1.4 KV | | 1.35 KV | |
| Co peak : Valley ratio | 5 : 1 | 3.7 : 1 | 1.9 : 1 | 2 : 1 |
| Resolution to Cs | ~9% | 8.4% | ~10% | 9.75% |

Testing of Fast Coincidence Unit with the Counters

In devising the dynode resistor chain described above the only check on the nature of the fast output pulses from the photomultiplier anode was that they should fire the fast trigger circuit. An oscilloscope capable of showing the rise time of the fast pulses was not available so it was necessary to ensure that these pulses were sharp enough to cause reliable triggering with as good a resolving time as was measured with the pulse generator. The resolving time was obtained by inserting a variable delay, consisting of 1 metre lengths of coaxial cable, giving 5 m/us delay per metre, between one of the counters and the fast coincidence unit, and finding the variation in coincidence rate with delay when a Co source was placed between the two counters, fig. 28. Ideally the coincidence rate should be constant until the delay is equal to the resolving time, after which it should be zero. Fig. 28 shows

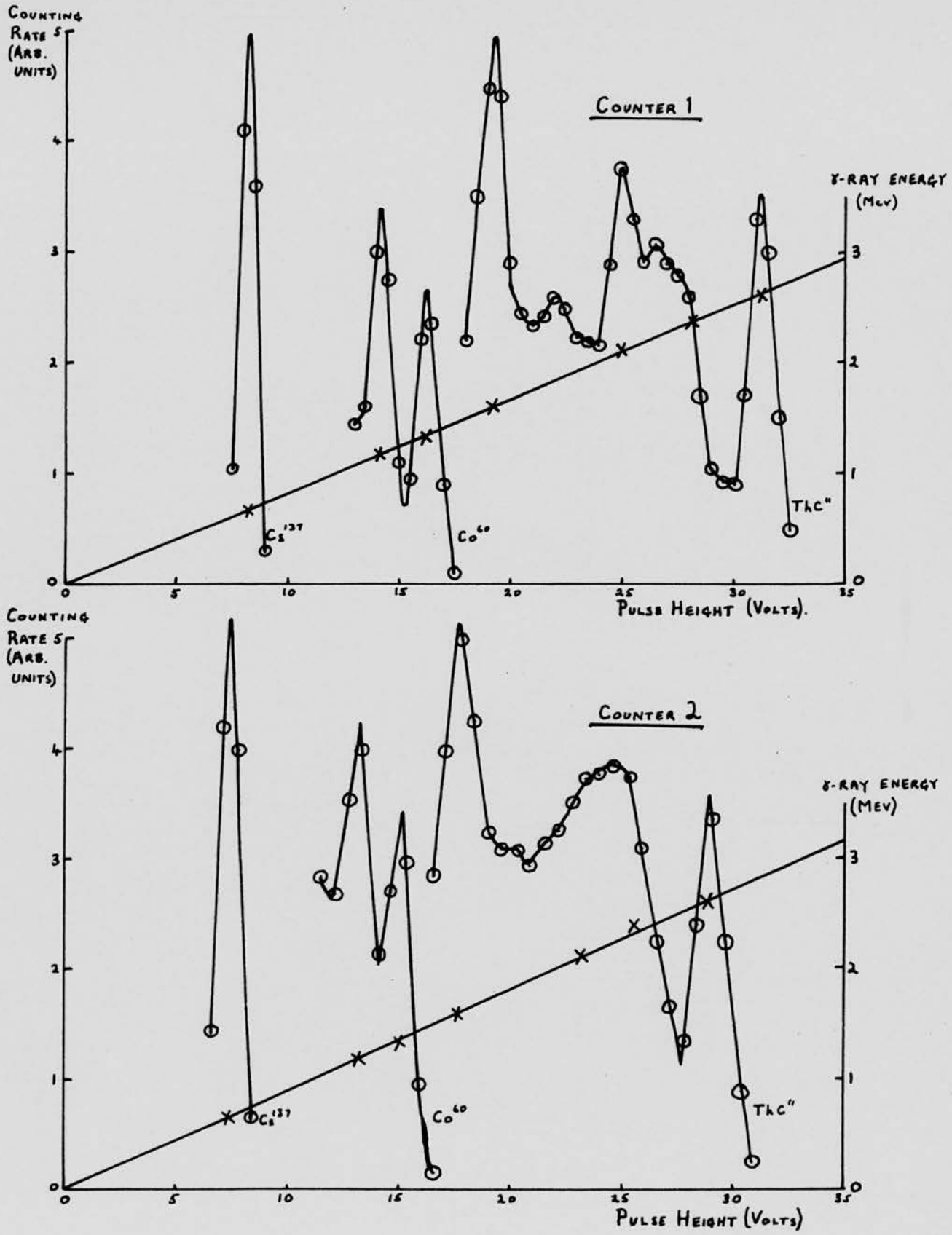


FIG 27. $Cs^{137}$, $Co^{60}$ AND ThC" SPECTRA.

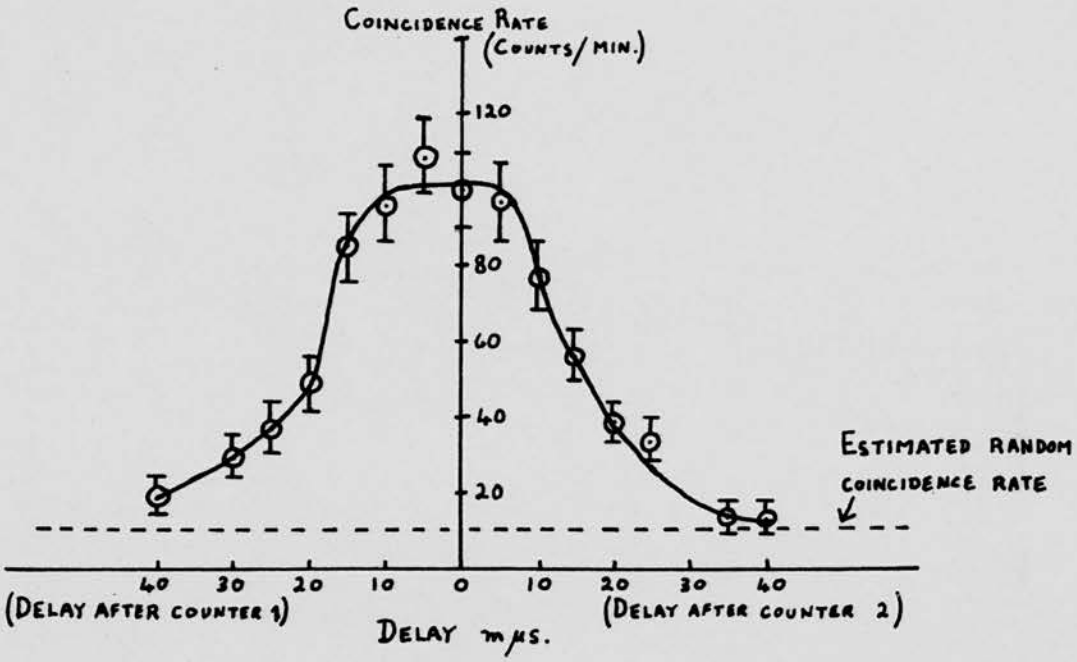


FIG. 28. COINCIDENCE COUNTING RATE AS A FUNCTION OF DELAY, DEMONSTRATING THE RESOLVING TIME OF THE FAST COINCIDENCE UNIT.

a resolving time of about 20 m/us, but the drop in the coincidence rate is not very sharp. By repeating the process with the pulse generator in place of the counter heads and still varying the delay by means of the cable delay-box a similar slow drop in coincidence rate was observed, in contrast with the reasonably sharp cut off found when using the double pulse generator directly. From this it was concluded that the poor appearance of fig. 28 is due mainly to the method of obtaining the variable delay.

There should be a small coincidence counting rate for all values of delay due to random coincidences. The random rate is $N_R = 2\tau N_1 N_2$, where $\tau$ is the resolving time and $N_1$ and $N_2$ are the counting rates in the two counters - each $2 \times 10^3$ per sec. in this case. Thus, $N_R = 2 \times 2 \times 10^{-8} \times 4 \times 10^6 = 16 \times 10^{-2}$/sec. or 9.6/min, as shown by the dotted line in fig. 28.

Testing the Fast-Slow Coincidence System with the Counters

The only unit required at this stage to complete the fast-slow coincidence system of fig. 20 was the slow coincidence unit, and for this a type 1036A coincidence unit, with its resolving time set at 2/us, was used.

First the efficiency of the electronic system was investigated by feeding pulses from one counter into both sides of the coincidence system, with the single channel replaced by a discriminator set at 5V (a switch for this purpose was provided in the single channel analyser used, Dynatron type N/101). In this way each pulse should gate itself into the kicksorter. The self-gated spectrum so obtained was distinguishable from the normal ungated one only by the small voltage shift introduced by the gate, indicating that no coincident pulses were missed.

While the system was connected in this way the discriminators in the fast coincidence unit were adjusted to reject all pulses smaller than those produced by 200 kev $\gamma$-rays, as they were too small to be of interest in the proposed experiment.

The complete system was finally arranged as in fig. 20 and set to gate on the 1.33 Mev, Co $\gamma$-rays. The spectrum in coincidence with this is shown in fig. 29, with an ungated Co spectrum for comparison. The coincidence spectrum has the shape due to $\gamma$-rays of a single energy 1.17 Mev, with, at 1.33 Mev, only a very small random contribution.

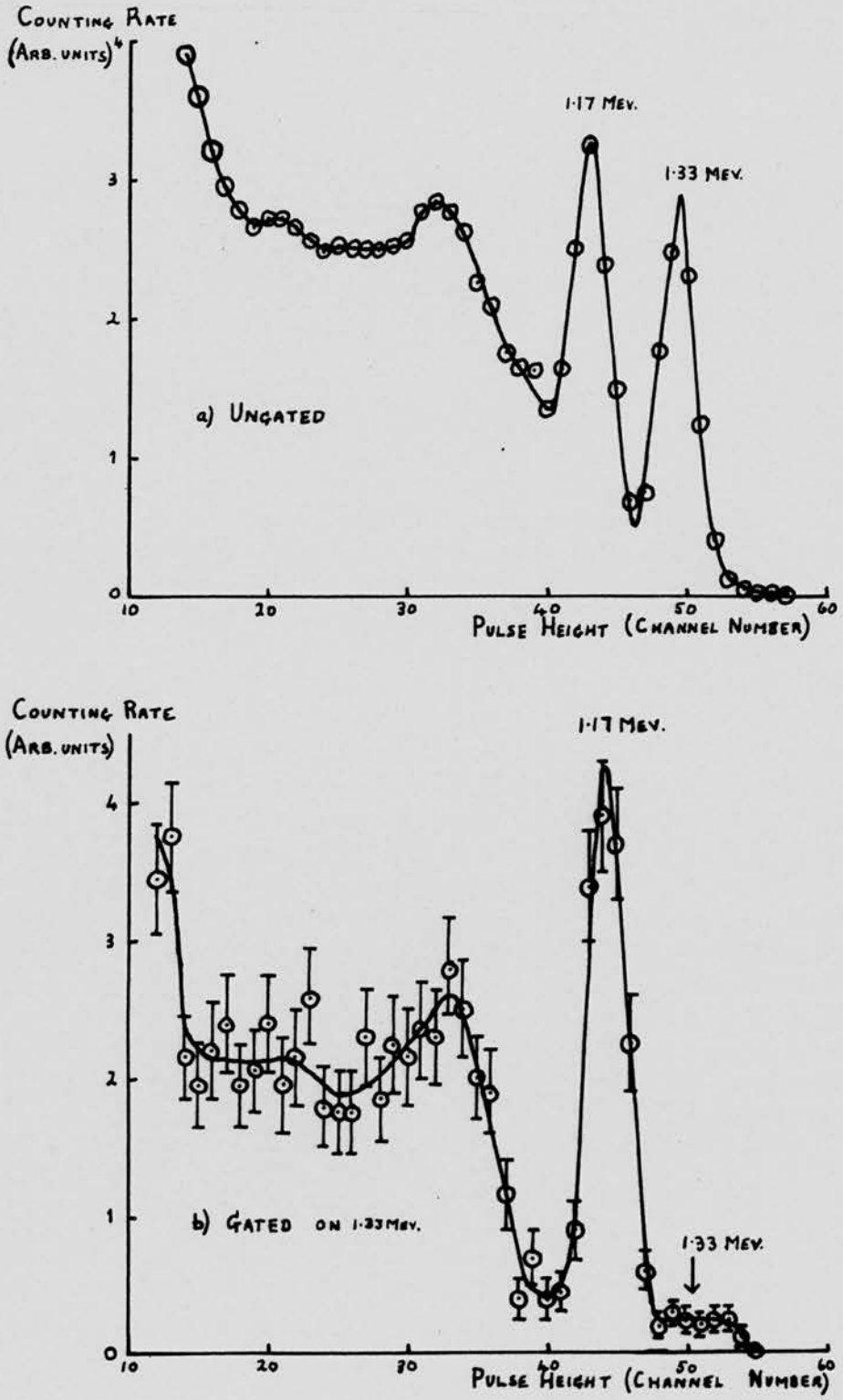


FIG 29. SPECTRA OF $Co^{60}$ $\gamma$-RAYS a) UNGATED

b) GATED ON THE 1·33 MEV PEAK (NOTE SMALL SHIFT DUE TO OPENING OF GATE).

# CHAPTER 4.

## EXPERIMENTAL METHOD.

In the experiment on the $B^{10}$ γ-ray cascades the fast-slow coincidence apparatus, described in sections 3.4 and 3.5, was used in conjunction with the Sunvic 80-channel kicksorter, as in section 3.3.

### 4.1. Choice of Cascades for Study

The γ-rays that might be found in the six possible gated spectra if a level existed near 2.86 Mev. are discussed below (see fig. 30).

Spectrum in Coincidence with 0.72 Mev

γ-rays of energies 0.41, 1.02, 1.43 and 2.86 Mev are to be expected in coincidence with 0.72 Mev according to the work of Shafroth and Hanna[16]. The possible γ-rays to or from a level near 2.86 Mev in coincidence with 0.72 Mev would have energies of about 0.7, 1.1, 2.1 and 2.9 Mev (fig. 30), although all of these need not occur. As at least two of the possible γ-rays from the 2.86 Mev level could be distinguished from the expected γ-rays from the well established levels, this would seem to be a coincidence spectrum worth investigating.

There are certain practical advantages in obtaining this spectrum. The single channel in the fast-slow coincidence system of fig. 20 has to be set on the full-energy peak of the 0.72 Mev γ-rays. This can be done quite accurately and easily as the 0.72 Mev peak is the strongest in the ungated spectrum (fig. 31). The peak efficiency of a scintillation counter, i.e. the probability that a γ-ray of given energy striking the scintillator will produce a pulse landing in the full-energy peak, drops rapidly with

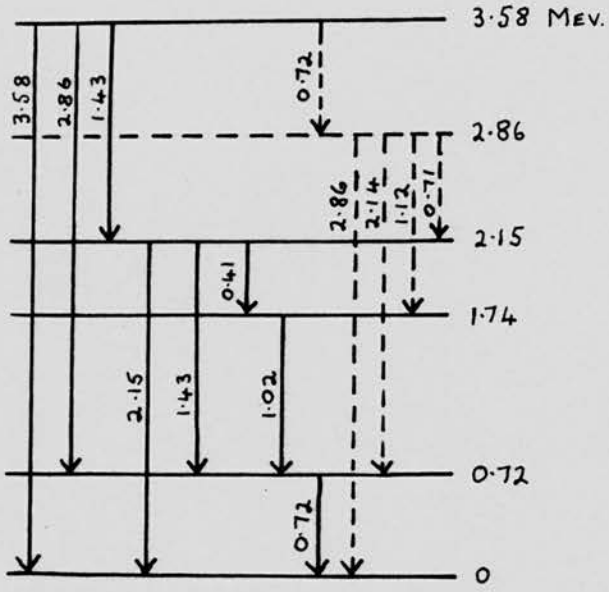


Fig 30. $B^{10}$ DECAY SCHEME SHOWING $\gamma$-RAYS THAT COULD ARISE FROM A LEVEL AT 2·86 MEV.

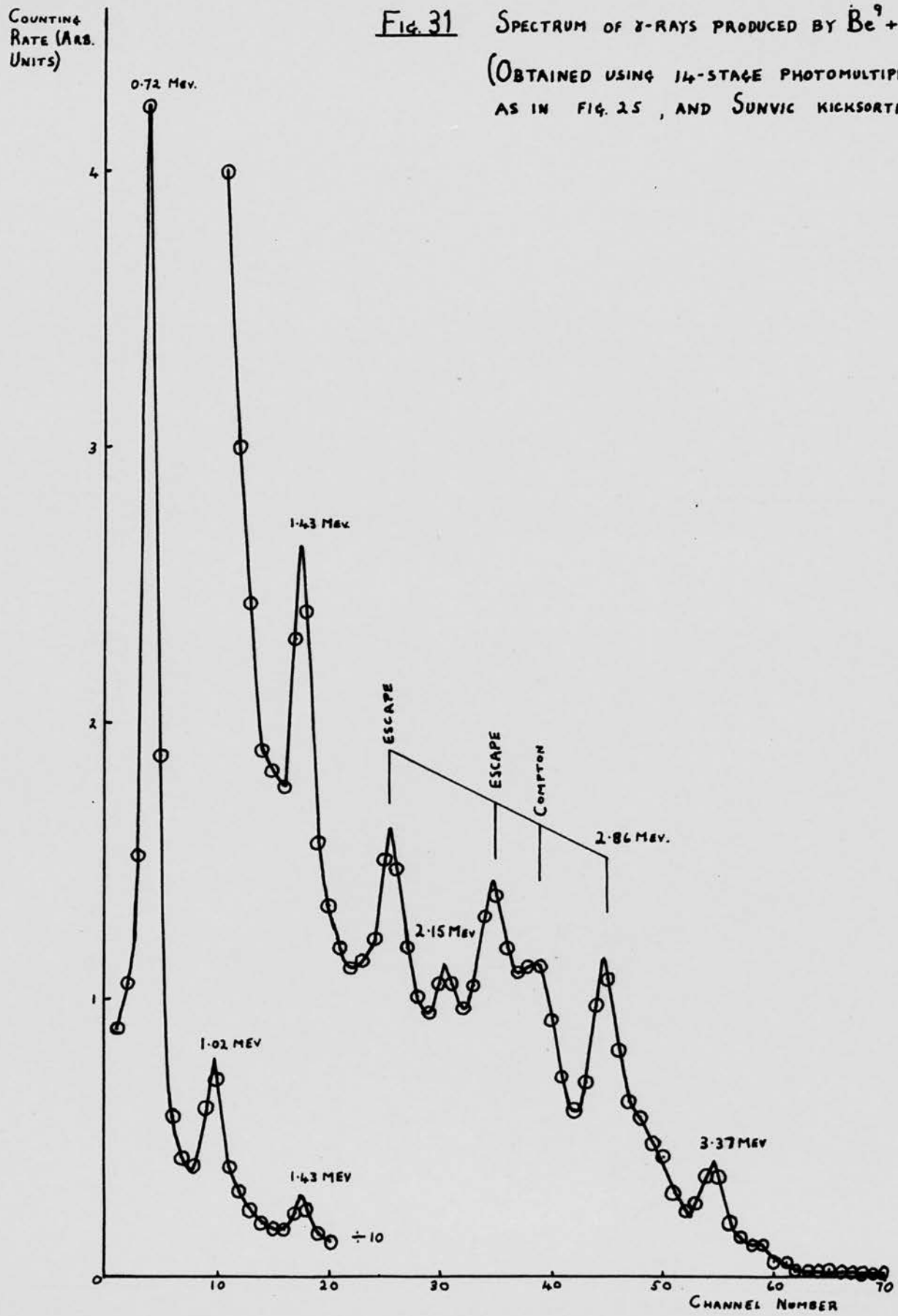


FIG. 31 SPECTRUM OF γ-RAYS PRODUCED BY $Be^9 + d$.
(OBTAINED USING 14-STAGE PHOTOMULTIPLIER AS IN FIG. 25, AND SUNVIC KICKSORTER).

increasing $\gamma$-ray energy. (Curves for NaI crystals are given in Lazar, Davis and Bell[24]). This means that the coincidence efficiency will be greater when gating on 0.72 Mev than in any other case, except that of the 0.41 Mev $\gamma$-ray.

Spectrum in Coincidence with 1.02 Mev

The well established levels should give rise to 0.41, 0.72 and 1.43 Mev $\gamma$-rays[16] and a level near 2.86 Mev could give $\gamma$-rays of energies about 0.7 and 1.1 Mev. The latter should be quite clear of the expected $\gamma$-rays and some work on this coincidence spectrum might be worthwhile.

Spectrum in Coincidence with 0.41 Mev

The decay scheme of Shafroth and Hanna[16] leads to 0.72, 1.02 and 1.43 Mev $\gamma$-rays and a level near 2.86 Mev could only give a $\gamma$-ray of about 0.7 Mev, so that there would seem to be nothing to recommend the investigation of this spectrum.

Spectrum in Coincidence with 1.43 Mev

$\gamma$-rays of energies 0.41, 0.72, 1.02, 1.43 and 2.15 Mev are to be expected[16]. Only a 0.7 Mev $\gamma$-ray could arise from the hypothetical level under investigation, so that this spectrum would not readily yield any valuable information.

Spectrum in Coincidence with 2.15 Mev

From the Shafroth and Hanna[16] decay scheme only a 1.43 Mev $\gamma$-ray is to be expected, whereas a level near 2.86 Mev could give rise to a 0.7 Mev $\gamma$-ray. However the 2.15 Mev peak is not sufficiently well separated from the escape peaks of the 2.86 Mev. $\gamma$-ray to allow this spectrum to be obtained accurately (fig. 31).

Spectrum in Coincidence with 2.86 Mev

0.72 Mev $\gamma$-rays in coincidence with 2.86 Mev can be accounted for by the well established levels or by a level at 2.86 Mev[16], so that this is not likely to be among the more interesting spectra.

The Neutron Spectrum of Karadeniz

Although the unpublished work of Karadeniz (fig. 2) indicates levels at 3.2 and 2.7 Mev considerations similar to those above suggest that the spectra in coincidence with 0.72 and 1.02 Mev are the most promising ones for study. It was accordingly decided to obtain these two coincidence spectra as accurately as is possible with the present equipment in a reasonable time.

## 4.2. Ratio of True to Random Coincidence Rates

### True Coincidence Rate

In the fast-slow coincidence system of fig. 20 the true coincidence counting rate Ne at the output of the gate will depend on the following factors:-

(i) the counting rate at the output of the single channel, say $n_k$,

(ii) the fraction f of the pulses accepted by the single channel that are truely in coincidence with other $\gamma$-rays emitted in the reaction.

(iii) a geometrical factor, G, which is the probability that one member of a truly coincident pair of $\gamma$-rays should strike counter 1 when the other member is detected by counter 2.

(iv) The detection efficiency of counter 1, $\phi$, for the appropriate energy of $\gamma$-rays.

Thus, $$N_c = fG\phi n_k \qquad (1)$$

Random Coincidence Rate

Random coincidences can occur in both the fast and the slow coincidence units and in the gate. The point of a fast-slow system is that the pulses fed out to the kicksorter should possess the freedom from random effects found in the fast coincidence unit. The slow coincidence unit is merely employed in amplitude selection and the gate is caused to pass a pulse only when a fast coincidence showing the desired amplitude requirements has occurred. It will be shown below that in fact under normal working conditions the random coincidence rate is that appropriate to the fast coincidence unit.

Random Coincidence Rate arising in the Fast Coincidence Unit, $N_R^f$

An output from the gate unit can only arise from a random fast coincidence if the associated slow pulse from counter 2 satisfies the amplitude requirement of the single channel. Thus only $n_k$ out of the n pulses/sec from counter 2 can contribute towards random coincidences that affect the output from the gate. If $\tau_f$ is the fast coincidence resolving time, the random rate in the kicksorter is $2\tau_f n_k n$, n being the counting rate in detector 1.

$$N_R^f = 2\tau_f n_k n.$$

Random Coincidence rate arising in the Slow Coincidence Unit, $N_R^s$

A random coincidence in the slow coincidence unit will open the gate and allow a pulse into the kicksorter. The random rate from this cause is

$$N_R^s = 2\tau_s n_f n_k$$

where $\tau_s$ is the slow coincidence resolving time and $n_f$ is the counting rate at the output of the fast coincidence unit.

Random Coincidence rate arising in the Gate, $N_R^g$

The gate is opened for $\tau_g$ secs., $n_s$ times per sec. so that

$$N_R^g = n_s \tau_g n.$$

Comparison of $N_R^f$, $N_R^s$ and $N_R^g$

The resolving times used were: $\tau_f = 2 \times 10^{-8}$ sec

$\tau_s = 2 \times 10^{-6}$ sec

$\tau_g = 5 \times 10^{-6}$ sec

Typical values for the counting rates would be:

$n \sim 10^3$/sec

$n_k \sim 10^2$/sec

$n_f \sim 10^{-1}$/sec

$n_s \sim 10^{-2}$/sec.

$$\therefore \quad N_R^f = 2\tau_f n_k n \approx 2 \times 2 \times 10^{-8} \times 10^2 \times 10^3 \approx 4 \times 10^{-3}/\text{sec} \quad (2)$$

$$N_R^s = 2\tau_s n_k n_f \approx 2 \times 2 \times 10^{-6} \times 10^2 \times 10^{-1} \approx 4 \times 10^{-5}/\text{sec}$$

$$N_R^g = n_s \tau_g n \approx 10^{-2} \times 5 \times 10^{-6} \times 10^3 \approx 5 \times 10^{-5}/\text{sec}$$

From these it can be seen that the random coincidence rate is effectively that arising in the fast coincidence unit, $N_R^f$.

The ratio of the true coincidence rate $N_c$ to the random rate $N_R$ is

$$\frac{N_c}{N_R} = \frac{f\, G\, \phi}{2\, \tau_f\, n}$$

from (1) and (2).

It is desirable to make this ratio as large as possible. $f$ is fixed by the cascade under investigation, $\phi$ by the crystal being used and $\tau_f$ by the electronic system. The counters were placed

as close as convenient to the target to obtain the most favourable value of G. The counting rate, n, must be kept low enough to give an acceptable value of $N_c/N_R$, but at the same time the counting rate must be sufficient to enable the experiment to be completed in a reasonable time.

4.3. The Choice of Counting Rate for the $B^{10}$ Experiment

An estimate of a suitable counting rate for the $B^{10}$ experiment was made practically, using the $\gamma$-rays from the $Be^9(d, n)B^{10}$ reaction. Spectra in coincidence with the 0.72 Mev $\gamma$-rays were obtained at several different counting rates. The monitor sealer (fig. 20) was used to check the counting rate at frequent intervals during the course of each run, and the controls of the H.T. set were adjusted as often as necessary to keep the counting rate constant. With a counting rate $\sim 5 \times 10^3$/sec. the shape of the coincidence spectrum was similar to an ungated one, indicating that random coincidences predominated. At about $\frac{1}{2} \times 10^3$/sec however the spectrum was clearly not of the ungated shape, the peaks corresponding to the $\gamma$-rays that would be expected in coincidence with 0.72 Mev from the work of Shafroth and Hanna[16] being more prominent. Under these conditions the counting rate at the high energy end of the coincidence spectrum was only $\sim 1$ count per channel per hour, and so it seemed that to seek further improvement by reducing the counting rate below $\frac{1}{2} \times 10^3$/sec would cause the experiment to last so long that drifts in the electronic units and possibly even the breakdown of one or more of them would seriously impair the coincidence spectra in other ways.

The expression derived above for $N_c/N_R$ was used to check that a counting rate of $\frac{1}{2} \times 10^3$/sec was a reasonable value to use in this experiment. The reliability of such a calculation

was first investigated by obtaining $N_c/N_R$ for the $Co^{60}$ coincidence spectrum of fig. 29.

$N_c/N_R$ for the $Co^{60}$ Coincidence Spectrum

$$\frac{N_c}{N_R} = \frac{f\,G\,\phi}{2\,\tau_f\,n}$$

The single channel was set on the 1.33 Mev peak. As the two $Co^{60}$ $\gamma$-rays are in cascade, each 1.33 Mev $\gamma$-ray has an associated 1.17 Mev $\gamma$-ray in coincidence with it, and f = 1.

The centres of the crystals were 9 cms from the Co source and the crystals are 3 cms in diameter. If we assume the angular correlation of the $Co^{60}$ $\gamma$-rays to be isotropic (as great accuracy is not required in a calculation of this kind) G is just the ratio of the area of the crystal facing the source to the area of a 9 cm sphere,

$$\text{i.e.} \quad G = \frac{\pi\, 9/4}{4\pi .81} = \frac{1}{144}$$

It is most useful to evaluate the ratio of true to random coincidences that occur in the 1.17 Mev peak, as this can be obtained easily from the coincidence spectrum. The efficiency for obtaining a pulse in the full energy peak when a 1 Mev $\gamma$-ray strikes a crystal of the size used is $\phi \sim 0.07$ (ref. 24).

In obtaining the spectrum of fig. 29 the counting rate n was 750/sec.

$$\therefore \quad \frac{N_c}{N_R} = \frac{1 \times \frac{1}{144} \times 0.07}{2 \times 2 \times 10^{-8} \times 750} \approx 20$$

When we gate on the 1.33 Mev $\gamma$-rays, ideally the only response in the coincidence spectrum should be due to 1.17 Mev

$\gamma$-rays. The response due to random coincidences should have the shape of an ungated spectrum, so the intensity of the random effect in the 1.17 Mev peak should be nearly the same as at 1.33 Mev (see fig. 29a). Applying this to the spectrum in fig. 29(b), the ratio of true to random coincidences in the 1.17 Mev peak is found to be 16, which is in reasonable agreement with the value 20 predicted above.

## $N_c/N_R$ for the $B^{10}$ Coincidence Spectrum

The value of $N_c/N_R$ is evaluated below for the 1 Mev peak in the spectrum in coincidence with 0.72 Mev, to check the suitability of a counting rate of $\frac{1}{2} \times 10^3$/sec. The counters were 9 cms from the target so the value of G may again be taken as 1/144.

In this case the value of f is not known accurately, but from a spectrum of the neutrons emitted during the reaction, e.g. fig. 2, it can be seen that many of the 0.72 Mev $\gamma$-ray quanta will result from the direct formation of $B^{10}$ in the state with 0.72 Mev excitation. Of the remainder of the 0.72 Mev quanta, some will be in coincidence with the 1.02 Mev $\gamma$-ray and others with the 1.43 or 2.86 Mev $\gamma$-rays (fig. 1). Because of these possibilities, f was rather arbitrarily assumed to be $\sim \frac{1}{4}$.

Then
$$\frac{N_c}{N_R} \approx \frac{\frac{1}{4} \times \frac{1}{144} \times 0.07}{2 \times 2 \times 10^{-8} \times \frac{1}{2} \times 10^3} \approx 6.$$

It was decided to accept a value of this order for $N_c/N_R$ in view of the low counting rate, $\sim$ 1/channel/hour, in the 2.8 Mev region of the coincidence spectrum, and to apply a correction to the spectrum for random coincidences. A total of at least about 50 counts per channel at the high energy end of the coincidence spectrum would seem desirable, so that about 50 hours of running

time would be required.

Some trial runs were also made on the spectrum in coincidence with 1.02 Mev $\gamma$-rays and they showed that a counting rate of $\frac{1}{2} \times 10^3$/sec would again be satisfactory if coupled with a running time of about 50 hours.

4.4. Outline of Method Used to Obtain the Coincidence Spectra.

The Sunvic multichannel kicksorter was available for this work only occasionally and the 100 hours total running time required had to be spread over three months. Both the coincidence spectra had therefore to be obtained by adding together the results of many short runs, and the method adopted, which is described below, was devised to minimise the effect of drifts in the electronic units on the resolution of the final total spectra, and to enable electronic faults to be spotted quickly. After each coincidence run, an ungated spectrum was obtained. These were combined in the same way as the gated spectra, and the resulting combined ungated spectrum was compared with a normal ungated spectrum as a test of the success of the method in maintaining the resolution.

A bombarding energy of 600 Kev was used and the deuteron beam current was adjusted to give the desired counting rate. As the monitor scaler consisted of a mechanical register, preceded by two dekatrons and a hard valve scale of 100, it was convenient to check the counting rate by measuring the time between successive counts on the register. This time was maintained within the range 25-30 secs, giving a counting rate just under $\frac{1}{2} \times 10^3$/sec. The scaler was left running continuously and frequent measurements of the time for $10^4$ monitor counts were made.

The Sunvic kicksorter was used with 80 channels, and was adjusted so that these covered the energy range of the $B^{10}$ $\gamma$-rays, i.e. from about 0.4 to 3.0 Mev. Before commencing each coincidence run an ungated $B^{10}$ spectrum was observed on the kicksorter and the positions of the peaks were found in order to detect drift in the sensitivity of the electronic system since the preceding run. A Muirhead 75 $\Omega$ constant impedance attenuator, variable in $\frac{1}{2}$ db steps, was included between the cathode follower and the amplifier before the Sunvic kicksorter (fig. 19) and was used to compensate any such drift.

The single channel analyser, with width switched to 1V, was next used to obtain the spectrum in the region of the peak to be used for gating. The width was then increased to 3V, and the channel set with the gating peak in its centre. This procedure was carried out prior to every run.

The coincidence run was then started. A scaler which monitored the coincidence rate served to show up faults in the coincidence system.

After each individual coincidence spectrum had been recorded, an ungated spectrum was again observed to ensure that no drift or other electronic trouble had developed during the run. If either the drift, or the number of coincidences recorded, seemed excessive the spectrum was rejected.

During the period in which spectra were being obtained the functioning of the coincidence system was tested at weekly intervals with a $Co^{60}$ source. The resolving time of the fast coincidence unit was also measured with a pulse generator several times.

Finally, the individual spectra were combined to give a result embodying about 50 hours of running. The details of the method used to combine the results, which included energy calibration of the individual spectra to reduce the effect of small unavoidable drifts, will be given in Chapter 5.

From the decay scheme, fig. 1, it is clear that there can be no 2.86 Mev $\gamma$-rays in coincidence with 1.02 Mev, so the response at the high energy end of the spectrum gated on 1.02 Mev will be entirely random in origin. A spectrum of the ungated shape was fitted to this high energy response to give the magnitude of the random contribution in the rest of the spectrum. The correction required to the other coincidence spectrum, gated on 0.72 Mev, was calculated from the random rate observed at the high energy end of the 1.02 Mev spectrum.

## 4.5. Comparison with the Method of Shafroth and Hanna[16]

In the experiment by Shafroth and Hanna[16] two sodium iodide scintillation spectrometers were used. The output from each photomultiplier was fed through a cathode follower and linear amplifier to a single channel pulse height analyser. The pulses from the two analysers triggered blocking oscillators to provide standard pulses for the coincidence mixer. A second coincidence circuit was provided to monitor random coincidences; it received delayed pulses from one analyser and undelayed pulses from the other. The resolving time of the coincidence circuits is not quoted in their paper.

To obtain a coincidence spectrum, one single-channel analyser was set on a chosen peak in the spectrum and the other was used to scan the region where coincidences could occur. The method

allowed only one point on the coincidence spectrum to be obtained at a time, so it would be very tedious to seek more than the minimum useful number of points for each spectrum. This was no great disadvantage as the main purpose of the experiment was to establish directly the decay scheme devised from the $Be^9(d,n)B^{10}$ neutron spectra and the energies of the $B^{10}$ $\gamma$-rays. In the coincidence spectra shown[16], channel widths of 3 to 8 volts were used, and the points were often placed so that there was one point for each possible peak and one for each possible valley, although two of the low energy spectra were obtained more accurately than this. The spectra were quite adequate for a discussion of the cascades involving the levels well known from the neutron spectra. However, the method was not well suited to give information about the low intensity regions of a spectrum, e.g. the response above 1 Mev. in coincidence with 0.72 Mev is not shown, and the use of wide channels on such a complex spectrum made accurate quantitative comparisons of spectra difficult.

It seems that the technique adopted in the present experiment, using a multichannel kicksorter, should produce more accurate spectra of better resolution, and so give a greater likelihood of observing any small effect due to a level near 2.8 Mev, which, on the evidence of the neutron spectra, should be very weak if it exists at all.

# CHAPTER 5.

## COINCIDENCE SPECTRA

Fourteen individual spectra were obtained gating on the 1.02 Mev peak, of which three were rejected either because of excessive drift in the sensitivity of the electronic system during the run, or because an abnormal coincidence rate was observed. Thirteen spectra were obtained gating on the 0.72 Mev peak, of which one was rejected. The length of the runs varied from 2 to 7 hours. Each time an ungated spectrum was also recorded.

### 5.1. Addition of Spectra

The spectra were first combined straightforwardly by adding together the number of counts recorded each time in corresponding channels. As precautions were taken during the experiment to keep any drift in the spectra to a minimum, the small residual drifts should do no more than spoil the resolution to some extent, and it is interesting to compare these total spectra with the ones obtained later with the aid of energy calibrations.

#### Spectrum gated on the 1.02 Mev peak

The eleven acceptable runs totalled 51 hours and when added together gave the spectrum in fig. 32.

#### Spectrum gated on the 0.72 Mev peak

Of the twelve acceptable runs, two showed evidence of drift that had not been adequately compensated before the run began, i.e. the peaks in these spectra were slightly displaced in relation to the corresponding peaks in the other ten results. These two were not included in fig. 33, but as they were quite acceptable in themselves, they were not finally rejected and will be referred to

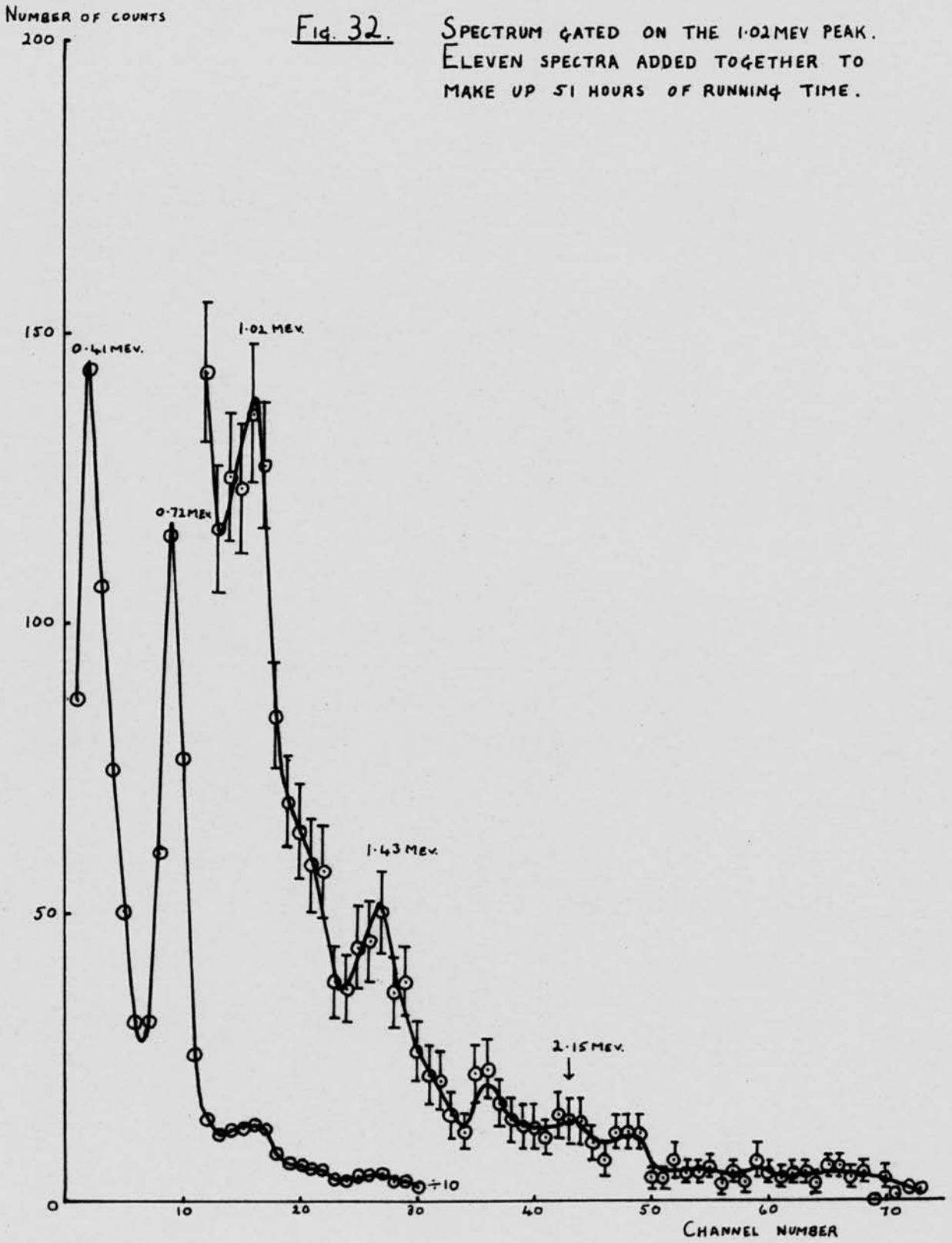


FIG. 32. SPECTRUM GATED ON THE 1·02 MEV PEAK. ELEVEN SPECTRA ADDED TOGETHER TO MAKE UP 51 HOURS OF RUNNING TIME.

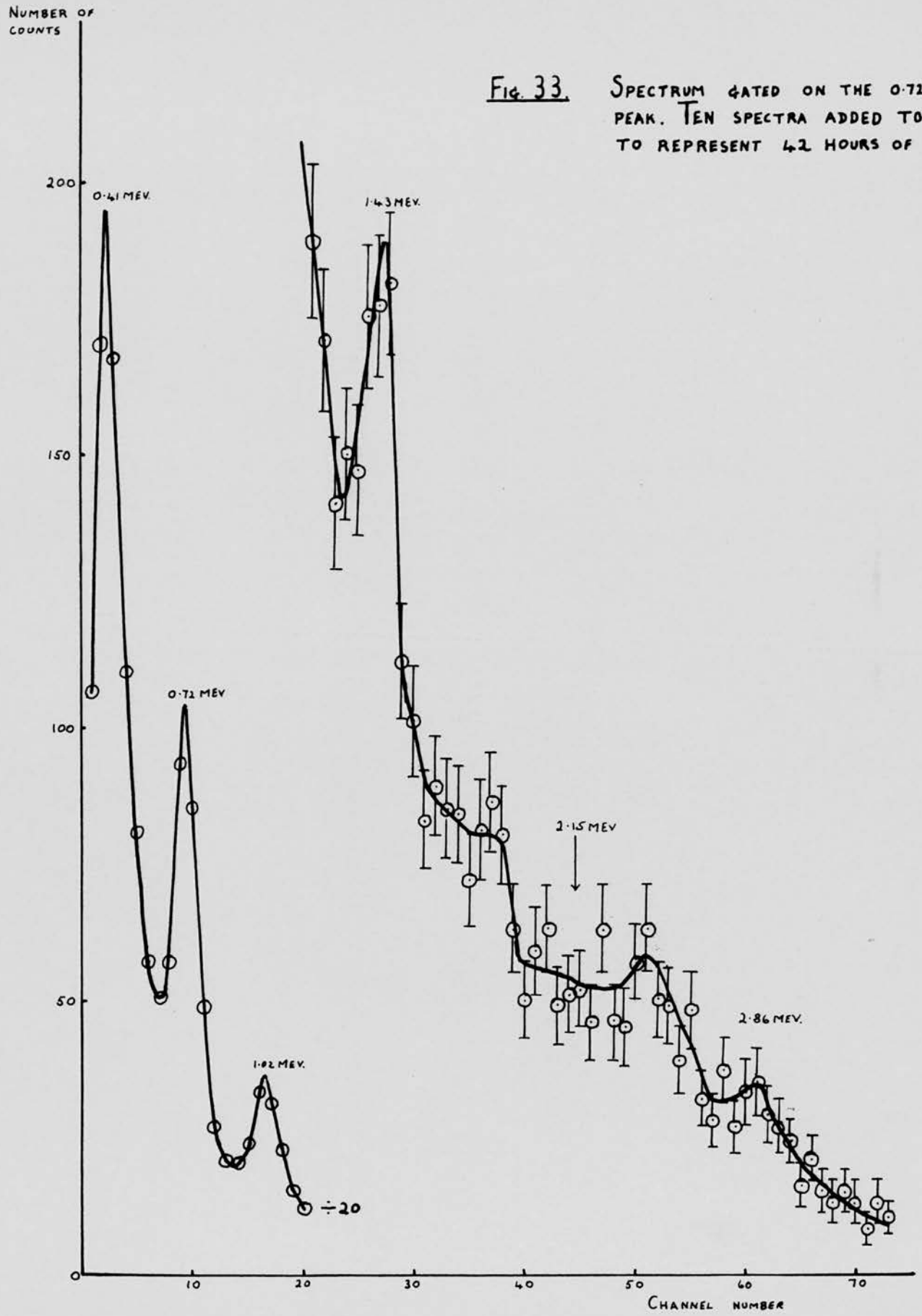


Fig. 33. Spectrum gated on the 0·72 MeV peak. Ten spectra added together to represent 42 hours of running.

again in section 5.2. The ten runs used totalled 42 hours.

Combined ungated spectra

The result of adding together the ungated spectra obtained over the same period as the spectrum gated on the 1.02 Mev peak is shown in fig. 34. The corresponding spectrum obtained over the same period as the spectrum gated on the 0.72 Mev peak is in fig. 35. Comparison of figs. 34 and 35 shows that drifts have had a worse effect on the latter result, although comparison of both these spectra with a normal ungated spectrum, e.g. fig. 31, indicates that the resolution has been considerably impaired in both cases. Presumably a similar spoiling of resolution has occurred, in the associated gated spectra, and in an attempt to overcome this a system of energy calibration of the individual runs prior to their combination was adopted.

## 5.2. Combination of Results, with Energy Calibration

### Spectrum gated on the 1.02 Mev peak

The method employed will be described for the case of the spectra gated on the 1.02 Mev peak.

The counting rate at the low energy end of the gated spectrum is very considerably larger than at the high energy end. In the spectrum resulting from a single run the positions of the peaks due to 0.41 Mev and 0.72 Mev $\gamma$-rays could be determined quite accurately and the peak due to 1.02 Mev $\gamma$-rays could be seen clearly, although it was not quite as well defined, see e.g. fig. 36. The positions of these peaks were used to draw a straight line energy calibration graph from which the energy corresponding to the centre of each channel of the kicksorter could be read off. From this a histogram was constructed showing the number of counts recorded in each channel against the energy of the channel. A histogram of this kind was

Fig. 34. Result of addition of ungated spectra obtained over the same period as the spectrum gated on the 1·02 MeV peak.

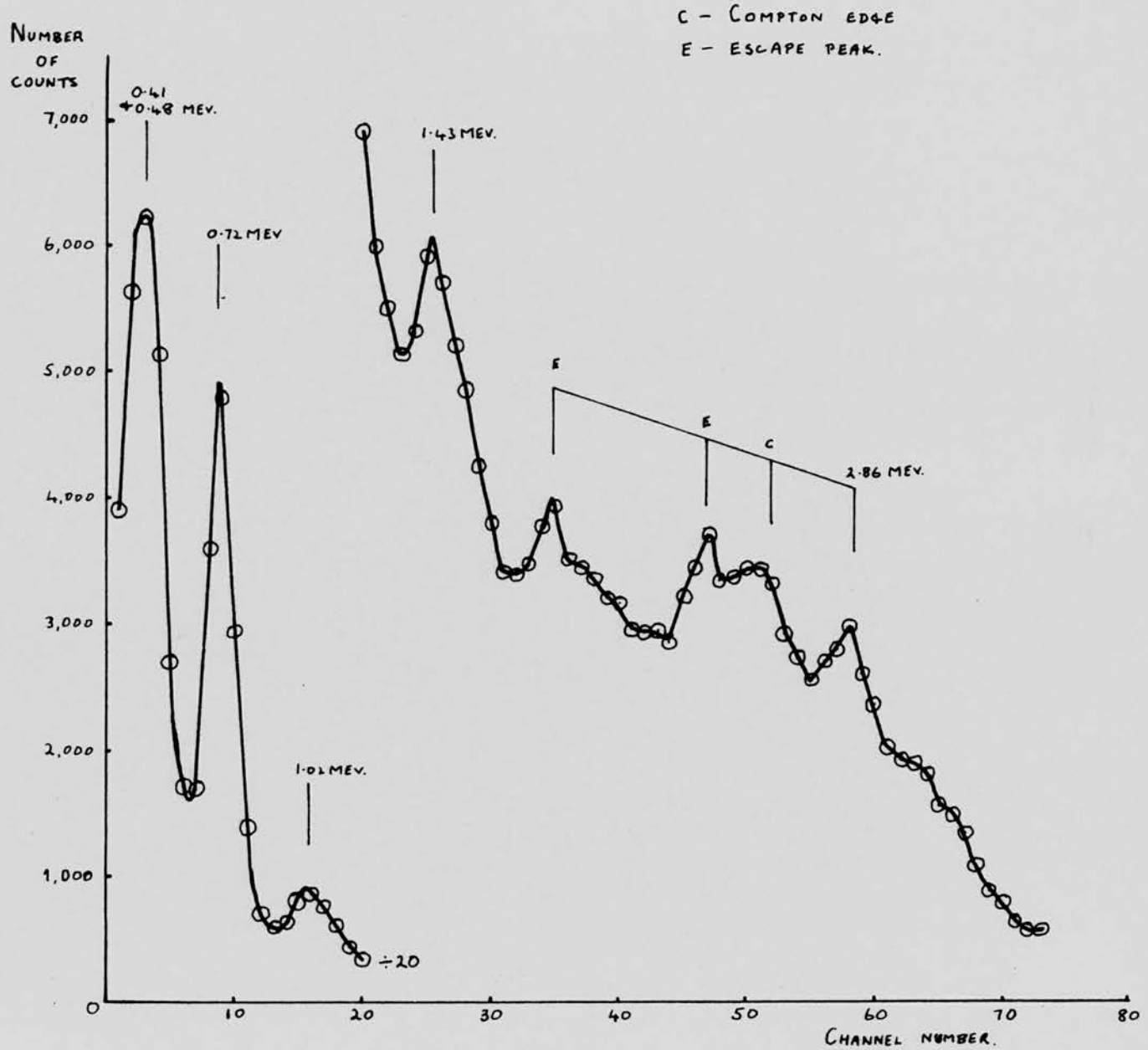

FIG. 35. RESULT OF ADDITION OF UNGATED SPECTRA OBTAINED OVER THE SAME PERIOD AS THE SPECTRUM GATED ON THE 0·72 MEV PEAK.

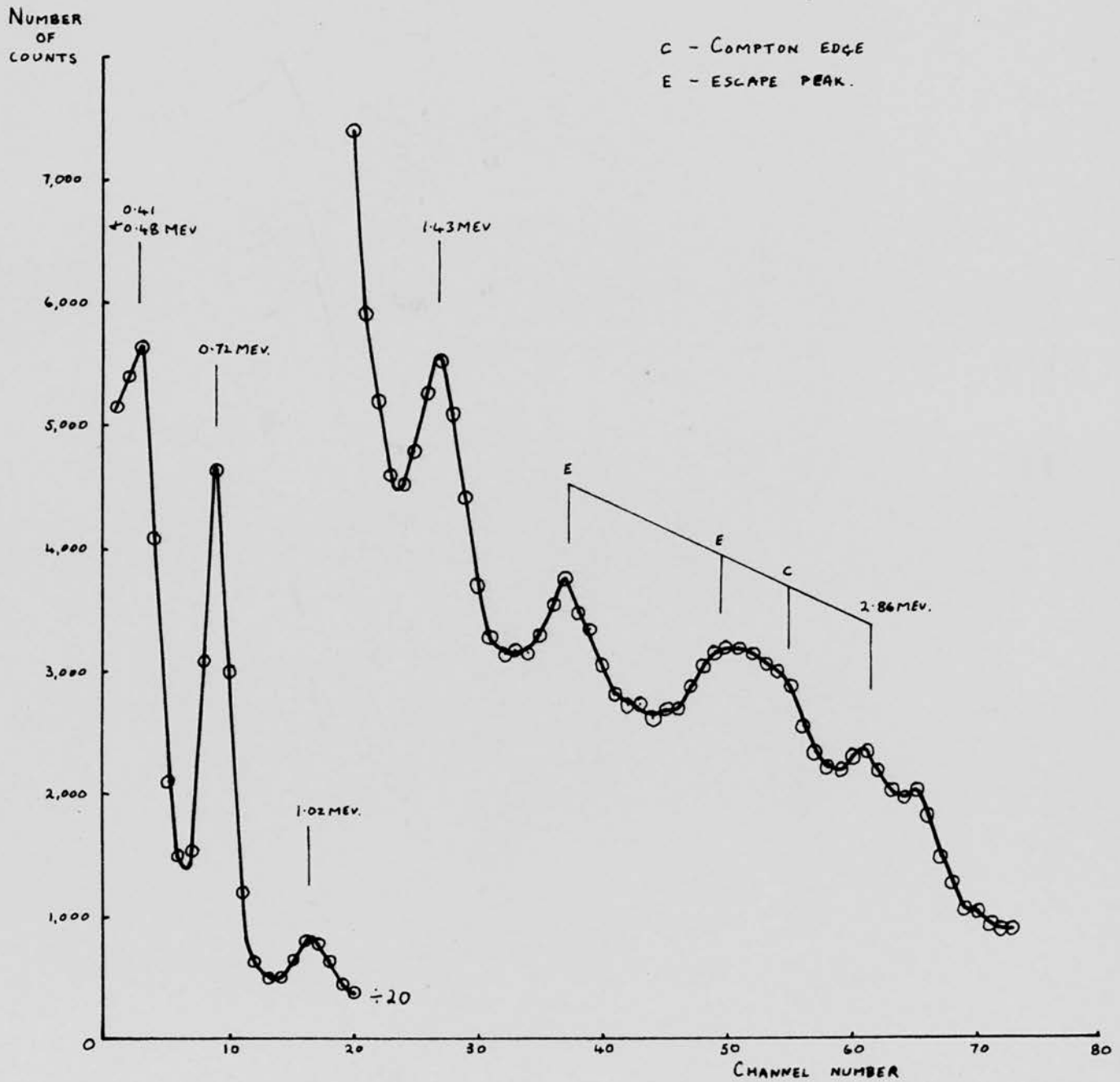

Fig 36 Result of a single typical run gating on the 1·02 MeV peak. The straight line energy calibration is also shown.

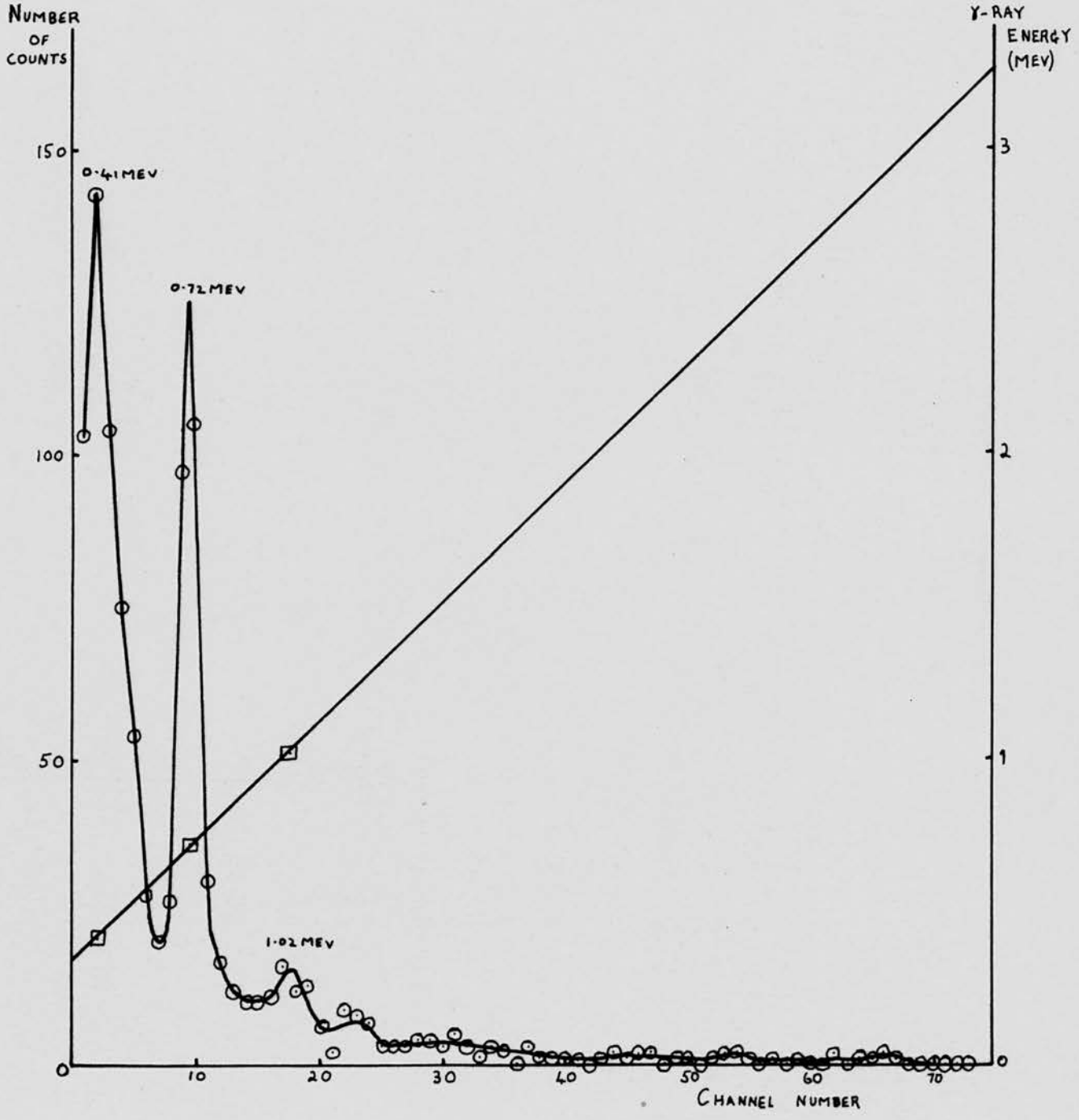

produced for each individual run. The energy range was divided into 0.05 Mev intervals and the area under the histogram (i.e. the number of counts) was found in each interval. The areas found in corresponding energy intervals from each histogram were then added together, to produce the spectrum in fig. 37. This is not substantially different from fig. 32, although the 1.43 Mev peak is perhaps better resolved.

Spectrum gated on the 0.72 Mev peak

The same procedure was followed with the ten results used to give the spectrum in fig. 33. The spectrum obtained using energy calibration is shown in fig. 38. In this the points defining the 1.43 Mev peak are more evenly distributed over the peak than in fig. 33 and above this energy the points suggest a slight improvement in resolution.

The two results that showed too large a drift for inclusion in the spectrum obtained by simple addition were energy calibrated and combined with the spectrum in fig. 38 to give fig. 39, which embodies 52.5 hours of running time.

Combined ungated spectra

The effectiveness of the technique of energy calibration was gauged by combining two sets of five ungated spectra and comparing the results. To make the conditions as similar as possible to those applying to the gated spectra, the energy calibrations were based on the positions of only three of the low energy peaks. The peak at 0.41 Mev could not be used in this case, as it was not resolved from the 0.48 Mev peak which arises from the $Be^9(d,\alpha)Li^7$ reaction, so the peaks at 0.72, 1.02 and 1.43 Mev were used. The

Fig. 37. Spectrum gated on the 1·02 MeV peak — result of combination of the spectra after energy calibration. The dotted curve is an estimate of the contribution due to random coincidences.

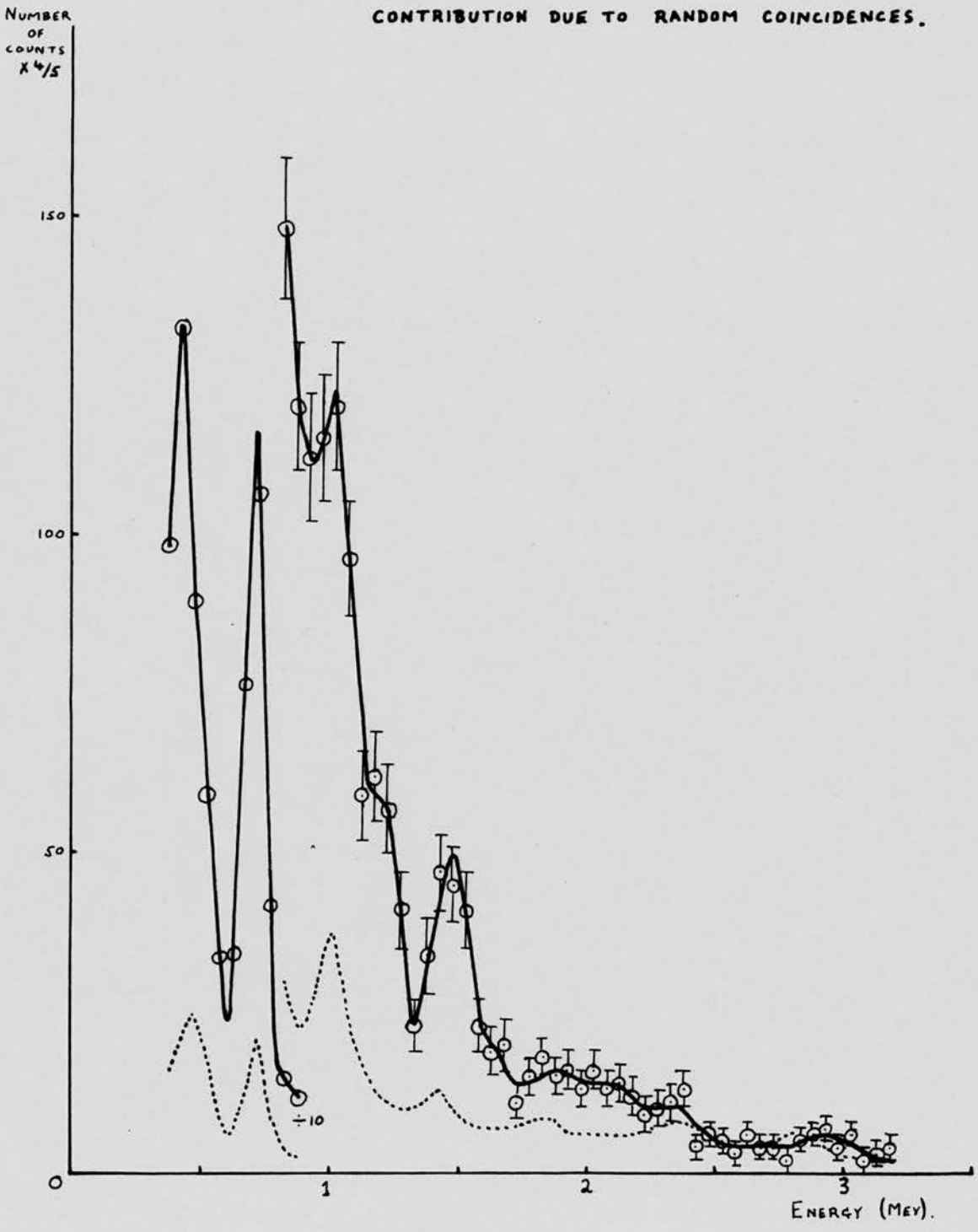

FIG. 38. SPECTRUM GATED ON THE 0·72 MEV. PEAK, OBTAINED AFTER ENERGY CALIBRATION OF THE RESULTS USED IN FIG. 33.

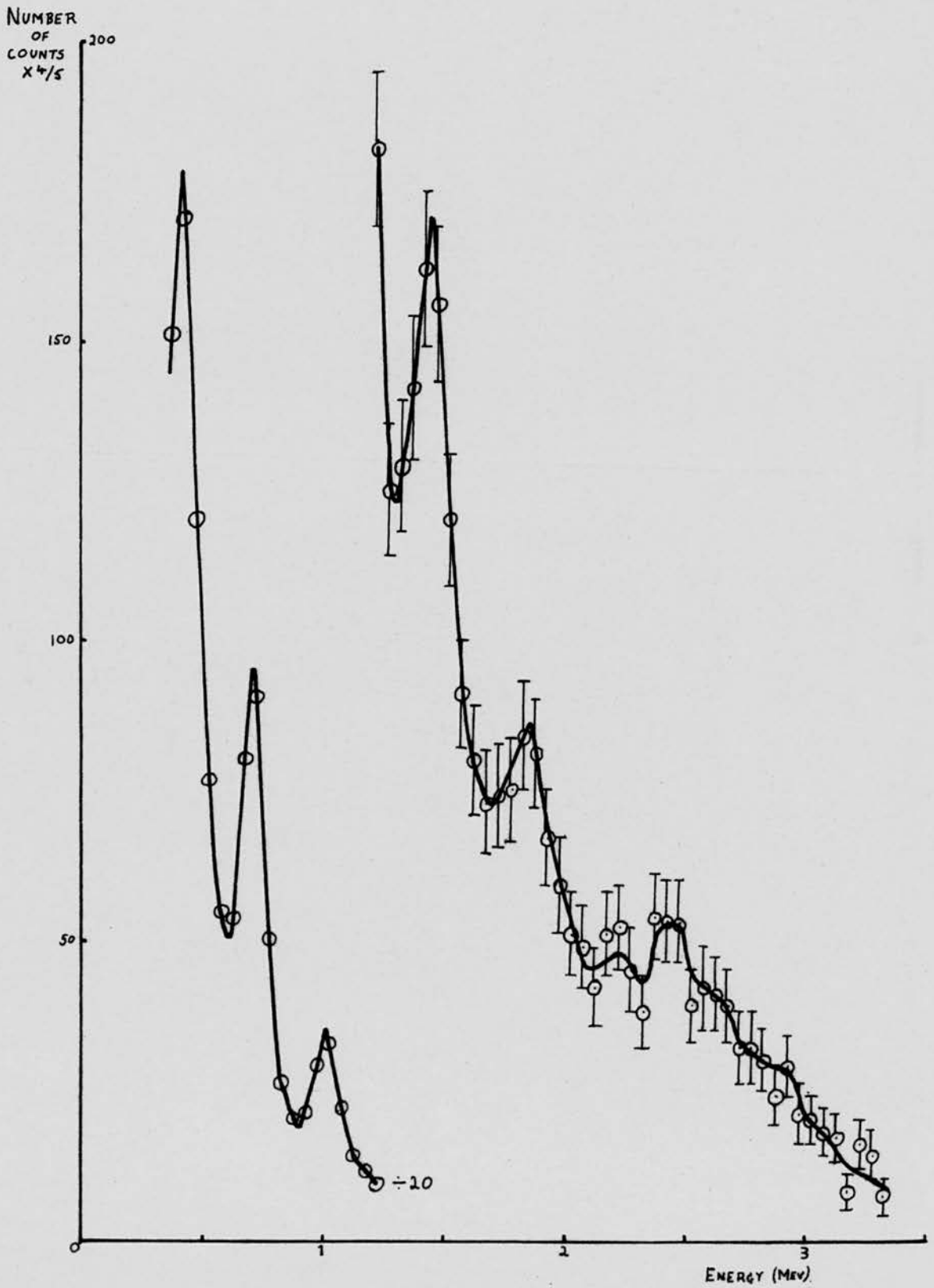

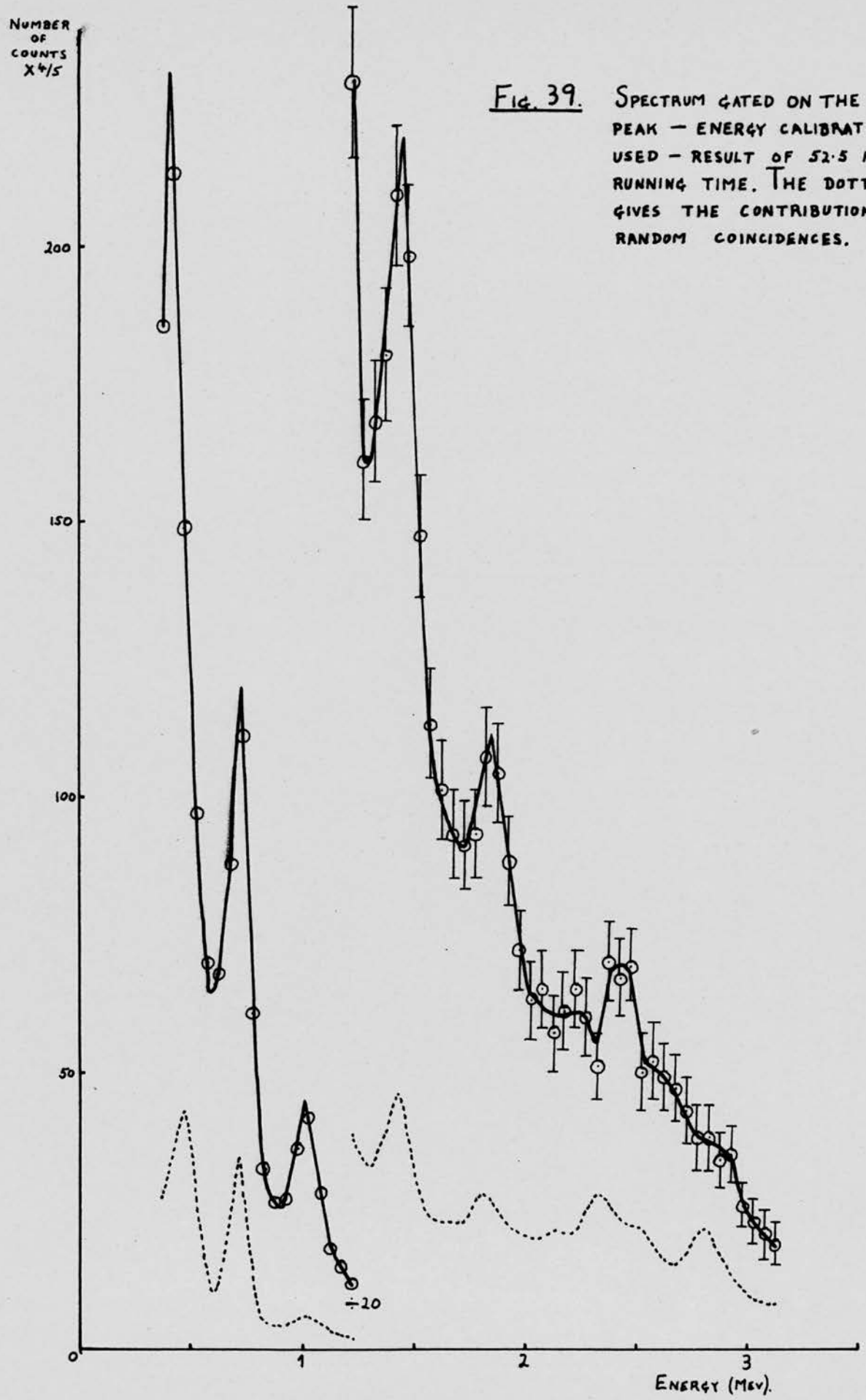


FIG. 39. SPECTRUM GATED ON THE 0·72 MEV. PEAK — ENERGY CALIBRATION TECHNIQUE USED — RESULT OF 52·5 HOURS OF RUNNING TIME. THE DOTTED CURVE GIVES THE CONTRIBUTION DUE TO RANDOM COINCIDENCES.

resulting pair of combined spectra are shown in fig. 40. It can be seen that they have very closely the same shape, much more so than the two ungated spectra produced by simple addition, figs. 34 and 35. The resolution also compares quite favourably with that observed in a normal spectrum, fig. 31.

The resolution in the gated spectra, figs. 37 and 39, would not be expected to be quite as good as in the ungated ones, fig. 40, as (a) the better statistical accuracy in the individual ungated spectra should enable a more accurate calibration line to be drawn, and (b) the use of the position of the 1.43 Mev peak should also help by providing a point on the calibration line nearer to the high energy end of the spectrum.

## 5.3. Correction for Random Coincidences

### Correction to the spectrum gated on the 1.02 Mev peak

A spectrum due to random coincidences should have the same shape as an ungated spectrum. The response in the 2.8 Mev region of the spectrum gated by 1.02 Mev $\gamma$-rays should be due entirely to random coincidences (see fig. 1 or fig. 30). A spectrum of the ungated shape fitted to the high energy end of the gated spectrum (Fig. 37, dotted curve), should therefore give the effect due to random coincidences over the whole energy range. The ungated spectrum used for this purpose was the sum of the two in fig. 40. The random contribution was subtracted from the experimental coincidence spectrum to give fig. 41. The curve giving the random contribution is fitted to points of poor statistical accuracy and consequently the magnitude of the random contribution can be altered by about $\pm$ 20% without significantly spoiling the fit. This is taken into account in the indication of the accuracy of the points in fig. 41.

Fig. 40. Combined ungated spectra obtained using energy calibration technique (each graph from a set of 5 results).

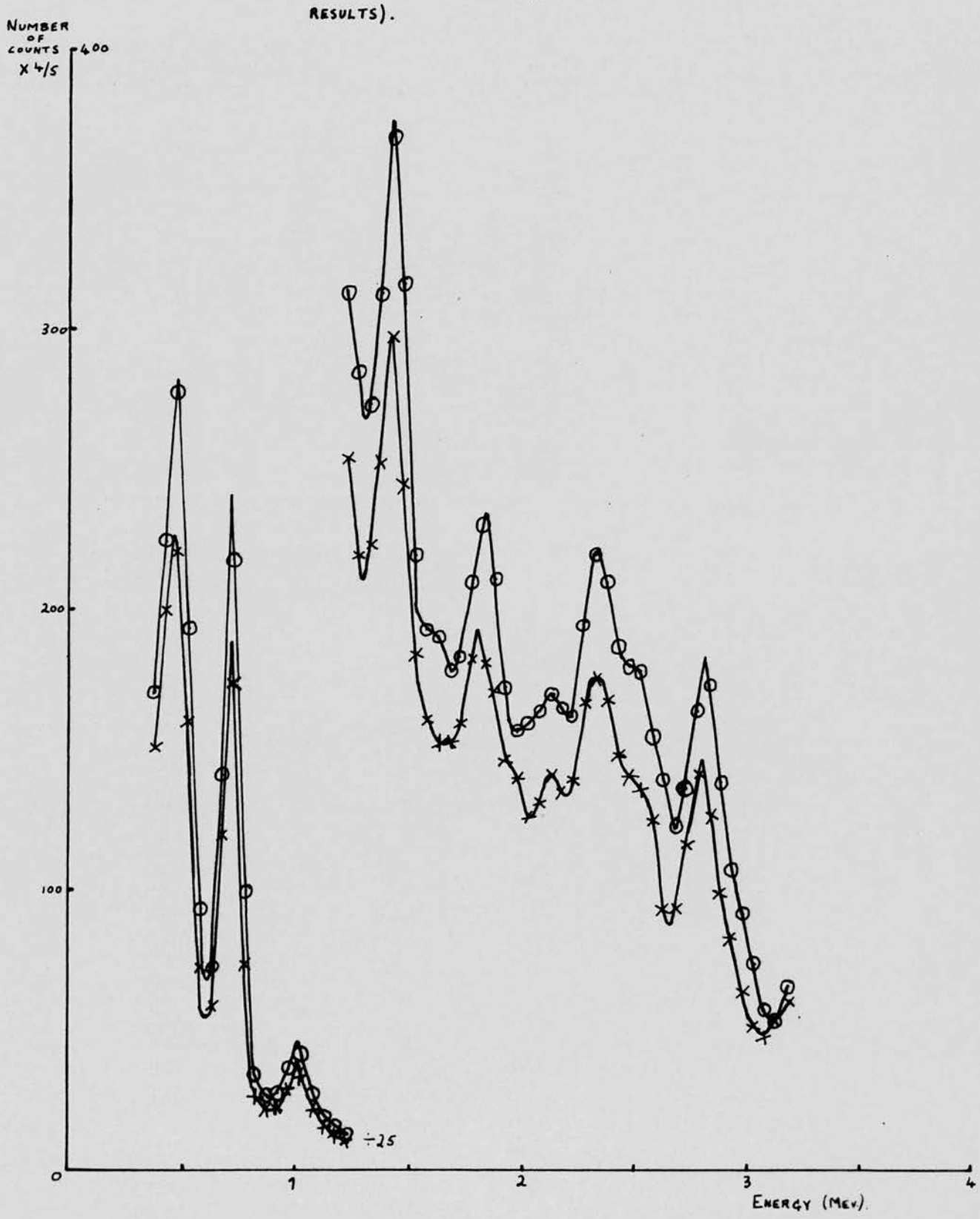

Fig. 41. Spectrum gated on the 1·02 MeV peak after correction for random coincidences.

( c - Compton edge.
E - Escape peak. )

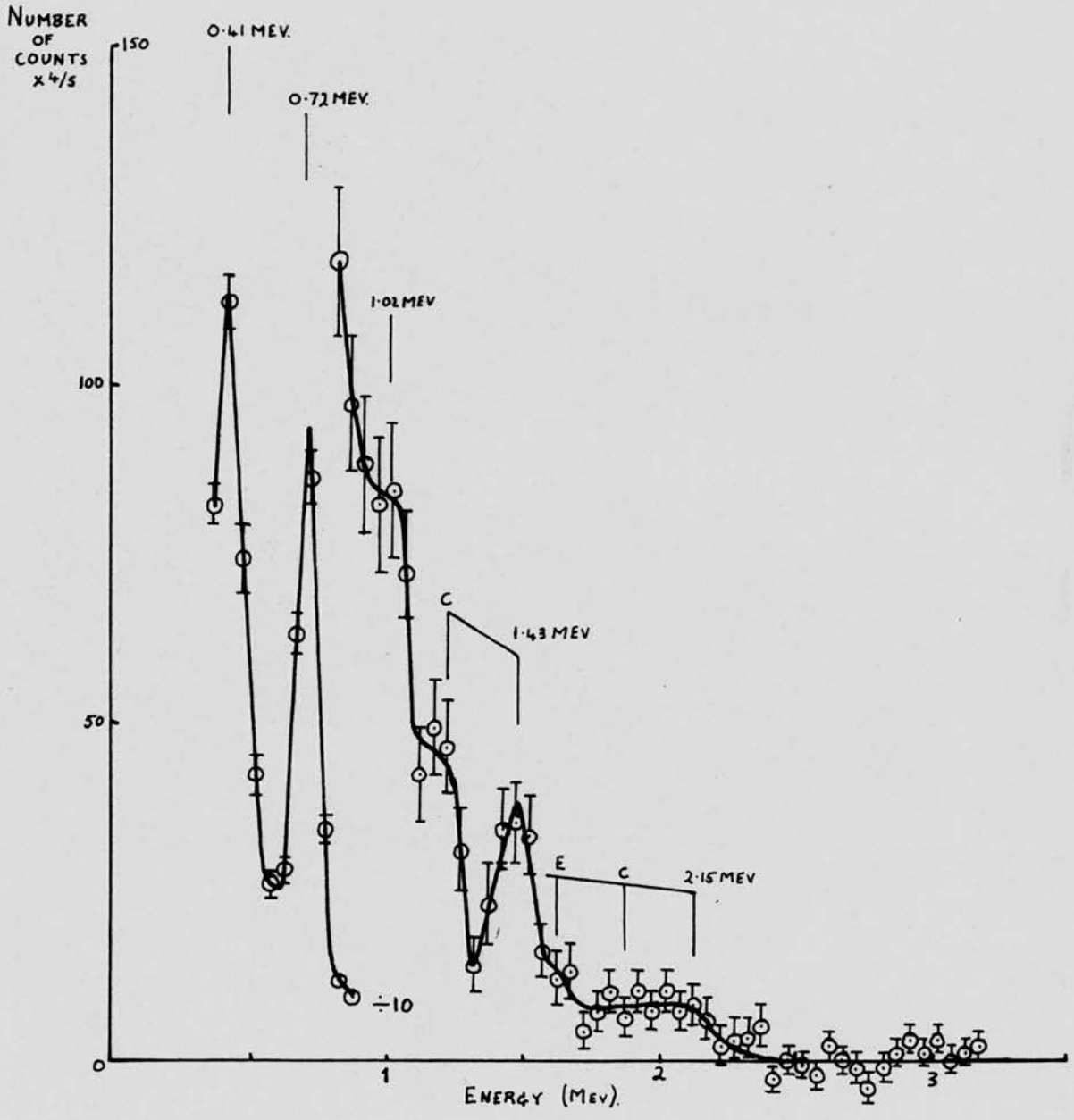

Correction to the spectrum gated on the 0.72 Mev peak

The random contribution to the spectrum gated on the 0.72 Mev peak was calculated from the random coincidence rate observed in the spectrum gated on the 1.02 Mev peak. The counting rate $N_R^k(E)$ in the gated spectrum at energy E due to random coincidences, when the single channel analyser is set on a peak of energy K Mev, is given by

$$N_R^k(E) = 2\tau_f n_k n(E)$$

where n(E) is the counting rate of pulses corresponding to -rays of energy E, at the output of the photomultiplier.

$$N_R^{0.72}(E) = 2\tau_f n_{0.72} n(E)$$

and $$N_R^{1.02}(E) = 2\tau_f n_{1.02} n(E)$$

$$\therefore \quad \frac{N_R^{0.72}(E)}{N_R^{1.02}(E)} = \frac{n_{0.72}}{n_{1.02}}$$

The ratio $n_{0.72}/n_{1.02}$ was calculated from the spectrum, fig. 42, obtained using the single channel analyser. The positions occupied by the 3 volt wide gating channel while obtaining the coincidence spectra are indicated.

$$\frac{N_R^{0.72}(E)}{N_R^{1.02}(E)} = \frac{n_{0.72}}{n_{1.02}}$$

$$= \frac{\text{area under 0.72 Mev peak between the channel limits}}{\text{area under 1.02 Mev peak between the channel limits}}$$

$$\approx 3.6$$

Since 52.5 hours were spent recording the spectrum gated on the 0.72 Mev peak and 51 hours on the one gated on the 1.02 Mev peak,

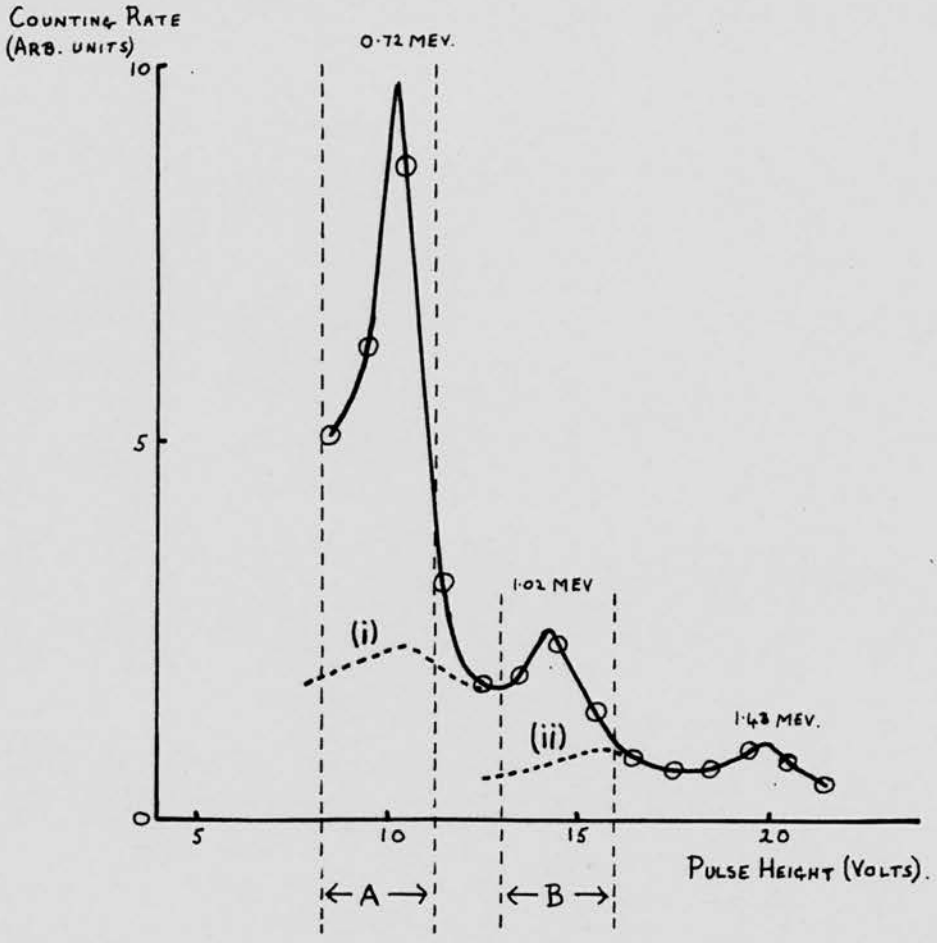


FIG. 42. SPECTRUM OF $B^{10}$ γ-RAYS OBTAINED USING THE SINGLE CHANNEL ANALYSER.

A INDICATES THE POSITION OF THE 3V WIDE CHANNEL WHEN GATING ON THE 0·72 MEV. PEAK.

B INDICATES THE POSITION OF THE 3V WIDE CHANNEL WHEN GATING ON THE 1·02 MEV PEAK.

CURVE (i) GIVES THE PART OF THE SPECTRUM DUE TO γ-RAYS OF ENERGY GREATER THAN 0·72 MEV.

CURVE (ii) GIVES THE PART OF THE SPECTRUM DUE TO γ-RAYS OF ENERGY GREATER THAN 1·02 MEV.

the number of random coincidences in the 0.72 Mev spectrum is $3.6 \times \frac{52.5}{51} \approx 3.7$ times the number in the 1.02 Mev case. The resulting curve giving the contribution due to random coincidences is shown dotted in fig. 39; fig. 43 gives the spectrum after the random effect has been subtracted.

5.4. The Effect of Pulses due to Compton Electrons accepted in the Gating Channel

When the single channel analyser was set on the 0.72 Mev peak a considerable number of the pulses it accepted would be due to electrons Compton-scattered by 1.02 Mev $\gamma$-rays (see fig. 42, curve (i)), while a small number of pulses caused by 1.43 Mev and higher energy $\gamma$-rays would also be present. These pulses would cause the spectrum gated on the 0.72 Mev peak, i.e. fig. 43, to contain peaks due to the $\gamma$-rays in coincidence with the 1.02 Mev $\gamma$-ray as well as much less intense peaks due to those in coincidence with the 1.43 Mev $\gamma$-rays.

The spectrum gated on the 1.02 Mev peak i.e. fig. 41, would be similarly affected by 1.43 Mev and higher energy $\gamma$-rays, see fig. 42 curve (ii). The spectrum gated on the 1.02 Mev peak should give a fairly good indication of the relative intensities of the unwanted peaks introduced, by 1.02 Mev and higher energy $\gamma$-rays into the spectrum gated on the 0.72 Mev peak.

The count $C_{0.72}$ at a given energy in the spectrum gated on the 0.72 Mev peak, due to $\gamma$-rays of energy greater than 0.72 Mev, is proportional to the area $A_1$ under curve (i) between limits A (see fig. 42), and to the time $T_1$ taken to obtain the spectrum. Thus

$$C_{0.72} \propto A_1 \times T_1$$

The count $C_{1.02}$ at the same energy in the spectrum gated on the

Fig. 43. Spectrum gated on the 0·71 MeV peak after correction for random coincidences. The dotted curve gives the contribution due to the acceptance of Compton electrons by the gating channel (see text).

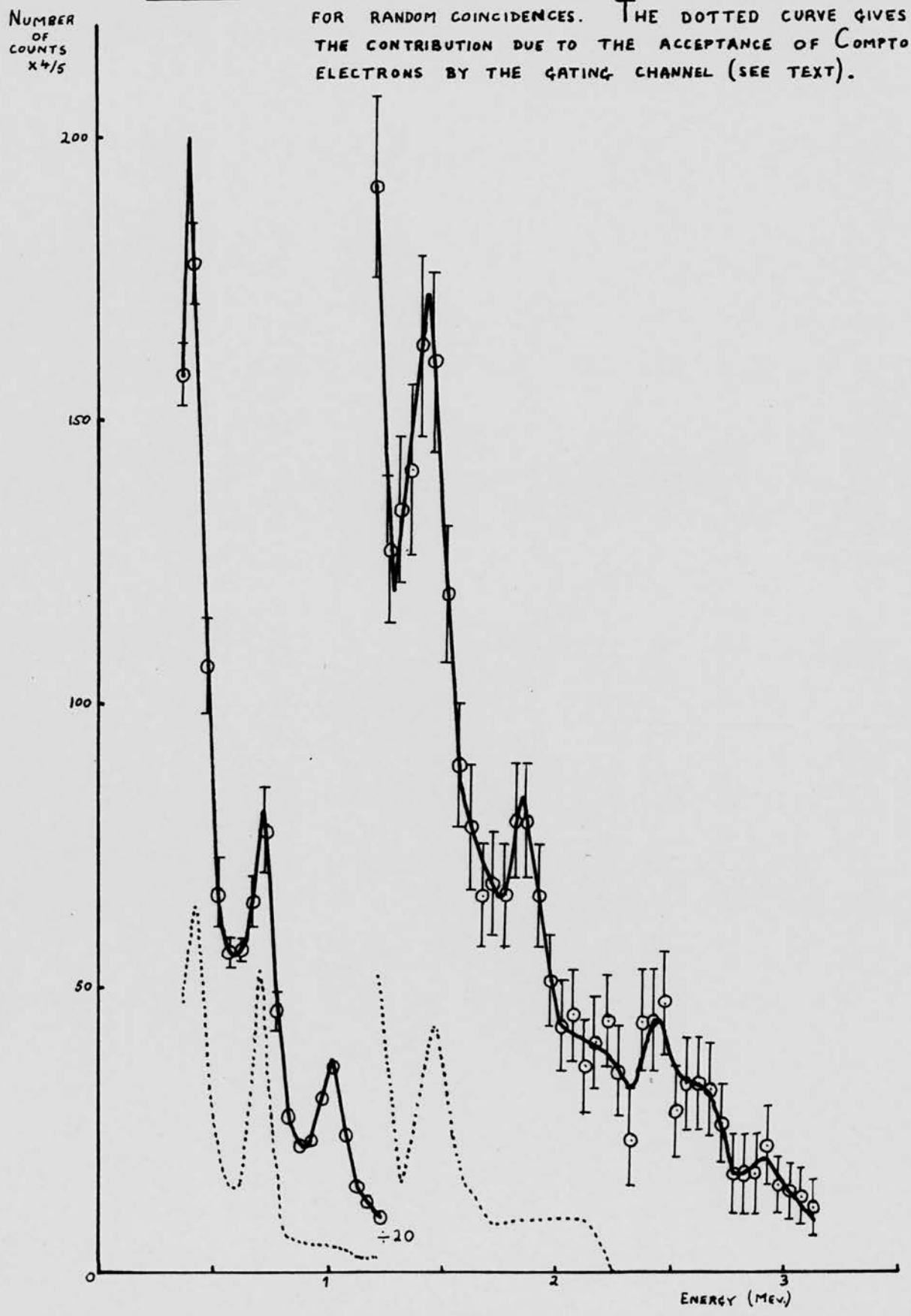

1.02 Mev peak is proportional to the area $A_2$ under the 1.02 Mev peak between limits B in fig. 42, and to the time $T_2$ taken to obtain the spectrum. Thus

$$C_{1.02} \propto A_2 \times T_2$$

$$\therefore \quad \frac{C_{0.72}}{C_{1.02}} = \frac{A_1}{A_2} \times \frac{T_1}{T_2}$$

$$= \frac{12.5}{11.5} \times \frac{52.5}{51.0}$$

$$1.1$$

The spectrum of fig. 41, was therefore multiplied by 1.1 to give the dotted curve in fig. 43, which was then subtracted from the spectrum in coincidence with 0.72 Mev. The resulting spectrum, fig. 44, should give the $\gamma$-rays in coincidence with the 0.72 Mev $\gamma$-ray free from all extraneous effects.

It was not possible to apply a similar correction to the spectrum gated on the 1.02 Mev peak as this would require a spectrum gated on the 1.43 Mev peak. From fig. 42 curve (ii) it was found that when the single channel analyser was set on the 1.02 Mev peak almost 2/5 of the gating pulses it accepted would be due to $\gamma$-rays of higher energy, principally 1.43 Mev; this was borne in mind when interpreting fig. 41.

## 5.5. Interpretation of the Coincidence Spectra

### $\gamma$-rays in coincidence with the 0.72 Mev $\gamma$-ray

The spectrum gated on the 0.72 Mev $\gamma$-ray, fig. 44, has peaks with energies of 0.4, 1.0, 1.45, 1.85, 2.45 and 2.9 Mev. The 2.45 Mev peak has shoulders at 2.2 and 2.65 Mev.

Fig. 44. Spectrum of the γ-rays in coincidence with the 0·72 MeV γ-ray.

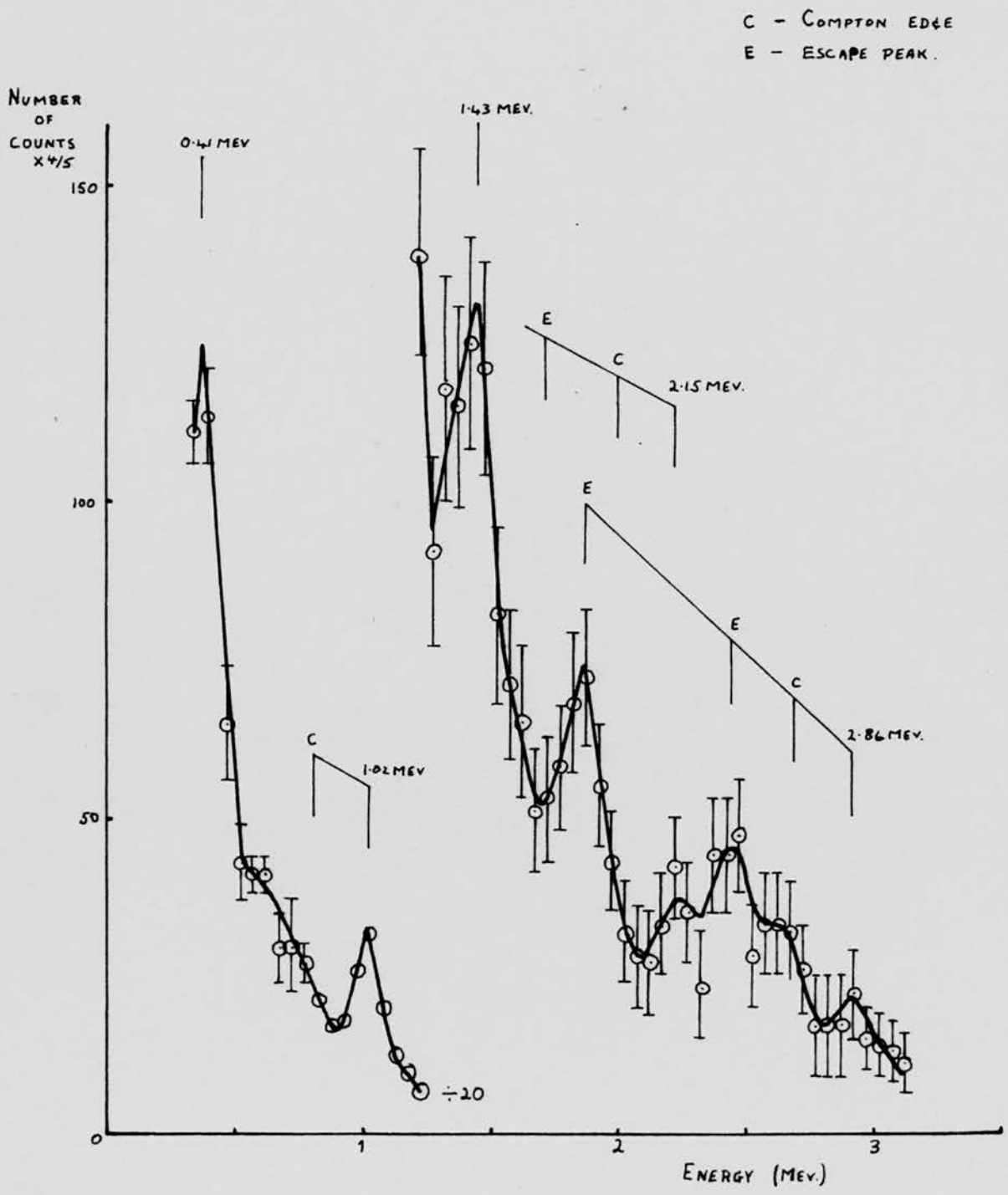

The peak at 2.9 Mev is taken to be the full energy peak of the 2.86 Mev $B^{10}$ $\gamma$-ray, with the shoulder at 2.65 Mev its Compton edge and the peaks at 2.45 and 1.85 Mev its escape peaks. It should be noted that as the energy calibration of the spectra was based on the positions of the low energy peaks, see fig. 36, errors $\sim$ 0.1 Mev are quite possible at the high energy end. From comparison with ungated spectra of the $B^{10}$ $\gamma$-rays and the 2.62 Mev $ThC^{11}$ $\gamma$-ray it would seem that the height of the full energy peak is rather low in relation to the Compton edge and single escape peak. However this is probably explained by an impairing of the resolution due to the inaccuracy of the energy calibration in this region of the individual coincidence spectra.

The shoulder at 2.2 Mev is interpreted as the full energy peak of the 2.15 Mev $B^{10}$ $\gamma$-ray. Its Compton edge and single escape peak would form a broad peak centred on 1.85 Mev. This is superposed on the 1.84 Mev escape peak due to the 2.86 Mev $\gamma$-ray, giving a 1.85 Mev peak much higher than the escape peak at 2.45 Mev. The presence of a 2.15 Mev $\gamma$-ray in this spectrum cannot be explained by the accepted $B^{10}$ decay scheme, fig. 1, although it could be in agreement with a decay scheme involving a level at 2.86 Mev (see fig. 30). The only way to avoid this interpretation would be to assume that the shoulder at 2.2 Mev is due to a "freak" statistical effect, and that the excessive height of the 1.85 Mev peak is attributable to the full energy peak of a 1.85 Mev $\gamma$-ray. A $\gamma$-ray of this energy from $B^{10}$ has not been reported. The only place such a $\gamma$-ray could be fitted into a decay scheme involving previously suggested levels would be from the 3.58 Mev level to the 1.74 Mev level, in which position it would be in coincidence with both the 0.72 Mev and the 1.02 Mev $\gamma$-rays. In

the spectrum gated on the 1.02 Mev $\gamma$-ray (fig. 41), which is discussed below, there is no peak at 1.85 Mev, and there can be little doubt that fig. 44 indicates coincidences between 2.15 Mev and 0.72 Mev $\gamma$-rays.

The remaining peaks in fig. 44 at 1.45, 1.0 and 0.4 Mev are taken to be full energy peaks due to 1.43, 1.02 and 0.41 Mev $B^{10}$ $\gamma$-rays. These $\gamma$-rays would all be expected from the accepted decay scheme.

A level at 2.86 Mev in $B^{10}$ could provide 0.72 Mev - 0.72 Mev coincidences (section 4.1 and fig. 30); there is no obvious sign of 0.72 Mev $\gamma$-rays in fig. 44.

Interpretation of the spectrum gated on the 1.02 Mev peak (fig. 41)

There are peaks in fig. 41 at 0.4, 0.7 and 1.45 Mev and shoulders at 1.0, 1.2 and 2.15 Mev. It should be recalled that about half of the gating pulses in this case were due to 1.43 Mev $\gamma$-rays (section 5.4).

The low intensity plateau from 2.15 Mev down to the 1.45 Mev peak is interpreted as being due to the full energy peak, Compton edge and escape peak of the 2.15 Mev $B^{10}$ $\gamma$-ray in coincidence with the 1.43 Mev $\gamma$-ray from the level at 3.58 Mev; the valley between the full energy peak and the Compton edge is unresolved because of the poor statistical accuracy associated with the small number of counts involved.

The peak at 1.45 Mev and the shoulder at 1.2 Mev are attributed to the 1.43 Mev $\gamma$-ray, being respectively the full energy peak and the Compton edge.

The shoulder at 1.0 Mev and the peaks at 0.7 and 0.4 Mev are attributed to the 1.02, 0.72 and 0.41 Mev $\gamma$-rays, the first

of these being necessarily in coincidence with the 1.43 Mev $\gamma$-ray.

This interpretation is consistent with the accepted decay scheme of fig. 1, as 0.41, 0.72 and 1.43 Mev $\gamma$-rays would be expected in coincidence with the 1.02 Mev $\gamma$-ray, while 0.41, 0.72, 1.02, 1.43 and 2.15 Mev $\gamma$-rays might occur in coincidence with the 1.43 Mev $\gamma$-rays.

A quantitative comparison of the gated and ungated spectra is made in the following chapter.

# CHAPTER 6.

## ANALYSIS OF THE RESULTS

Before discussing the $B^{10}$ decay scheme a quantitative analysis of the observed spectra is presented.

### 6.1. The Relative Intensities of the $B^{10}$ $\gamma$-rays

The ungated spectra in figs. 9 and 31 were used to find the relative intensities of the $\gamma$-rays resulting from the $Be^{9}(d, n)B^{10}$ reaction at a deuteron energy of 600 Kev.

The line shape resulting from the detection of a $\gamma$-ray within the energy range covered by the experiment could be sketched fairly accurately, as the shapes associated with $\gamma$-rays having energies of 0.66 Mev (from $Cs^{137}$), 1.17 Mev (from a coincidence spectrum showing one of the $\gamma$-rays from $Co^{60}$, e.g. fig. 29b) and 2.62 Mev (from $ThC^{11}$) are well known from many spectra obtained while testing the equipment. Single line spectra appropriate to the $\gamma$-rays in the spectrum shown in fig. 31 were drawn and their relative intensities adjusted until the curve obtained by summing them agreed as well as possible with the experimental points. Fig. 45 shows the result obtained; the line shapes of the individual $\gamma$-rays are shown dotted, the sum of the dotted curves is shown as a full line, and the experimental points are circled. The agreement between the observed points and the synthesised spectrum is very good, only one point, in the valley between the 1.02 Mev and the 1.43 Mev peaks being noticeably off the curve. Fig. 45 does not include the 0.41 Mev $B^{10}$ $\gamma$-ray, or the 0.48 Mev $Li^{7}$ $\gamma$-ray. A more expanded spectrum is necessary to separate the peaks caused by these two $\gamma$-rays, so the analysis of the low energy end of the spectrum

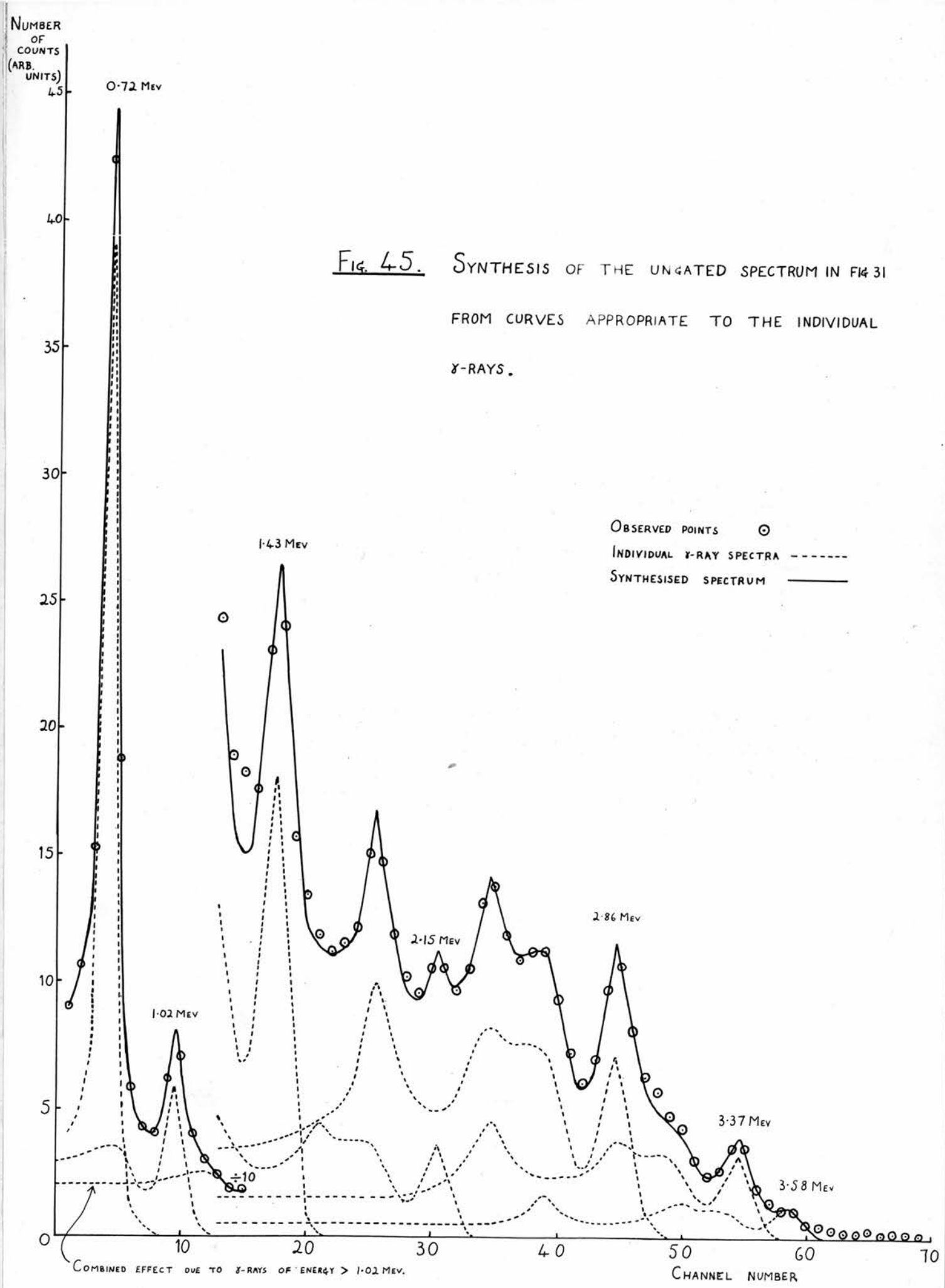


FIG. 45. SYNTHESIS OF THE UNGATED SPECTRUM IN FIG 31 FROM CURVES APPROPRIATE TO THE INDIVIDUAL γ-RAYS.

was carried out on fig. 9, which shows only the 0.41, 0.48 and 0.72 Mev peaks. Fig. 46 shows the experimental points from fig. 9, together with the line shapes attributed to the $\gamma$-rays concerned and the curve obtained by summing them, which agrees well with the points.

The relative intensities of the $\gamma$-rays were found by measuring from figs. 45 and 46 the area under the full energy peak of each $\gamma$-ray and correcting for the variation of detection efficiency with energy from the appropriate curve in Lazar, Davis and Bell[24]. The results are given in the table below.

From fig. 46 the area under the 0.41 Mev peak is 0.41 times the area under the 0.72 Mev peak, and this was used to calculate the area appropriate to the 0.41 Mev $\gamma$-ray on the scale of fig. 45. The present measurements were made using $1\frac{1}{4}$" x 1" NaI crystals with the target 8 cms. from the front face of the crystal; the peak efficiencies used were taken from a curve[24] relating to a $1\frac{1}{2}$" x 1" crystal with a source distance of 7 cms. This curve is drawn for energies up to 1.5 Mev only and the peak efficiencies for 2.15, 2.86 and 3.58 Mev $\gamma$-rays were obtained by extrapolation. Lazar, Davis and Bell give a similar curve for the same size of crystal, but with a source distance of 2.5 cms, and extending up to 2.2 Mev; from this it is clear that the efficiency quoted below for 2.15 Mev $\gamma$-rays cannot be far wrong. There is unfortunately no similar check on the values used for 2.86 and 3.58 Mev $\gamma$-rays.

Published values of the relative intensities of the $B^{10}$ $\gamma$-rays from the $Be^9(d, n)B^{10}$ reaction are included in the table for comparison, although it should be noted that they were obtained with a deuteron bombarding energy of 1.2 Mev, twice that used in the present experiment.

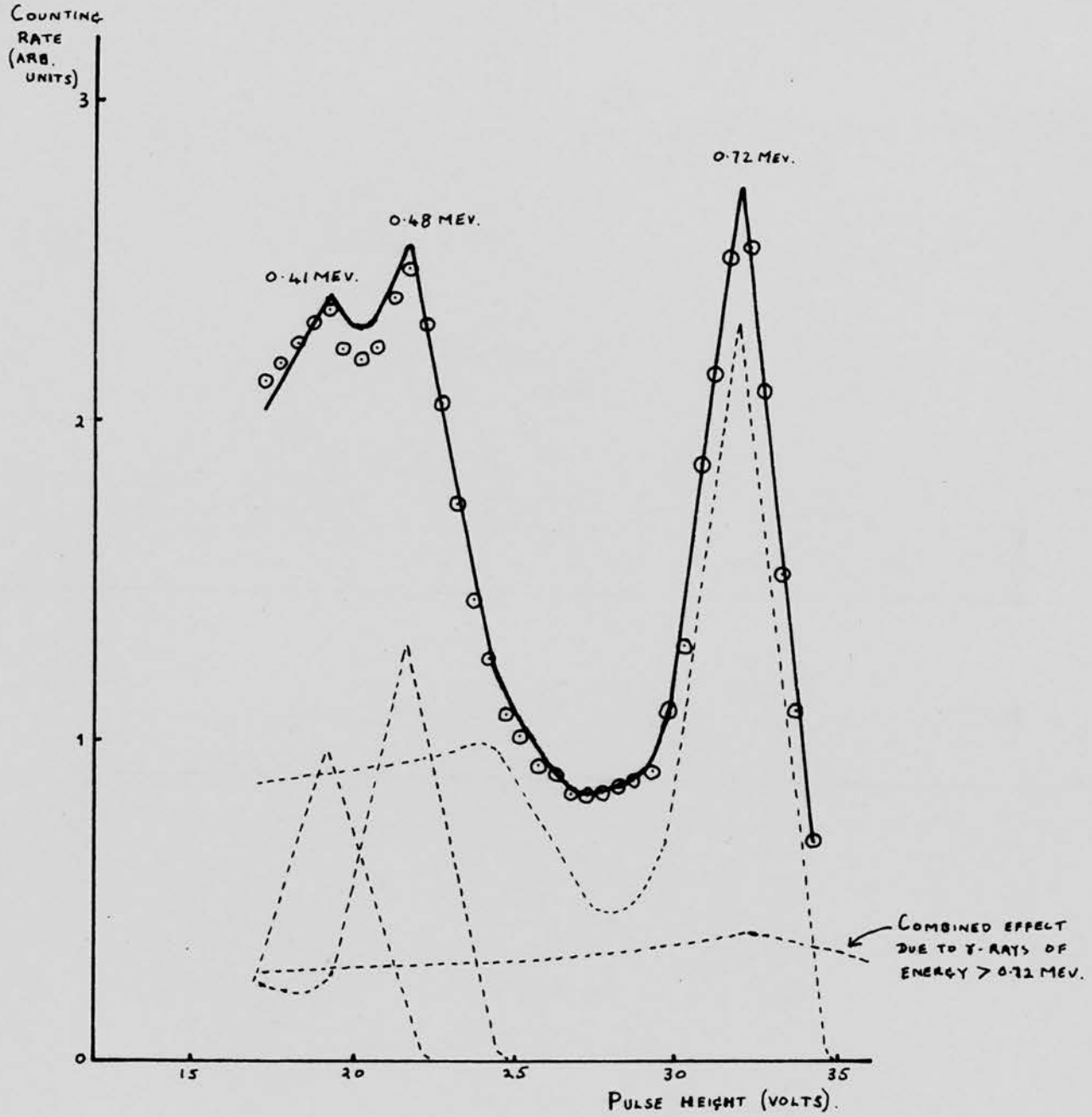


FIG. 46. SYNTHESIS OF THE SPECTRUM IN FIG. 9.

OBSERVED POINTS ⊙

SINGLE γ-RAY SPECTRA - - - - - - - -

SYNTHESISED SPECTRUM ——————

## Relative Intensities of the γ-rays from $Be^9(d, n)B^{10}$

| Present Experiment, $E_d$ = 0.6 Mev | | | | $E_d$ = 1.2 Mev | |
|---|---|---|---|---|---|
| γ-ray energy (Mev) | Area under full energy peak (fig. 45) (Arb. units) | Peak efficiency[24] | Relative Intensity % | Rasmussen et al.[14] Rel. Int. * % | Ajzenberg and Lauritsen[25] Rel. Int. % |
| 3.58 | 36 | 0.010 † | 3 ± 1 | 1.5 | 3 ± 1 |
| 2.86 | 213 | 0.015 † | 12 ± 3 | 4.6 | 10 ± 3 |
| 2.15 | 98 | 0.022 † | 4 ± 1 | 2.9 | 5 ± 1 |
| 1.43 | 522 | 0.040 | 11 ± 3 | 8.7 | 10 ± 3 |
| 1.02 | 1,218 | 0.050 | 20 ± 5 | 13 | 15 ± 4 |
| 0.72 | 5,850 | 0.120 | 42 ± 10 | 56 | 53 ± 14 |
| 0.41 | 0.41 x 5,850 | 0.270 | 7 ± 2 | 14 | 5 ± 1 |

† Obtained by extrapolation

* Accuracy quoted as within a factor of two.

Rasmussen, Hornyák and Lauritsen[14], who used a magnetic lens spectrograph to study the photoelectrons emitted by a thorium converter irradiated by the $B^{10}$ γ-rays, comment that their intensities "may be in error by as much as a factor of two". The intensities in the last column are those given by Ajzenberg and Lauritsen[25], here converted into percentages. In their 1952 review[25], Ajzenberg and Lauritsen attribute these intensities to the experiment by Rasmussen, Hornyák and Lauritsen[14] (1949) and to Rasmussen's Ph.D. thesis (California Institute of Technology, 1950), so it is probably reasonable to assume that they are the more reliable values, being based either on a reappraisal of the earlier results or on a later experiment. Despite the difference in bombarding energy, the present results are in good agreement with the figures given by Ajzenberg and Lauritsen[25] and follow the general trend of the intensities given by Rasmussen et al.[14].

## 6.2. Analysis of the Spectrum in Coincidence with the 0.72 Mev $B^{10}$ γ-ray

The spectrum of the γ-rays in coincidence with the 0.72 Mev γ-ray (fig. 44) was analysed in a similar way to the ungated spectra. Fig. 47 shows the experimental points from fig. 44, and the curve obtained by summing spectra appropriate to the various γ-rays present. It can be seen (as explained in section 5.5.) that a contribution from a 2.15 Mev γ-ray is necessary to explain the intensity of the peak at 1.84 Mev, as well as to give good agreement at 2.15 Mev. A small contribution due to a 0.72 Mev γ-ray is included to improve the agreement in this region between the synthesised spectrum and the experimental points. The

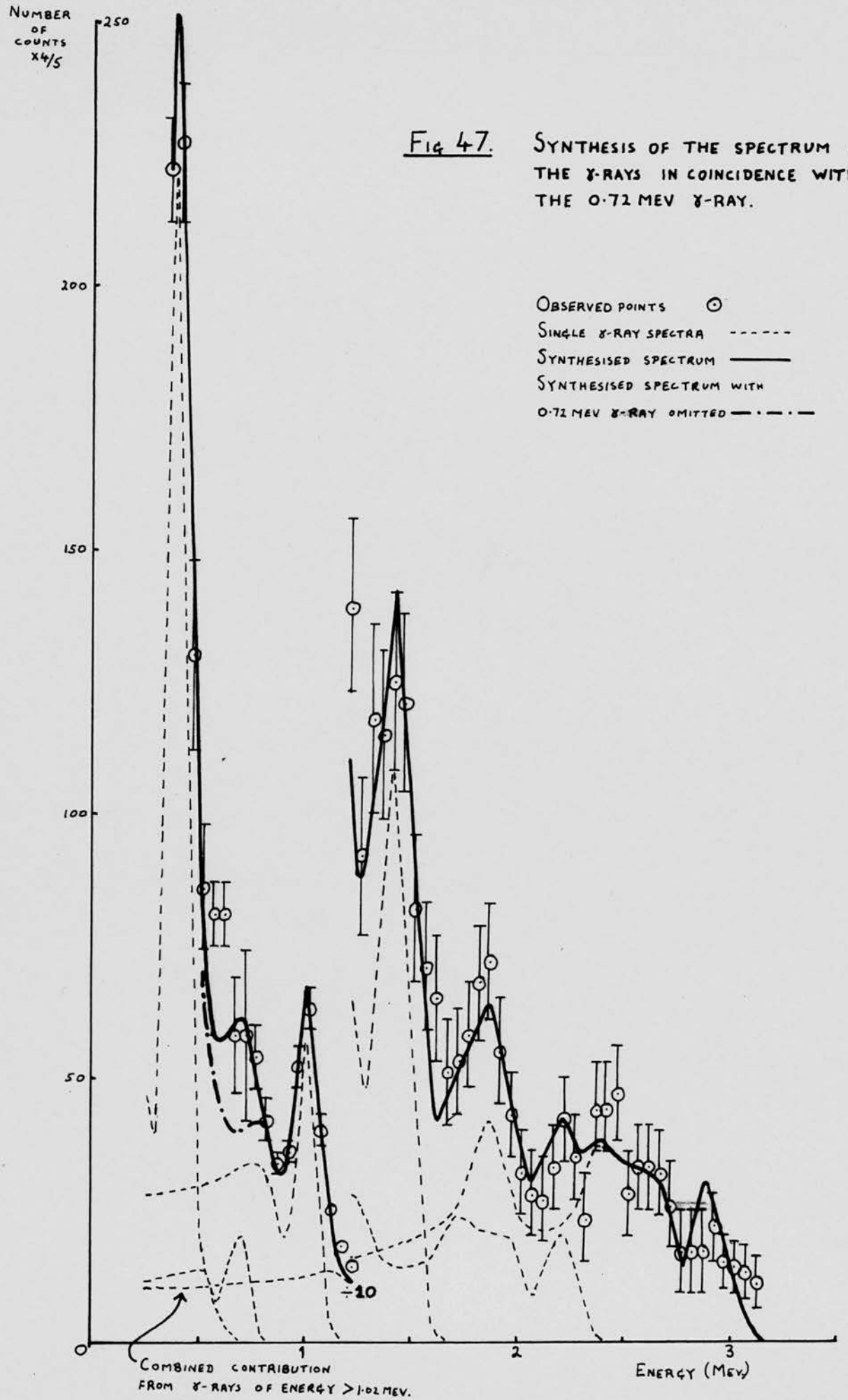


FIG 47. SYNTHESIS OF THE SPECTRUM OF THE γ-RAYS IN COINCIDENCE WITH THE 0.72 MEV γ-RAY.

"dot-dash" curve shows the effect of omitting this 0.72 Mev contribution; taking the accuracy of the points and of the ɣ-ray line shapes into account the agreement is not too bad and it is doubtful whether a 0.72 Mev contribution is needed to explain the shape of the observed spectrum. The relative intensities of the ɣ-rays in this spectrum, found from the areas under the full energy peaks in the same way as for the ungated spectrum, are listed below.

Relative Intensities of the ɣ-rays
in Coincidence with the 0.72 Mev ɣ-ray

| ɣ-ray energy (Mev) | Relative intensity (%) |
|---|---|
| 2.86 | $10 \pm 3$ |
| 2.15 | $5 \pm 1$ |
| 1.43 | $16 \pm 4$ |
| 1.02 | $39 \pm 10$ |
| (0.72) | $(5 \pm 4)$ |
| 0.41 | $26 \pm 10$ |

The intensity of the 0.41 Mev ɣ-ray is less accurate as the experimental points define only the higher energy side of its peak (fig. 47).

The presence of a 2.15 Mev ɣ-ray in this spectrum is clearly at variance with the accepted decay scheme (fig. 1), but could readily be explained by a level at about 2.86 Mev (fig. 30). A small contribution to the coincidence spectrum from a ɣ-ray of energy about 0.72 Mev could also be explained by a level at 2.86 Mev.

If the decay scheme in fig. 1 were valid, all the 2.86 Mev γ-rays should be in coincidence with 0.72 Mev γ-rays, and all the 1.02 Mev and 0.41 Mev γ-rays should also be in coincidence with 0.72 Mev γ-rays. In that case the relative intensities of the 2.86, 1.02 and 0.41 Mev γ-rays should be the same in a spectrum gated on the 0.72 Mev γ-ray as in an ungated spectrum, provided that the intensities in the coincidence spectrum do not depend on the angle between the detectors. The angular anisotropies observed by Shafroth and Hanna[16] are not large (~10%) and the error introduced by assuming isotropy is small compared with the accuracy of the measurements. The table below lists, for these γ-rays, in column (1) the relative intensities in the spectrum gated on the 0.72 Mev γ-ray, and in column (2) the relative intensities in an ungated spectrum.

| γ-ray energy | (1) | (2) |
|---|---|---|
| 2.86 Mev | 10 ± 3 | 24 ± 6 |
| 1.02 Mev | 39 ± 10 | 40 ± 10 |
| 0.41 Mev | 26 ± 10 | 14 ± 4 |

Within the accuracy of the measurements the relative intensities of the 1.02 and 0.41 Mev γ-rays may be the same in both spectra, but only about half of the 2.86 Mev γ-rays appear to be present in the spectrum gated on the 0.72 Mev γ-ray (column (1)). This could be explained if the $Be^9(d, n)B^{10}$ reaction gave rise to a 2.86 Mev excited state in $B^{10}$ which decayed directly to the ground state; it would be necessary to assume that about half of

the 2.86 Mev $\gamma$-rays arose in this way and that the other half were produced, in coincidence with a 0.72 Mev $\gamma$-ray, by the decay of the 3.58 Mev level.

The presence of a 2.15 Mev $\gamma$-ray in this spectrum, and the evidence that only about half of the 2.86 Mev $\gamma$-rays are in coincidence with 0.72 Mev $\gamma$-rays, provide strong support for the existence of a 2.86 Mev level in $B^{10}$. However it is necessary to consider whether these two features of the coincidence spectrum could be due to an inaccuracy in the magnitude of either of the corrections made to the observed spectrum - the correction for random coincidences or the correction for the acceptance by the gating channel of pulses caused by electrons Compton-scattered by higher energy $\gamma$-rays.

An error in the correction made for random coincidences could not explain the above effects. If the correction made for random coincidences was inadequate, a further subtraction of a spectrum of the ungated shape would have to be made from the coincidence spectrum. This would reduce further the fraction of the 2.86 Mev $\gamma$-rays observed in the coincidence spectrum and would in any case introduce an unacceptable valley at 0.72 Mev. An excessive correction for random coincidences would mean that the contribution at 0.72 Mev and 2.15 Mev should be even larger.

A further correction for the effect of pulses caused by higher energy $\gamma$-rays being accepted by the gating channel would result in a similar unacceptable valley at 0.72 Mev, whereas again, if the correction is already too large, the intensities of the 0.72 Mev and 2.15 Mev $\gamma$-rays should be increased.

A combination of the correction for random coincidences too large with the other correction too small could perhaps cause the effects under consideration, but the error in each case would have to be at least a factor of two or more, and errors of this magnitude are decidedly unlikely.

Fig. 47 thus seems to provide definite evidence for a level at 2.86 Mev in $B^{10}$.

6.3. Analysis of the Spectrum Gated on the 1.02 Mev Peak

The spectrum gated on the 1.02 Mev peak, fig. 41, was analysed in the same way as the spectra discussed above; the result is shown in fig. 48. The agreement between the synthesised curve and the experimental points is good, with only two points, at 0.85 and 0.90 Mev, noticeably off the curve. The relative intensities from fig. 48 are listed below.

Relative Intensities of the $\gamma$-rays in the Spectrum Gated on the 1.02 Mev Peak

| $\gamma$-ray energy (Mev) | Relative intensities (%) |
|---|---|
| 2.15 | $6 \pm 2$ |
| 1.43 | $10 \pm 3$ |
| 1.02 | $17 \pm 4$ |
| 0.72 | $53 \pm 13$ |
| 0.41 | $18 \pm 8$ |

It should be recalled that in obtaining this spectrum about half of the gating pulses were due to 1.02 Mev $\gamma$-rays and half to 1.43 Mev $\gamma$-rays (section 5.4.) This spectrum is consistent with

FIG. 48. SYNTHESIS OF THE SPECTRUM GATED ON THE 1·02 MEV PEAK.

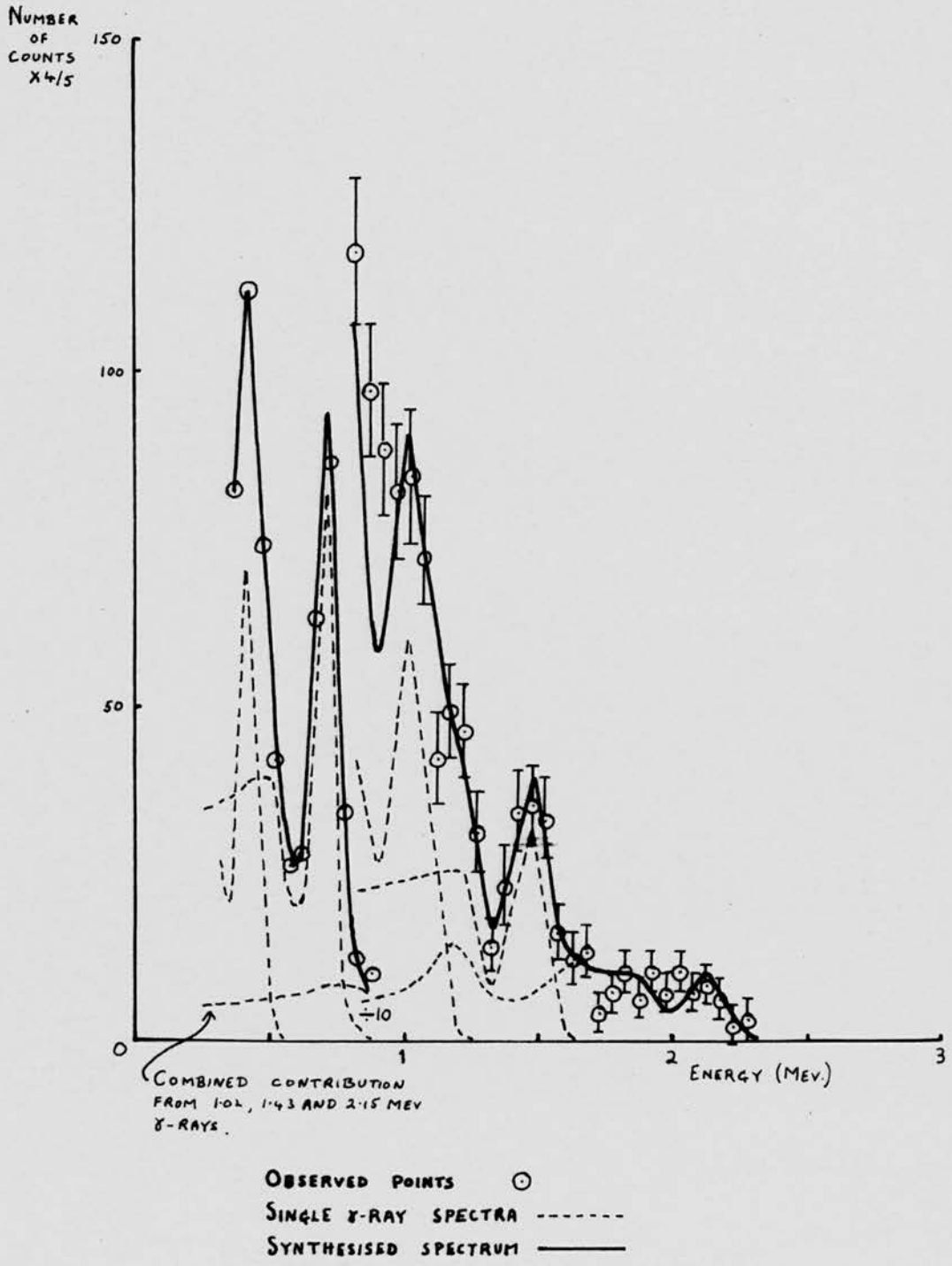

the decay scheme in fig. 1. According to it the 1.43, 0.72 and 0.41 Mev $\gamma$-rays would be in coincidence with the 1.02 Mev $\gamma$-ray, and all the $\gamma$-rays observed would be in coincidence with one or other of the 1.43 Mev $\gamma$-rays.

## 6.4. Relative Intensities of the Neutron Groups from the Reaction $Be^9(d, n)B^{10}$.

If the angular distribution of the neutrons from the $Be^9(d, n)B^{10}$ reaction is isotropic, the relative intensities of the neutron groups in a spectrum give the probabilities for the formation of the corresponding levels in $B^{10}$. The relative intensities were found of the groups in the spectrum (fig. 2) of the neutrons emitted at $0^\circ$ to the deuteron beam. On the assumption that any anisotropy is small these intensities, tabulated below, are used later to ensure that decay schemes that are consistent with the $\gamma$-ray spectra are also consistent with the neutron intensities. The relative intensities obtained by other workers, at different bombarding energies, are listed for comparison.

Relative Intensities of the Neutron Groups from $Be^9(d, n)B^{10}$

(from the spectrum by Karadeniz, fig. 2. $E_d$ = 0.6 Mev)

| Energy of level in $B^{10}$ (Mev) | Relative intensity | Relative intensities observed by other workers[25] | |
|---|---|---|---|
| | | Pruitt et al[25] $E_d$ = 0.94 Mev | Ajzenberg[5&25] $E_d$ = 3.4 Mev |
| 0 | 17 ± 4 | 38 | 49 |
| 0.72 | 34 ± 8 | 43 | 46 |
| 1.74 | 13 ± 3 | 7 | 10 |
| 2.15 | 22 ± 5 | 24 | 19 |
| (2.70) | (8 ± 2) | - | - |
| (3.20) | (4 ± 1) | - | - |
| 3.58 | 20 ± 5 | 26 | 26 |

The intensities of the groups corresponding to the excited levels of $B^{10}$ follow the same general trend in all the results, although the ground state would seem to be excited less strongly at the lower bombarding energy. This also seems to be the case in the spectra shown by Dyer and Bird[7] ($E_d$ = 0.6 Mev), although they do not quote relative intensities. The intensities obtained by Pruitt et al. were based on spectra obtained at angles from 15° to 140° to the deuteron beam and those of Ajzenberg were obtained at angles between 0° and 80°, so that these results should take some account of the anisotropic distribution of the emitted neutrons. It is reasonable to expect the anisotropy to become less at the lower bombarding energy used by Karadeniz, as at least the effects due to stripping should be reduced. The idea of making a correction to the intensities from Karadeniz's neutron spectrum based on the angular distributions obtained by Green et al.[9]

(bombarding energy 860 Kev) was investigated, but it did not improve the agreement with the other results in any way, and in view of the difference in the bombarding energies used in the two experiments such a correction would be of doubtful validity.

As only the intensities of the groups corresponding to the excited levels are used for comparison with the proposed decay schemes, the reasonable agreement between the intensities of these groups, despite the different bombarding energies, encourages the belief that the use of the values from Karadeniz's spectrum, taking into account the accuracy quoted, will not lead to any substantially wrong conclusions.

## 6.5. The $B^{10}$ Decay Scheme

It is clear from the discussion of the spectrum in coincidence with the 0.72 Mev $\gamma$-ray that a level in $B^{10}$ at 2.86 Mev is necessary to explain the results obtained. This would seem to be the only modification necessary to the accepted scheme in fig. 1, so a scheme of the kind shown in fig. 30 is considered.

Of the transitions that could involve the 2.86 Mev level, only the transition to the 1.74 Mev level, which would give a $\gamma$-ray of energy 1.12 Mev, can be immediately ruled out. There is no evidence for a $\gamma$-ray of this energy in any of the observed spectra. The $\gamma$-ray transition from the 2.86 Mev level to the ground state must be included, because of the evidence that all of the 2.86 Mev $\gamma$-rays are not in coincidence with 0.72 Mev $\gamma$-rays. The possibility of a 0.72 Mev $\gamma$-ray between the 3.58 Mev and 2.86 Mev levels, and an energetically indistinguishable 0.71 Mev $\gamma$-ray between the 2.86 Mev and 2.15 Mev levels, could only be rejected if there were definitely no 0.72 Mev - 0.72 Mev coincidences

observed. The occurrence of either or both of these $\gamma$-rays must be considered. The "upper" of them (between the 3.58 and 2.86 Mev levels) followed by the 2.86 Mev $\gamma$-ray to the ground state could possibly be responsible for the observed 0.72 Mev - 2.86 Mev coincidences, in which case the 2.86 Mev transition between the 3.58 Mev and 0.72 Mev levels might not occur at all. Likewise the observed 0.72 Mev - 2.15 Mev coincidences could be due to either the 2.14 Mev $\gamma$-ray transition between the 2.86 Mev and 0.72 Mev levels followed by the 0.72 Mev $\gamma$-ray to the ground state or the 0.71 Mev $\gamma$-ray transition between the 2.86 Mev and 2.15 Mev levels followed by the 2.15 Mev $\gamma$-ray to the ground state.

Possible decay schemes embodying these possibilities are outlined below, and the agreements they give with the observed $\gamma$-ray and neutron-group relative intensities are discussed.

Decay Scheme I

Fig. 49 shows one possible decay scheme, which includes all the possible $\gamma$-rays except the 0.71 Mev transition between the 2.86 Mev and 2.15 Mev levels (which is indicated by a dotted line). The number beside each transition indicates its relative intensity. The relative intensities of the neutron groups that fit the decay scheme are shown at the right hand side. The table below compares the relative intensities resulting from the decay scheme with those observed.

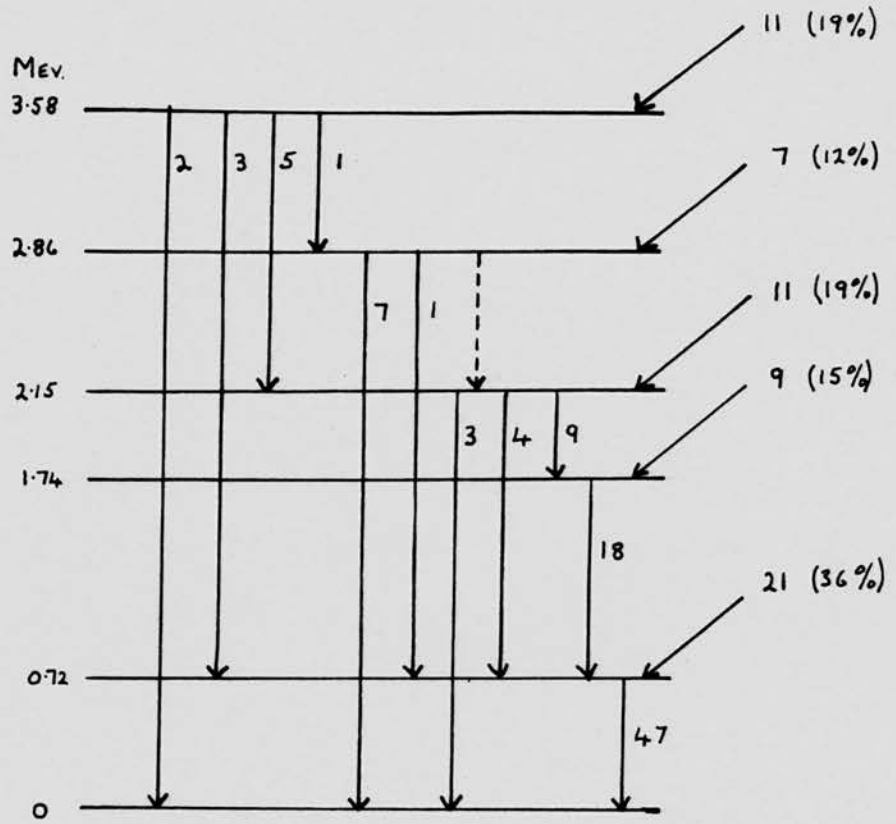


FIG. 49. DECAY SCHEME I.

THE NEUTRON INTENSITIES ARE QUOTED IN BRACKETS AS PERCENTAGES OF THE NUMBER OF NEUTRONS ASSOCIATED WITH THE FIVE EXCITED LEVELS.

## Relative Intensities from Decay Scheme I.

| γ-ray intensities | | | | | | | neutron groups | | |
|---|---|---|---|---|---|---|---|---|---|
| γ-ray energy (Mev) | Ungated spectrum | | Gated on 0.72 Mev | | Gated on 1.02 Mev | | $B^{10}$ level (Mev) | Decay scheme intensities | Observed intensities (Karadeniz) |
| | Decay scheme | Observed | Decay scheme | Observed | Decay scheme | Observed | | | |
| 3.58 | 2% | 3 ± 1% | 0% | 0% | 0% | 0% | 3.58 | 19% | 20 ± 5% |
| 2.86 | 10 | 12 ± 3 | 10 | 10 ± 3 | 0 | 0 | 2.86 | 12 | 8 ± 2 |
| 2.15 | 4 | 4 ± 1 | 3 | 5 ± 1 | 2 | 6 ± 2 | 2.15 | 19 | 22 ± 5 |
| 1.43 | 9 | 11 ± 3 | 20 | 16 ± 4 | 11 | 10 ± 3 | 1.74 | 15 | 13 ± 3 |
| 1.02 | 18 | 20 ± 5 | 45 | 39 ± 10 | 6 | 17 ± 4 | 0.72 | 36 | 34 ± 8 |
| 0.72 | 48 | 42 ± 10 | 1 | 5 ± 4 | 55 | 53 ± 13 | | | |
| 0.41 | 9 | 7 ± 2 | 23 | 26 ± 10 | 26 | 18 ± 8 | | | |

In the column listing the observed intensities of the neutron groups from Karadeniz's spectrum, the value quoted for the 2.86 Mev level was that observed at 2.7 Mev. The intensities from the decay scheme for comparison with the spectrum gated on the 1.02 Mev peak take account of the fact that the observed spectrum is really a combination of equal contributions from the spectra in coincidence with the 1.02 Mev and the 1.43 Mev $\gamma$-rays.

This decay scheme gives good agreement with the relative intensities observed in the ungated spectrum, in the spectrum in coincidence with the 0.72 Mev $\gamma$-ray, and with the intensities of the neutron groups. It only disagrees appreciably over the intensity of the 1.02 Mev $\gamma$-ray in the spectrum gated on the 1.02 Mev peak. In this decay scheme the agreement over this point could be improved only by considerably increasing the intensity of the upper 1.43 Mev $\gamma$-ray (between the 3.58 and 2.15 Mev levels) at the expense of the lower one. The agreement would still not be very good, even if the lower 1.43 Mev $\gamma$-ray were omitted, and this would spoil the agreement in the intensities of the neutron groups corresponding to the 3.58 Mev and 2.15 Mev levels. More important, the presence of 1.43 Mev - 1.43 Mev $\gamma$-ray coincidences is well established by Shafroth and Hanna[16].

The weak 0.72 Mev transition between the 3.58 Mev and 2.86 Mev levels could be doubled in intensity without spoiling the agreement with the observed intensities. If it is omitted there is no explanation of the small number of observed 0.72 Mev - 0.72 Mev coincidences.

If a weak 0.71 Mev transition between the 2.86 Mev and 2.15 Mev levels is included as an addition to the scheme shown, it

would tend to spoil the agreement in the intensities of the neutron groups associated with the2.86 Mev and 2.15 Mev levels, by increasing the intensity of the former and reducing that of the latter. Altering the intensities of other transitions to compensate for this produces other discrepancies, although an intensity of about 1% of the total number of $\gamma$-rays for this 0.71 Mev transition cannot be definitely ruled out - hence its inclusion as a dotted line in the decay scheme. An intensity of about 4% would be required for this transition if it were to explain the observed 0.72 Mev - 2.15 Mev coincidences, and the explanation adopted in the decay scheme is therefore preferable (i.e. 2.14 Mev $\gamma$-ray between 2.86 Mev and 0.72 Mev levels followed by 0.72 Mev $\gamma$-ray to ground).

The intensity of the upper 2.86 Mev $\gamma$-ray (between the 3.58 Mev and 0.72 Mev levels) cannot be increased above the value shown.

Decay Scheme II

A satisfactory decay scheme can be devised (fig. 50) in which all the 2.86 Mev $\gamma$-rays occur between the 2.86 Mev level and ground.

The table below compares the relative intensities from this decay scheme with those observed.

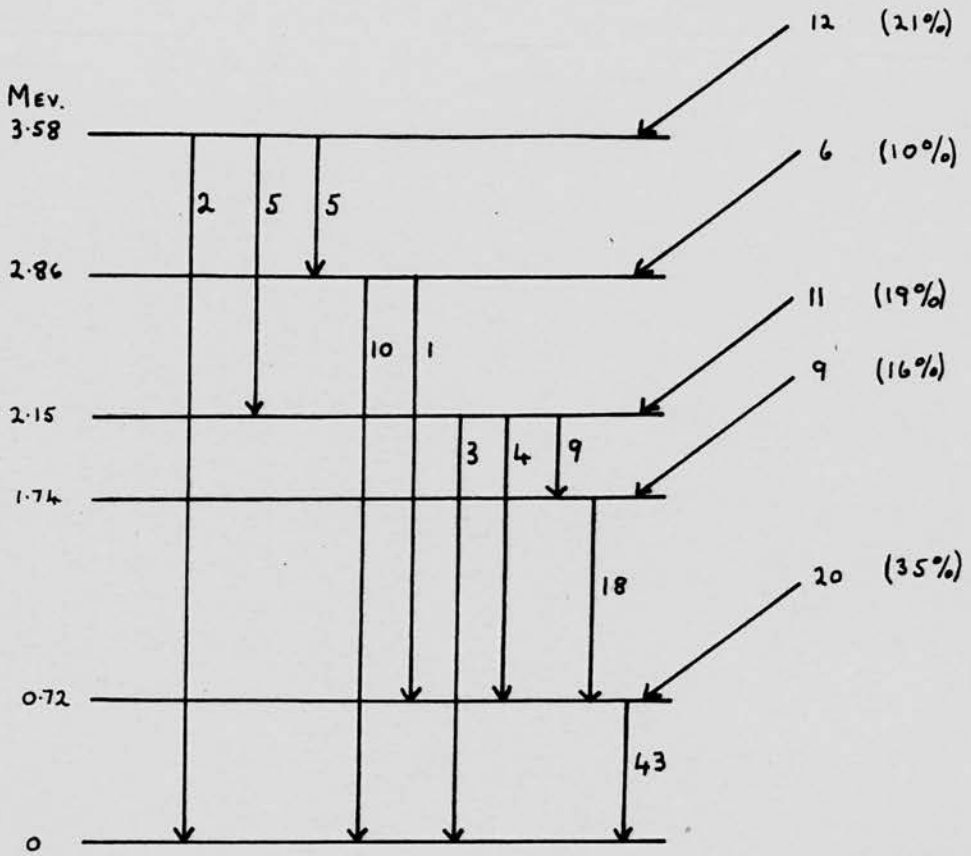


FIG 50. DECAY SCHEME II

## Relative Intensities from Decay Scheme II.

| γ-ray intensities | | | | | | | neutron groups | | |
|---|---|---|---|---|---|---|---|---|---|
| γ-ray energy (Mev) | Ungated spectrum | | Gated on 0.72 Mev | | Gated on 1.02 Mev | | $B^{10}$ level (Mev) | Decay scheme intensities | Observed intensities (Karadeniz) |
| | Decay scheme | Observed | Decay scheme | Observed | Decay scheme | Observed | | | |
| 3.58 | 2% | 3 ± 1% | 0% | 0% | 0% | 0% | 3.58 | 21% | 20 ± 5% |
| 2.86 | 10 | 12 ± 3 | 10 | 10 ± 3 | 0 | 0 | 2.86 | 10 | 8 ± 2 |
| 2.15 | 4 | 4 ± 1 | 2 | 5 ± 1 | 2 | 6 ± 2 | 2.15 | 19 | 22 ± 5 |
| 1.43 | 9 | 11 ± 3 | 16 | 16 ± 4 | 11 | 10 ± 3 | 1.74 | 16 | 13 ± 3 |
| 1.02 | 18 | 20 ± 5 | 36 | 39 ± 10 | 6 | 17 ± 4 | 0.72 | 35 | 34 ± 8 |
| 0.72 | 48 | 42 ± 10 | 2 | 5 ± 4 | 55 | 53 ± 13 | | | |
| 0.41 | 9 | 7 ± 2 | 18 | 26 ± 10 | 26 | 18 ± 8 | | | |

The agreement between the observed intensities and those derived from the decay scheme is generally good; the largest disagreement is in the case of the 1.02 Mev γ-ray in the spectrum gated on 1.02 Mev. This was also the point of worst agreement in decay scheme I.

As in the case of decay scheme I there is nothing to be gained by including a 0.71 Mev γ-ray transition between the 2.86 Mev and 2.15 Mev levels, although one with an intensity of about 1% of the total number of γ-ray transitions cannot be definitely excluded. It is not shown, as decay scheme II is intended to produce a satisfactory explanation of the observed intensities with the minimum necessary number of transitions.

Both decay schemes fit the results equally well and on the data available there is no way of deciding between them. In going from decay scheme I to decay scheme II, the intensities of four transitions are altered; provided they are altered in step with one another they can have any intermediate value between the limits set by these two schemes, without spoiling the agreement with the observed intensities. This is summarised in fig. 52.

Evidence for a level at about 3.2 Mev

The neutron spectrum due to Karadeniz contains a weak group that could correspond to a level in $B^{10}$ at 3.2 Mev. In the γ-ray spectrum gated on the 1.02 Mev peak, the excess of the intensity of the 1.02 Mev γ-ray over that deduced from the above decay schemes might suggest that there are 1.02 Mev - 1.02 Mev γ-ray coincidences. This would be possible if there were a level in $B^{10}$ at 3.17 Mev giving 1.02 Mev transition to the level at 2.15 Mev and so producing a 1.02 - 0.41 - 1.02 - 0.72 Mev cascade (see

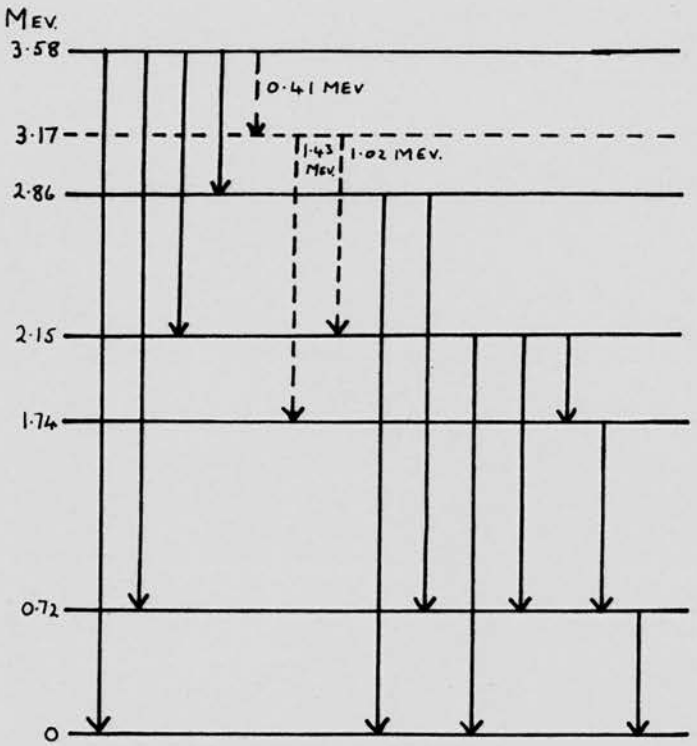


FIG. 51. POSSIBLE γ-RAYS INVOLVING A HYPOTHETICAL LEVEL IN $B^{10}$ AT 3·17 MEV. (SHOWN DOTTED). THE OTHER TRANSITIONS ARE SHOWN AS FULL LINES.

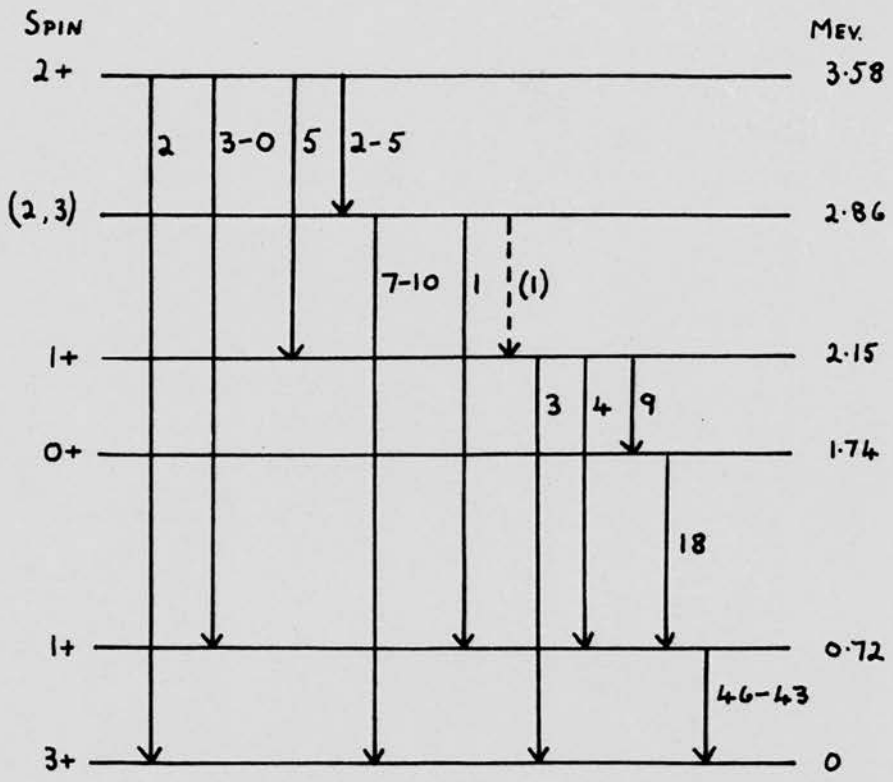


FIG. 52. $B^{10}$ DECAY SCHEME

fig. 51). However such a cascade would also cause the 1.02 Mev γ-ray in the spectrum in coincidence with the 0.72 Mev γ-ray to have an intensity in excess of that predicted by the decay schemes, and this is not the case. Further, to attribute an appreciable intensity to any of the possible γ-rays involving a 3.17 Mev level (fig. 51) makes good agreement between the decay scheme and the observed intensities of the neutron groups impossible to achieve without introducing other discrepancies.

Thus there is no good evidence from the γ-ray spectra for a level near 3.2 Mev and it is assumed that the corresponding group in the neutron spectrum must have some other explanation. It may be, for example, that there should be only one group in this region of the spectrum corresponding to a level at 2.86 Mev and that because of the poor statistical accuracy of the observed points it has by chance taken on the appearance of two groups, one on either side of the true position. If this explanation were valid, the intensity of the neutron-group corresponding to the 2.86 Mev level would be increased to 12%; this would not affect the agreement between the observed intensities and those deduced from the decay scheme in fig. 52.

## 6.6; Conclusions from the Experiment

The γ-ray coincidence spectra provide definite evidence for a level in $B^{10}$ at 2.86 Mev, and the decay scheme presented in fig. 52 provides a good explanation of the observed relative intensities of the γ-rays both in the gated and ungated spectra. This decay scheme is also in agreement with the relative intensities of the neutron groups from this reaction observed by Karadeniz, at the same bombarding energy. The accuracy of the relative intensities quoted in fig. 52 is probably about ± 50%, although

the intensities of the 1.02 Mev and the stronger 0.72 Mev transitions are possibly more accurate, say ± 25%.

It is possible to speculate on a spin assignment for the 2.86 Mev level. The generally accepted spin values[17] for the other levels are shown in fig. 52. Spin values of 0 or 1 for the 2.86 Mev level seem unlikely as they would make the transition to the ground state the least favoured. A spin of 2 might be possible as it would lead one to expect the transition to the 1.74 Mev level to be inhibited relative to the transitions observed. Similarly a spin of 3 might be acceptable. A value of 4 is less likely as it would make the transition to the ground state the only probable one. Spin values of 2 or 3 are therefore tentatively suggested.

# CHAPTER 7.

## DISCUSSION

The conclusions reached about the $B^{10}$ decay scheme are here compared with those derived from previous experiments.

The coincidence spectra obtained by Shafroth and Hanna[16], which they cited as evidence for the decay scheme in fig. 1, do not differ significantly from the corresponding parts of the spectra resulting from the present experiment. However, as explained in section 4.5, their equipment made it difficult for them to study the low intensity parts of a coincidence spectrum, or to attempt accurate quantitative comparisons. In their spectrum of the $\gamma$-rays in coincidence with the 0.72 Mev $\gamma$-ray they show only the energy range 0.2 - 1.1 Mev and not the lower-intensity higher-energy end, which was the part of the spectrum that yielded evidence for the 2.86 Mev $B^{10}$ level in the present experiment.

Some published spectra of the neutrons from the $Be^9(d, n)B^{10}$ reaction would support arguments for the existence of a level at 2.86 Mev in $B^{10}$, while others would not. It may be significant that the spectra that do show a neutron group corresponding to such a level were obtained using a lower deuteron bombarding energy than the others. The spectra due to Karadeniz, which have been referred to frequently, were obtained with the same bombarding energy as was used in the present experiment, 600 Kev. This was also the energy employed by Dyer and Bird[7], who obtained neutron spectra at three angles to the deuteron beam, each of which showed a group that could be attributed to a level in $B^{10}$ at 2.85 Mev. Dyer and Bird[7] drew attention to similar weak neutron groups

in the spectra obtained at low bombarding energies by Staub and Stephens[2] and Powell[3]. It must however be admitted that these groups are of very doubtful statistical significance, as are those corresponding to a 2.9 Mev level observed by Reid[8] in spectra obtained at $0^{\circ}$ and $90^{\circ}$ to a 750 Kev deuteron beam. It should be noted that Reid and Karadeniz both used the same beryllium target in their experiments; a different target was used in the present work.

Of the neutron spectra that show no group corresponding to a 2.86 Mev level, that obtained with the lowest bombarding energy is due to Green, Scanlon and Willmott[9] who employed 865 Kev deuterons. There is no evidence for a 2.86 Mev level in spectra by Pruitt, Swartz and Hanna[6], who used 950 Kev deuterons, nor in the results of Ajzenberg[5] who employed a bombarding energy of 3.5 Mev.

Bockelman et al.[11] who studied protons and deuterons inelastically scattered by $B^{10}$ found no suggestion of a 2.86 Mev level.

The $Li^{7}(\alpha, n)B^{10}$ reaction has not been studied at sufficiently high $\alpha$-particle bombarding energy to enable any $B^{10}$ levels above that at 2.15 Mev to be observed[12 and 13].

There seems to be no obvious and truly satisfactory explanation for the detection of the 2.86 Mev level only at low bombarding energies. There is however another similar feature in the behaviour of the $B^{10}$ nucleus that requires explanation. The experiments on the $Li^{7}(\alpha, n)B^{10}$, reaction[12, 13] both lead one to expect a level at 1.3 Mev in $B^{10}$, which has not been observed from any other reaction.

The energies and spins calculated for the first four excited states of $B^{10}$ by Kurath[19] agree quite well with those observed for the 0.72, 1.74, 2.15 and 3.58 Mev levels and there is no suggestion from these "intermediate coupling" calculations of a level near 2.8 Mev.

## CHAPTER 8.

## PROPOSALS FOR FUTURE EXPERIMENTS ON $B^{10}$

A spectrum of the neutrons from the $Be^9(d, n)B^{10}$ reaction provides information on the energy levels of $B^{10}$ which requires less interpretation than do the results of a coincidence experiment on the $\gamma$-rays. To study further the postulated 2.86 Mev level in $B^{10}$ it would seem desirable to observe its neutron group in a spectrum of good resolution (at least as good as that obtained by Karadeniz or by Green et al.[9]) and of statistical accuracy considerably exceeding that which can reasonably be obtained using emulsion techniques. The requirement of statistical accuracy indicates an electronic system, and a time-of-flight spectrometer would be likely to provide the best resolution. With such an instrument it would be quite feasible to obtain spectra at several bombarding energies to find whether the level is excited only at low energies.

A spectrometer similar to the one described by Batchelor and Towle[26] would be suitable. The idea is to obtain the velocities of the neutrons, and therefore their energies, by measuring the time taken by them to traverse a fixed distance. In order to discuss the modification that would be necessary to the system used by Batchelor and Towle to make it suitable for use with an H.T. set, the working of their instrument is outlined briefly.

The beam of bombarding particles is pulsed so as to strike the target in very short bursts. A "zero-time pulse" indicates the arrival of the beam on the target, i.e. the time at which

neutrons are emitted. The electronic equipment measures the time interval between the arrival of this pulse and a pulse from the neutron detector at the end of the flight path, and feeds out this information as a pulse whose amplitude is proportional to the time interval. A multichannel kicksorter is used to give a spectrum of the flight times.

An H.T. set has inevitably a ripple voltage superimposed on the accelerating potential which would cause the beam, after deflection by the analysing magnet, to sweep the target at the ripple frequency (200 c/s in the case of the Edinburgh set). In the spectrometer described by Batchelor and Towle[26], which was used with a Van de Graaff accelerator, the beam is pulsed by passing between deflector plates to which is applied a sinusoidal potential of about 10 KV amplitude and frequency 2.5 Mc/s, and the zero-time pulse is derived from this r.f. voltage. Thus in a spectrometer with a similar pulsing system used with an H.T. set the beam would sweep the target with a combination of the motions due to the r.f. deflection and the ripple voltage. Under these circumstances it might be preferable to obtain the zero time pulse by detecting the $\gamma$-rays emitted when the beam strikes the target. This should be quite satisfactory as the level in $B^{10}$ with the longest lifetime is probably the 0.72 Mev level with a lifetime of $\sim 10^{-9}$ sec.[27], which is quite short compared with the time ($10^{-7}$ sec.) for the most energetic neutron (5 Mev) from this reaction to travel a distance of 3 metres, which is a reasonable length for a flight path. To use the $\gamma$-rays as an indication of the time of emission of the neutrons would have the additional advantage to a University laboratory that only one hundred-channel kicksorter would be required, instead of the two used for the experiment of

reference 26.

The principal improvement that could be made to the γ-ray spectrometers for a future experiment would be to use larger crystals, with the γ-rays collimated to strike each crystal in a narrow beam along its axis. The spectrometers would then have an improved peak efficiency and each full energy peak would be much more prominent than its associated Compton edge and escape peaks. The interpretation of the spectra would be more reliable as a much smaller correction would be required for the unwanted pulses accepted in the gating channel. A γ-ray spectrometer with a larger crystal might also separate the 2.15 Mev peak from the escape peaks of the 2.86 Mev γ-ray sufficiently to enable a spectrum gated on the 2.15 Mev γ-ray to be obtained. An improvement by a factor of not more than four could perhaps be obtained in the coincidence resolving time, and would reduce the correction for random coincidences.

A study of the neutron spectrum should probably take precedence over a further study of the γ-rays, although a combination of accurate neutron spectra at several angles to the deuteron beam, with good γ-ray coincidence spectra should enable the relative intensities of the γ-ray transitions to be determined.

The idea of observing the spectrum of the γ-rays in coincidence with each of the neutron groups is attractive. Unfortunately the experimental difficulties are very large, because any neutron spectrometer with a worthwhile resolution is very inefficient. A high beam current of deuterons could be used to get the maximum counting rate in the neutron spectrometer but this would probably result in a γ-ray counting rate so large as to give considerable

distortion of the spectrum. However, if a time of flight spectrometer were constructed and a suitable $\gamma$-ray spectrometer were at hand, it might be interesting to set up a delayed coincidence system to attempt to observe the $\gamma$-ray spectra in coincidence with even some of the neutron groups, although in view of the difficulties, really good coincidence spectra are hardly to be expected.

A relevant experiment that would require less complex equipment would be to obtain the $\alpha$-particle threshold energies for slow neutron production in the $Li^7(\alpha, n)B^{10}$ reaction, studying particularly the regions that could give evidence for 2.86 Mev and 1.3 Mev levels in $B^{10}$. Spectra of the $\gamma$-rays could also be obtained with $\alpha$-particle bombarding energies chosen to excite the $B^{10}$ nucleus up to each level in turn. It would then be interesting to seek evidence for $\gamma$-rays involving the 1.3 Mev level, which has so far been observed only in studies of the neutrons. The Q value for the production of the ground state of $B^{10}$ is about -3 Mev[12, 13] and so a source of $\alpha$-particles of energy about 10 Mev would be required to excite the $B^{10}$ nucleus up to about 3 Mev.

## ACKNOWLEDGMENTS

My grateful thanks go to Professor N. Feather, F.R.S. for providing the facilities for the experiment, and to Mr. R.M. Sillitto for his interest, encouragement and valuable advice. I am also grateful to Dr. M.C. Karadeniz for the use of his unpublished neutron spectrum, to my colleague Mr. G. Bradford for interesting discussions, and to the members of the Department who co-operated over the use of electronic equipment.

The help given by Mr. A. Headridge and his technical staff with the construction of apparatus, and by Mr. C. McAnna with the maintenance of electronic equipment is gratefully acknowledged. My thanks go also to Mr. H. Napier for his willing assistance in running the H.T. set, often at quite abnormal hours.

The receipt of a Maintenance Grant from the Department of Scientific and Industrial Research, and later of a Post-Graduate Studentship from Edinburgh University, is acknowledged with thanks.

## REFERENCES


1. Bonnar and Brubaker, Phys. Rev. 50, 308 (1936)
2. Staub and Stephens, Phys. Rev. 55, 131 (1939)
3. Powell, Proc. Roy. Soc. A. 181, 344 (1943)
4. Whitehead and Mandeville, Phys. Rev. 77, 732 (1950)
5. Ajzenberg, Phys. Rev. 82, 43 (1951)
   and Phys. Rev. 88, 298 (1952)
6. Pruitt, Swartz and Hanna, Phys. Rev. 92, 1456 (1953)
7. Dyer and Bird, Aust. J. Phys. 6, 45 (1953)
8. Reid, Proc. Phys. Soc. A. 67, 466 (1954)
9. Green, Scanlon and Willmott, Proc. Phys. Soc. A. 68, 386 (1955)
10. Craig, Donahue and Jones, Phys. Rev. 88, 808 (1952)
11. Bockelman, Browne, Sperduto and Buechner, Phys. Rev. 92, 665 (1953)
12. Haxel and Stuhlinger, Z. Physik, 114, 178 (1939)
13. Robbins, Phys. Rev. 101, 1,373 (1956)
14. Rasmussen, Hornyák and Lauritsen, Phys. Rev. 76, 581 (1949)
15. Day and Huus, Phys. Rev. 85, 761 (1952)
16. Shafroth and Hanna, Phys. Rev. 95, 86 (1954)
17. Ajzenberg and Lauritsen, Revs. Mod. Phys. 27, 77 (1955)
18. Bird and Spear, Aust. J. Phys. 8, 567 (1955)
19. Kurath, Phys. Rev. 101, 216 (1956)
20. Folkierski, J. Sci. Instrum. 33, 187 (1956)
21. Wilkinson, Proc. Camb. Phil. Soc. 46, 508 (1950)

22. Collinge, Morrison and Eccleshall, J. Sci. Instrum. 33, 72 (1956)

23. Fisher and Schute, Phil. Mag. 2, 1,255 (1957)

24. Lazar, Davis and Bell, Nucleonics 14(4), 52 (April, 1956)

25. Ajzenberg and Lauritsen, Revs. Mod. Phys. 24, 321 (1952)

26. Batchelor and Towle, Proc. Phys. Soc. 73, 193 (1959)

27. Bloom, Turner and Wilkinson, Phys. Rev. 105, 232 (1957)